EUROPEAN ORGANIZATION FOR NUCLEAR RESEARCH

October 26, 2012

A survey of backward proton and pion production in p+C interactions at beam momenta from 1 to 400 GeV/c

O. Chvala[4,6], H. G. Fischer[3,a)], M. Makariev[5], A. Rybicki[2], D. Varga[1], S. Wenig[3]

[1]Eötvös Loránd University, Budapest, Hungary
[2]H. Niewodniczański Institute of Nuclear Physics, Polish Academy of Sciences, Cracow, Poland
[3]CERN, Geneva, Switzerland
[4]Charles University, Faculty of Mathematics and Physics, Institute of Particle and Nuclear Physics, Prague, Czech Republic
[5]Institute for Nuclear Research and Nuclear Energy, BAS, Sofia, Bulgaria
[6]now at University of Tennessee, Knoxville, TN, USA

to be published in EPJC

Abstract

New data on proton and pion production in p+C interactions from the CERN PS and SPS accelerators are used in conjunction with other available data sets to perform a comprehensive survey of backward hadronic cross sections. This survey covers the complete backward hemisphere in the range of lab angles from 10 to 180 degrees, from 0.2 to 1.4 GeV/c in lab momentum and from 1 to 400 GeV/c in projectile momentum. Using the constraints of continuity and smoothness of the angular, momentum and energy dependences a consistent description of the inclusive cross sections is established which allows the control of the internal consistency of the nineteen available data sets.

a) e-mail: Hans.Gerhard.Fischer@cern.ch

1 Introduction

An impressive amount of data on backward hadron production in p+C interactions has been collected over the past four decades. A literature survey reveals no less than 19 experiments which have contributed a total amount of more than 3500 data points covering wide areas in projectile momentum, lab angle and lab momentum.

Looking at the physics motivation and at the distribution in time of these efforts, two distinct classes of experimental approaches become evident. 15 experiments cluster in a first period during the two decades between 1970 and 1990. All these measurements have been motivated by the nuclear part of proton-nucleus collisions, in particular by the width of the momentum distributions in the nuclear rest system which reach far beyond the narrow limits expected from nuclear binding alone. These studies have ceased in the late 1980's with the advent of relativistic heavy ion collisions and their promise of "new" phenomena beyond the realm of classic nuclear physics.

A second class of very recent measurements has appeared and is being pursued after the turn of the century, with publications starting about 2008. Here the motivation is totally different. It is driven by the necessity of obtaining hadronic reference data for the study of systematic effects in cosmic ray and neutrino physics, in particular concerning atmospheric and long base line experiments as well as eventual novel neutrino factories. The main aim of these studies is the comparison to and the improvement of hadronic production models – models which are to be considered as multi-parameter descriptions of the non-calculable sector of the strong interaction, with very limited predictive power.

This new and exclusive aim has led to the strange situation that if all recent publications contain detailed comparisons to available production models, no comparison to existing data is attempted. It remains therefore unclear how these new results compare to the wealth of already available data and whether they in fact may over-ride and replace the existing results.

In this environment the studies conducted since 15 years by the NA49 experiment at the CERN SPS have a completely different aim. Here it is attempted to trace a model-independent way from the basic hadron-nucleon interaction via hadron-nucleus to nucleus-nucleus collisions. This aim needs precision data from a large variety of projectile and target combinations as well as a maximum phase space coverage. As the acceptance of the NA49 detector is limited to lab angles below 45 degrees, it is indicated to use existing backward data in the SPS energy range in order to extend the acceptance coverage for the asymmetric proton-nucleus interactions. This requires a careful study of the dependence on cms energy and of the reliability of the results to be used.

In the course of this work it appeared useful and even mandatory to provide a survey of all available data over the full scale of interaction energies, the more so as no overview of the experimental situation is available to date. This means that the present study deals with projectile momenta from 1 to 400 GeV/c, for a lab angle range from 10 to 180 degrees, and for lab momenta from 0.2 to 1.2 GeV/c.

2 Variables and kinematics

Most available data have been obtained as a function of the lab momentum p_{lab} (or kinetic energy T_{lab}) at constant lab angle Θ_{lab}. In this publication all given yields are transformed to the double differential invariant cross section

$$f(p_{\text{lab}}, \Theta_{\text{lab}}) = \frac{E}{p_{\text{lab}}^2} \frac{d^2\sigma}{dp_{\text{lab}} d\Omega}. \quad (1)$$

In this context the term ”backward” needs a precise definition. One possibility would be to define as ”backward” the region of lab angles $\Theta_{\rm lab} > 90$ degrees. The present paper uses instead a definition which refers to the cms frame with the basic variables Feynman x_F and transverse momentum p_T, defining as ”backward” the particle yields at $x_F < 0$. This allows a clear separation of the projectile fragmentation region at positive x_F with a limited feed-over into negative x_F and the target fragmentation region at negative x_F with a limited feed-over into positive x_F. At the same time the notion of ”kinematic limit” in participant fragmentation is clearly brought out at x_F = $\pm$ 1 and the contributions from intranuclear cascading may be clearly visualized and eventually separated.

The correlation between the two pairs of variables is presented in Fig. 1 which shows lines of constant $p_{\rm lab}$ and $\Theta_{\rm lab}$ in the coordinate frame of x_F and p_T for protons and pions for the two values of projectile momentum at 158 and 3 GeV/c which are representative of the typical range of interaction energies discussed in this paper.

Several comments are due in this context. The definition of Feynman x_F has been modi-

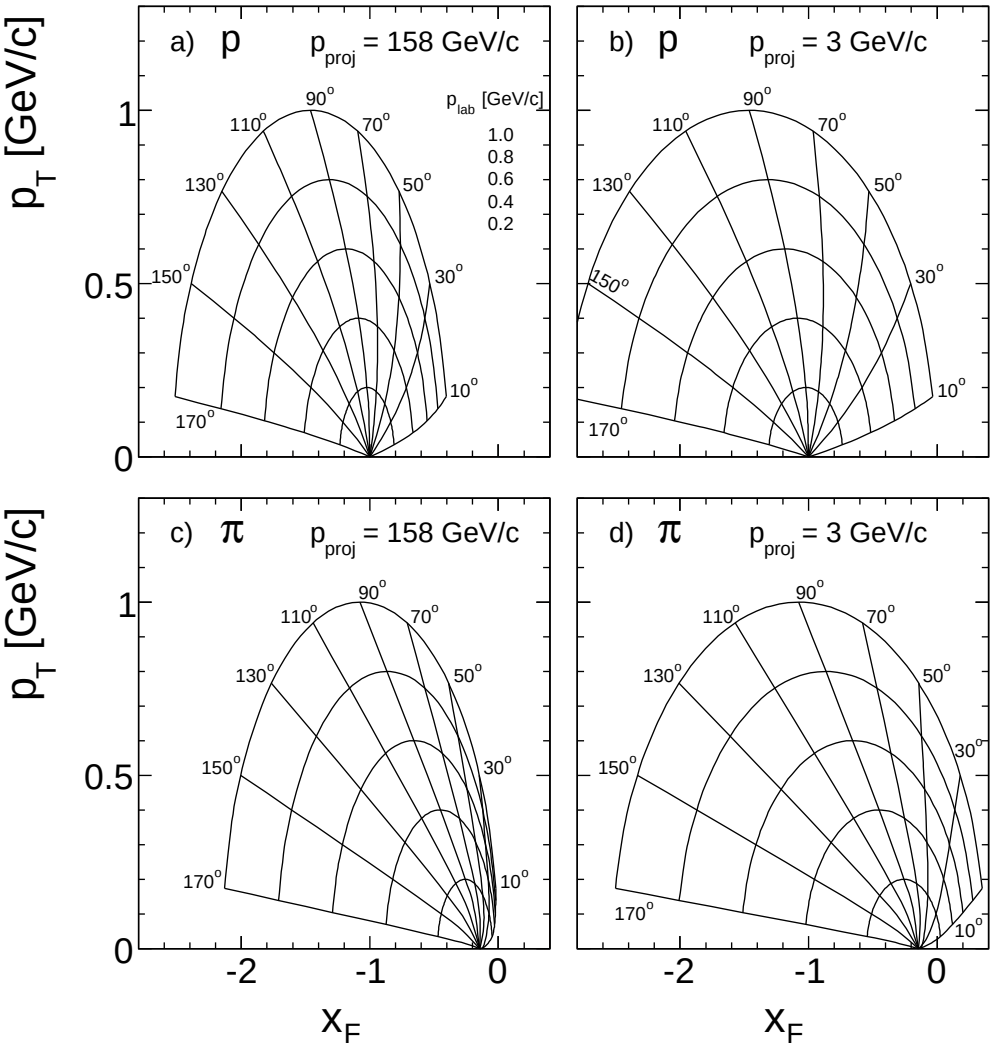

Figure 1: Lines of constant $p_{\rm lab}$ and $\Theta_{\rm lab}$ in the cms frame spanned by Feynman x_F and p_T for protons and pions at two different projectile momenta, a) protons at 158 GeV/c, b) protons at 3 GeV/c, c) pions at 158 GeV/c and d) pions at 3 GeV/c

fied from the standard one,

$$x_F = \frac{p_l}{p_{\text{max}}} = \frac{p_l}{\sqrt{s}/2} \tag{2}$$

to

$$x_F = \frac{p_l}{\sqrt{s/4 - m_p^2}} \tag{3}$$

with m_p the proton mass. This takes care of baryon number conservation and regularises the kinematic borders at low interaction energies. The s dependence in Fig. 1 is small to negligible for lab angles above about 50 degrees both for pions and protons but becomes noticeable at small Θ_{lab}. If at SPS energy the full range of lab momenta up to 1.4 GeV/c and angles above 10 degrees is confined to the backward region both for protons and pions, the coverage for pions extends to positive x_F at low lab angles and low beam momenta.

Another remark concerns the overlap between target fragmentation and nuclear cascading. For protons, at all lab angles above about 70 degrees the kinematic limit for fragmentation of a target nucleon at rest in the lab system is exceeded. For pions on the other hand this is not the case as their x_F value for p_{lab} = 0 is at

$$|x_F| = \frac{m_\pi}{m_p} = 0.148 \tag{4}$$

This means that over the full range of lab angles and up to large p_{lab} values the contribution from target participants mixes with the nuclear component. The separation of the two processes therefore becomes an important task, see Sect. 10 of this paper.

A last remark is due to the limits of experimental coverage. All existing experiments run out of statistics at cross section levels of about 10 μb, that is about 4 orders of magnitude below the maximum yields. As visible from the momentum ranges indicated in Tables 1 and 2, this corresponds to a typical upper momentum cut-off in the region of 1 GeV/c.

3 The Experimental Situation

The backward phase space coverage in p+C interactions is surprisingly complete if compared with the forward direction and even with the available data in the elementary p+p collisions. This is apparent from the list of experiments given in Tables 1 and 2 with their ranges in beam momentum, lab angle, and lab momentum. Although some effort has been spent to pick up all published results, this list is not claimed to be exhaustive as some results given as ”private communication”, in conference proceedings or unpublished internal reports might have escaped attention.

For secondary protons, Table 1, the important amount of low energy n+C data by Franz et al. [10] has been added to the survey as the isospin factors for the transformation into p+C results have been studied and determined with some precision, see Sect. 5.

For secondary pions, Table 2, the situation is somewhat complicated by the fact that two independent sets of results have been published by the HARP-CDP [4] and the HARP [15] groups, based on identical input data obtained with the same detector. An attempt to clarify this partially contradictory situation is presented in Sect. 9.3 of this paper.

Unfortunately, no commonly agreed scale in the three basic variables Θ_{lab}, p_{lab} and p_{beam} of the double-differential cross sections has been defined by the different collaborations providing the data contained in Tables 1 and 2. This leads to the fact that not a single couple out

interaction	Experiment	projectile momentum (GeV/c)	lab angle coverage (degrees)	p_{lab} coverage (GeV/c)	number of data points	errors [%] $\langle\sigma_{stat}\rangle$	$\langle\sigma_{syst}\rangle$
p+C	Bayukov [1]	400	70, 90, 118, 137, 160	0.4–1.3	35	6	20
	NA49 [2]	158	10, 20, 30, 40	0.3–1.6	40	7	5
	Belyaev [3]	17, 23, 28, 34 ,41, 49, 56	159	0.3–1.2	125	5	15
	HARP-CDP [4]	3, 5, 8, 12, 15	25, 35, 45, 55, 67, 82, 97, 112	0.45–1.5	202	4	6
	Burgov [5]	2.2, 6.0, 8.5	162	0.35–0.85	36	15	5
	Bayukov [6]	1.87, 4.5, 6.57	137	0.3–1.1	55	10	20
	Geaga [7]	1.8, 2.9, 5.8	180	0.3–1.0	50	17	15
	Frankel [8]	1.22	180	0.45–0.8	6	7	
	Komarov [9]	1.27	105, 115, 122, 130, 140, 150, 160	0.34–0.54	∼200	8	15
n+C	Franz [10]	0.84, 0.99, 1.15	51, 61, 73, 81, 98, 120, 140, 149, 160	0.3–0.8	553	5	10

Table 1: Data sets for proton production in p+C and n+C collisions from seven experiments giving the ranges covered in projectile momentum, lab angle, and lab momentum, the number of measured data points and errors

Experiment	projectile momentum (GeV/c)	lab angle coverage (degrees)	p_{lab} coverage (GeV/c)	number of data points	errors [%] $\langle\sigma_{stat}\rangle$	$\langle\sigma_{syst}\rangle$
Nikiforov [11]	400	70, 90, 118, 137, 160	0.2–1.3	59	12	
NA49 [12]	158	5, 10, 15, 20, 25, 30, 35, 40, 45	0.1–1.2	174	5	4
Belyaev [13]	17, 22, 28, 34, 41, 47, 57	159	0.25–1.0	218	4	15
Abgrall [14]	31	0.6–22.3	0.2–18	624	6	7
HARP-CDP [4]	3, 5, 8, 12, 15	25, 35, 45, 55, 67, 82, 97, 112	0.2–1.6	829	6	8
HARP [15]	3, 5, 8, 12	25, 37, 48, 61, 72, 83, 95, 106,117	0.125–0.75	605	12	
Burgov [16]	2.2, 6.0, 8.5	162	0.25–0.6	29	20	
Baldin [17]	6.0, 8.4	180	0.2–1.25	45	10	
Cochran [18]	1.38	15, 20, 30, 45, 60, 75, 90, 105, 120, 135, 150	0.1–0.7	199	3	12
Crawford [19]	1.20	22.5, 45, 60, 90, 135	0.1–0.4	50	8	7

Table 2: Data sets for pion production in p+C collisions from seven experiments giving the ranges covered in projectile momentum, lab angle, and lab momentum, the number of measured data points and errors

of the more than 3500 data points contained in these Tables may be directly compared. The application of an interpolation scheme as described in Sect. 4 is therefore an absolute necessity. Ideally the thus obtained interpolated cross sections would form an internally consistent sample of results which would be coherent within the given experimental errors. As will become apparent in the following data comparison, this assumption is surprisingly well fulfilled for the majority of the experiments. Only four of the 20 quoted groups of results fall significantly out of this comparison; those will be discussed in Sect. 9 of this paper. In this sense the overall survey of the backward proton and pion production results in a powerful constraint for the comparison with any new data sample.

4 Data comparison

As stated above the main problem in bringing the wealth of available data into a consistent picture is given by the generally disparate position in phase space and interaction energy of the different experiments. The triplet of lab variables given by the beam momentum p_{beam}, the lab momentum p_{lab} and the lab angle Θ_{lab} has been used for the establishment of the following interpolation scheme. In addition and of course, the statistical and systematic errors have to be taken into account in the data comparison.

4.1 Errors

The last columns of Tables 1 and 2 contain some information about the statistical and systematic errors of the different experiments. The given numbers are to be regarded as mean values excluding some upward tails as they are inevitable at the limits of the covered phase space in particular for the statistical uncertainties. In some cases only rudimentary information about the systematic errors is available or the systematic and statistical errors are even combined into one quantity. In the latter cases these values are given in between the respective columns of Table 2.

Inspection of these approximate error levels reveals a rather broad band of uncertainties ranging from about 4% to about 20%, the latter limit being generally defined by overall normalization errors. The presence of extensive data sets well below the 10% range of both statistical and systematic errors gives however some hope that a resulting overall consistency on this level might become attainable by the extensive use of data interpolation.

The term "interpolation" is to be regarded in this context as a smooth interconnection of the data points in any of the three phase space variables defined above. This interconnection is generally done by eyeball fits which offer, within the error limits shown above, sufficient accuracy. If the distributions in Θ_{lab} and interaction energy are anyway not describable by straightforward arithmetic parametrization, the p_{lab} dependences are, as discussed in Sect. 4.4 below, in a majority of cases approximately exponential. In these cases exponential fits have been used if applicable.

As additional constraint physics asks of course for smoothness and continuity in all three variables simultaneously. Therefore the resulting overall data interpolation has to attempt a three-dimensional consistency.

If the data interpolation helps, by the inter-correlation of data points, to reduce the local statistical fluctuations, it does of course not reduce the systematic uncertainties. It is rather on the level of systematic deviations that the consistency of different experimental results is to be judged. It will become apparent from the detailed discussion described below that the majority of the quoted experiments allows for the establishment of a surprisingly consistent overall description in all three variables.

4.2 Dependence on cms energy s

As the data discussed here span an extremely wide range of cms energy from close to production threshold to the upper range of Fermilab energies, a suitable compression of the energy scale has been introduced in order to be able to present the results in a close-to-equidistant fashion against energy. The form chosen here is the variable $1/\sqrt{s}$. This choice is suggested by the considerable amount of work invested in studying the approach of hadronic cross sections to the scaling limit at high energy in the 1970's [20]. In fact the Regge parametrization suggested a smooth dependence of the cross sections as $s^{-\alpha}$, with α = 0.25–0.5 depending on the choice of trajectories involved. Such behaviour was indeed found experimentally. In the present study the cross sections turn out to have only a mild $1/\sqrt{s}$ dependence for $\sqrt{s} \gtrsim 5$ GeV, a dependence which is however different for pions and protons. This dependence is strongly modified below $\sqrt{s} \sim 2.5$ GeV due to threshold effects.

4.3 Angular dependence

A convenient and often used scale for the lab angle dependence is given by $cos(\Theta_{\text{lab}})$. This scale has the advantage of producing shapes that are again to zero order exponential. Of

course, continuity through $\Theta_{\rm lab}$ = 180 degrees imposes an approach to 180 degrees with tangent zero. As the data samples are generally not measured at common values of $\Theta_{\rm lab}$, a fixed grid of angles has been defined based on the $\Theta_{\rm lab}$ values of the HARP-CDP experiment [4] dominating the range from 25 to 112 degrees. Measured values down to 10 degrees and in the higher angular range at 137, 160, and 180 degrees have been added. Measurements not corresponding to these grid values are interpolated using the $cos(\Theta_{\rm lab})$ distributions specified below.

4.4 Lab momentum dependence

All data discussed here have been transformed into invariant cross sections (1). This facilitates the presentation in different coordinate systems and eliminates the trivial approach of the phase space element to zero with decreasing momentum. In addition, most of the invariant $p_{\rm lab}$ distributions are close to exponential within the measured $p_{\rm lab}$ range. There are notable deviations mostly at low momentum and in the lower (higher) range of lab angles for pions and protons, respectively, as well as in the approach to threshold. In these cases an eyeball fit has been used which can be reliably performed within the error margins indicated above.

At low lab momenta physics requires a deviation from the exponential shape as the invariant cross sections must approach $p_{\rm lab}$ = 0 with tangent zero. This limit appears in general at $p_{\rm lab} < 0.2$ GeV/c for pions and $p_{\rm lab} < 0.5$ GeV/c for protons. The data presented here fall practically all above these momentum limits. Only the HARP experiment [15] gives results at $p_{\rm lab}$ = 0.125 GeV/c for pions where indeed a substantial deviation from the exponential shape is visible. This is shown in Fig. 2 where the deviation from exponential fits at this $p_{\rm lab}$ is given in percent for all angles and beam momenta together with similar deviations observed in p+p interactions [21].

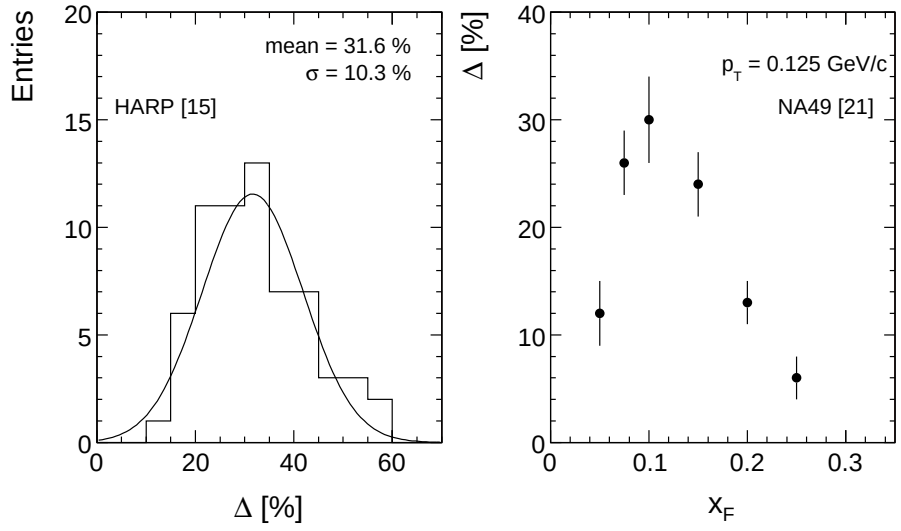

Figure 2: a) Distribution of the deviation of the data points at $p_{\rm lab}$ = 0.125 GeV/c from the exponential fits for π^+ and π^- at all angles and beam momenta, b) Deviation of π^+ cross sections at p_T = 0.125 GeV/c from exponential fits to the higher p_T region in p+p interactions as a function of x_F

A number of examples of momentum distributions for protons and pions is given in the following Figs. 3 and 5 which show the invariant cross sections as a function of $p_{\rm lab}$ and the corresponding exponential fits

$$f(p_{\rm lab}, \Theta_{\rm lab}, p_{\rm beam}) = A(\Theta_{\rm lab}, p_{\rm beam}) * exp(-p_{\rm lab}/B(\Theta_{\rm lab}, p_{\rm beam})) \quad (5)$$

which are, whenever necessary, supplemented by hand interpolations into the non-exponential regions.

A first group of distributions in the medium angular range at 45 and 97 degrees is presented in Fig. 3 for the HARP-CDP data concerning protons and pions, including exponential fits.

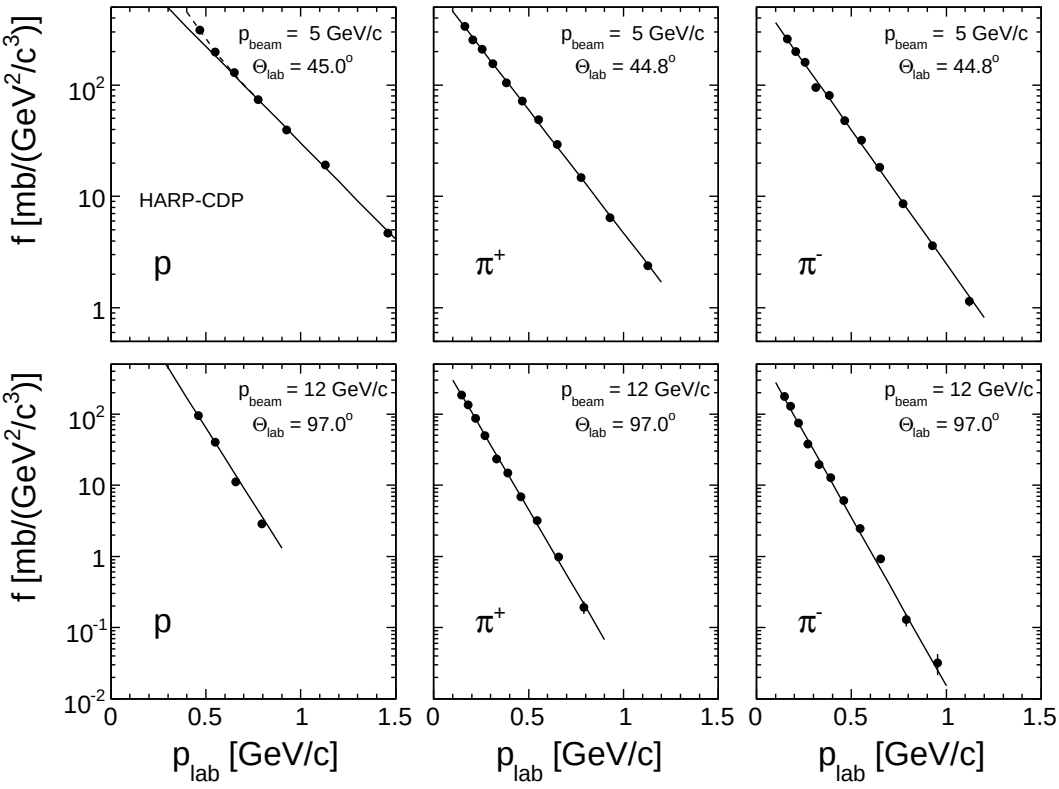

Figure 3: Invariant cross sections for protons, π^+ and π^- as a function of $p_{\rm lab}$ at $\Theta_{\rm lab}$ = 45 and 97 degrees. Full lines: exponential fits. Broken line: hand-interpolation into the non-exponential region

Evidently the exponential shape is within errors in general a good approximation to the momentum dependence. More quantitative information is contained in the normalized residual distributions of the data points,

$$r_{\rm norm} = \Delta/\sigma \quad (6)$$

where Δ is the difference between data and fit and sigma the statistical error of the given data point. Should the fit describe the physics and should systematic effects be negligible, the distribution of $r_{\rm norm}$ is expected to be Gaussian with rms equal to unity. The $r_{\rm norm}$ distributions are given for the totality of the HARP-CDP data in Fig. 4.

These distributions are well described by centred Gaussians. The resulting rms values are however somewhat bigger than one signalling systematic experimental effects or a deviation of physics from the simple exponential parametrization. In view of the statistical errors of 4% to 6% given by HARP-CDP (Tables 1 and 2) these deviations are on the level of a few percent which is below the error margin to be anyway expected from the present general data survey.

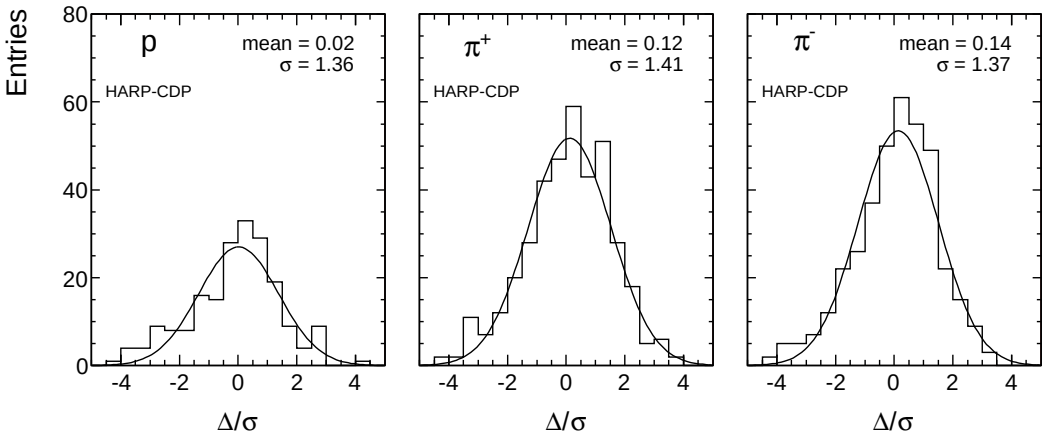

Figure 4: Normalized residual distributions for protons and pions for the complete set of beam momenta and angles of the HARP-CDP data with the exception of a few points at low angles and momenta which clearly exhibit non-exponential behaviour

Further examples of $p_{\rm lab}$ distributions from other experiments are given in Fig. 5 for a selection of particle type, beam momenta and angles.

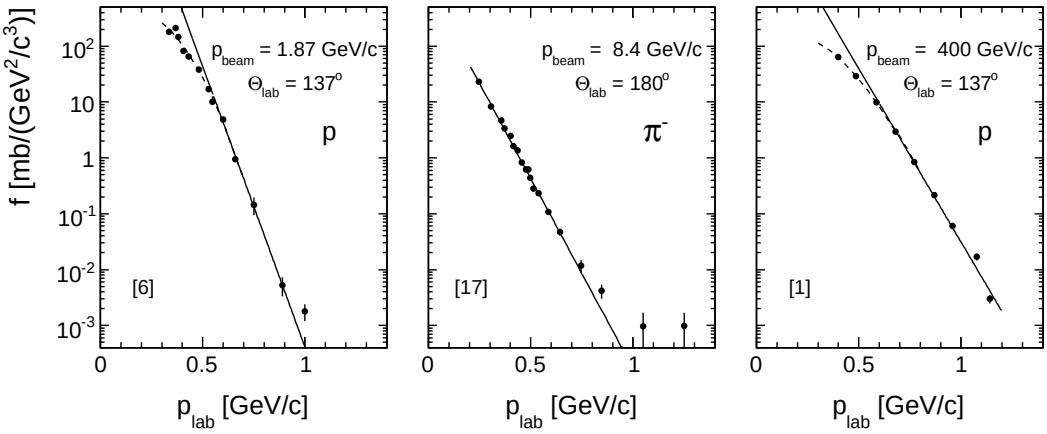

Figure 5: Several examples of invariant cross sections as a function of $p_{\rm lab}$ for a variety of particle type, lab angle and beam momenta including exponential fits (full lines) and, when necessary, eyeball fits into the non-exponential regions of $p_{\rm lab}$ (broken lines).

Again the basically exponential shape of these distributions is evident. Characterizing the exponential fits by their inverse slopes $B(\Theta_{\rm lab}, p_{\rm beam})$ a smooth and distinct dependence on lab angle and beam momentum becomes visible as shown in Fig. 6.

Compared to the strong dependence of B on $\Theta_{\rm lab}$ which ranges from 0.3 to 0.05 GeV/c, the only modest dependence on $p_{\rm beam}$ of $\sim$0.03 GeV/c for beam momenta from 3 to 158 GeV/c is noticeable.

Following the above data parametrization a generalized grid of $p_{\rm lab}$ values between 0.2 and 1.2 GeV/c, in steps of 0.1 GeV/c, may now be established. Concerning the lower and upper limits of this grid, an extrapolation beyond the limits given by the experimental values has been performed in some cases. This extrapolation does not exceed the bin width of the respective data lists and is therefore defendable in view of the generally smooth, gentle and well-defined $p_{\rm lab}$ dependences.

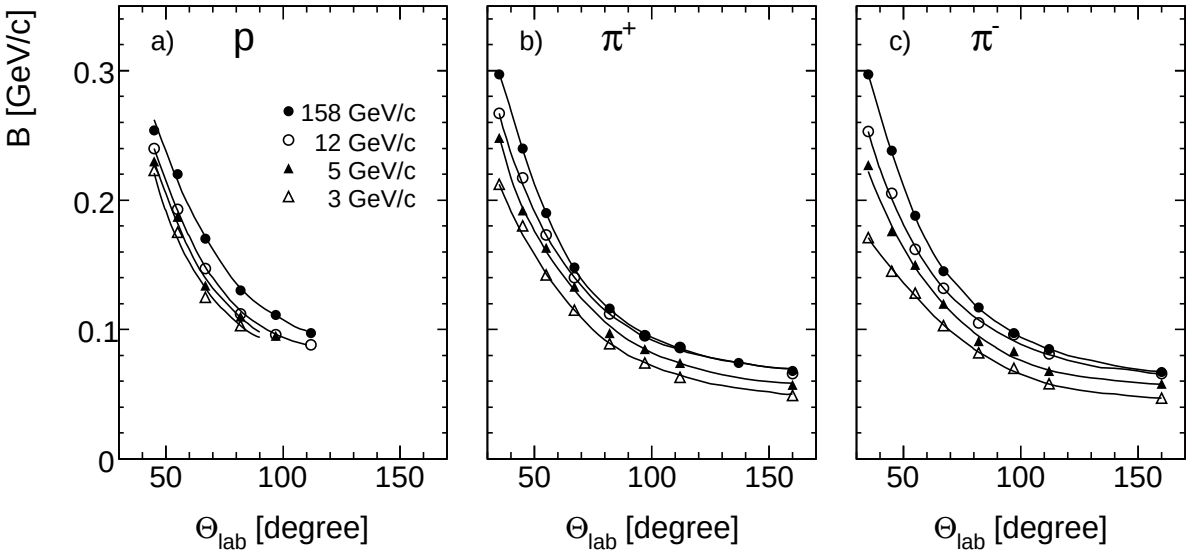

Figure 6: Inverse slopes $B(\Theta_{\rm lab}, p_{\rm beam})$ as a function of $\Theta_{\rm lab}$ for four beam momenta from 3 to 158 GeV/c, a) for protons, b) for π^+ and c) for π^-. The full lines are drawn to guide the eye

4.5 Physics constraints

In the absence of theoretical predictability in the soft sector of the strong interaction, any attempt at bringing a multitude of experimental results into a common and consistent picture has to rely on a minimal set of model-independent physics constraints. In fact a "democratic" averaging of eventually contradictory data sets would only add confusion instead of clarity.

4.5.1 Continuity

Two examples of the continuity constraint have already been mentioned above: invariant $p_{\rm lab}$ distributions have to approach zero momentum horizontally that is with tangent zero. The same is true for angular distributions in their approach to 180 degrees.

4.5.2 Smoothness

It is a matter of experimental experience in the realm of soft hadronic interactions that in general distributions in any kind of kinematic variable tend to be "smooth" in the sense of absence of abrupt local upwards or downwards variations. The widespread use of simple algebraic parametrizations has its origin in this fact, specifically in the absence of local maxima and minima, with the eventual exception of threshold behaviour of which some examples will become visible below.

4.5.3 Charge conservation and isospin symmetry

Charge conservation has of course to be fulfilled by any type of experimental result. This means for instance that for the interaction of a positively charged projectile (proton) with an isoscalar nucleus (Carbon) the π^+/π^- ratio has to be greater or equal to unity over the full phase space invoking isospin symmetry (and of course the experience from a wide range of experimental results). The presence of data with $\pi^+/\pi^- < 1$ therefore immediately indicates experimental problems. The inspection of π^+/π^- ratios has the further advantage that a large part of the systematic uncertainties, notably the overall normalization errors, cancel in this ratio.

4.5.4 Isospin rotation of secondary baryons and projectile

It has been shown that in proton induced nuclear collisions the yields of the secondary protons and neutrons are related by a constant factor of about 2 which is in turn related to the ratio of the basic nucleon-nucleon interaction [22]. Similarly, when rotating the projectile isospin from proton to neutron, it has been predicted that the yield ratio of secondary protons from proton and neutron projectiles

$$R^{\mathrm{p/n}} = \frac{f(p + C \rightarrow p')}{f(n + C \rightarrow p)} \tag{7}$$

should be constant and equal to 2.5 for light nuclei [23]. The extensive and precise low-energy data set of Franz et al. [10] from n+C interactions has therefore been included in the present survey. These data present a welcome extension of the $1/\sqrt{s}$ scale into the region 0.47 to 0.49 which is not covered for most of the angular range with proton projectiles. As shown below, these data fit indeed very well, after re-normalization, into the general $1/\sqrt{s}$ dependence of secondary protons where the low energy data by Frankel et al. [8] and Komarov et al. [9] at angles between 112 and 180 degrees provide an independent control of the normalization.

4.5.5 Establishing a consistent set of data

With these constraints in mind, and having established the parametrization and interpolation of the p_{lab} distributions as discussed above, one may now proceed to the attempt at sorting the 19 available experiments into a consistent global data set. It would of course be rather surprising if all experiments would fit into this global picture within their respective error limits. In fact it turns out that this procedure establishes a very strong constraint for possible deviations, as a large majority of results is creating a perfectly consistent picture both for protons and for pions. Only four of the 19 data sets cannot be brought into consistency with all other experiments without gravely affecting and contradicting the above constraints. These data are not included in the following global interpolation scheme. They will be discussed separately in Sect. 9 below.

5 The proton data

5.1 $1/\sqrt{s}$ dependence

The invariant proton cross sections are shown in Fig. 7 as a function of $1/\sqrt{s}$ for a grid of ten lab angles between 25 and 180 degrees and constant lab momenta between 0.3 and 1.2 GeV/c. The interpolated data points in each panel are identified by symbols corresponding to the different experiments.

The solid lines are eyeball interpolations through the data points. A first remark concerning this Figure concerns the smoothness and continuity of the $1/\sqrt{s}$ dependences. The achieved overall consistency of all data is rather impressive even if single points are deviating in some areas of phase space. The salient features of the physics contained in these plots may be summarized as follows:

- a strong yield suppression between $1/\sqrt{s} \sim 0.45$ and the elastic limit at $1/\sqrt{s} = 0.53$ is evident
- the n+C data [10] are well consistent with the p+C results in the overlap regions; they define a broad maximum of the cross sections at $1/\sqrt{s} \sim 0.46$ at medium angles and low p_{lab}

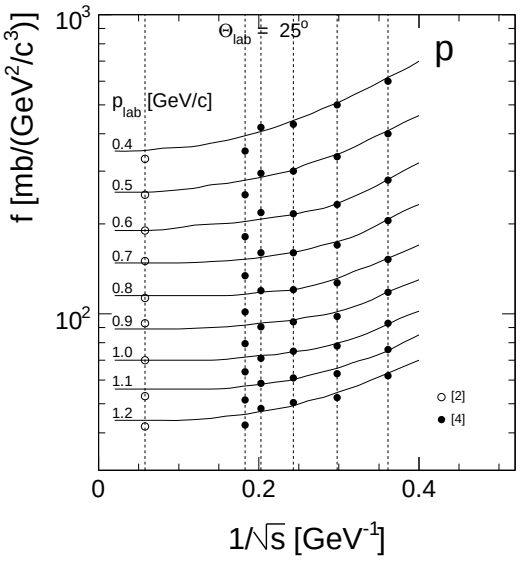
Θ_{lab} = 25°
p
p_{lab} [GeV/c]
0.4
0.5
0.6
0.7
0.8
0.9
1.0
1.1
1.2
○ [2]
● [4]
f [mb/(GeV²/c³)]
1/√s [GeV⁻¹]

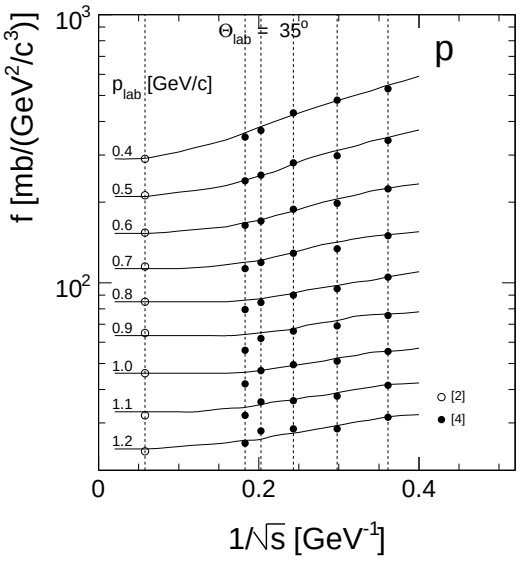
Θ_{lab} = 35°
p
p_{lab} [GeV/c]
0.4
0.5
0.6
0.7
0.8
0.9
1.0
1.1
1.2
○ [2]
● [4]
f [mb/(GeV²/c³)]
1/√s [GeV⁻¹]

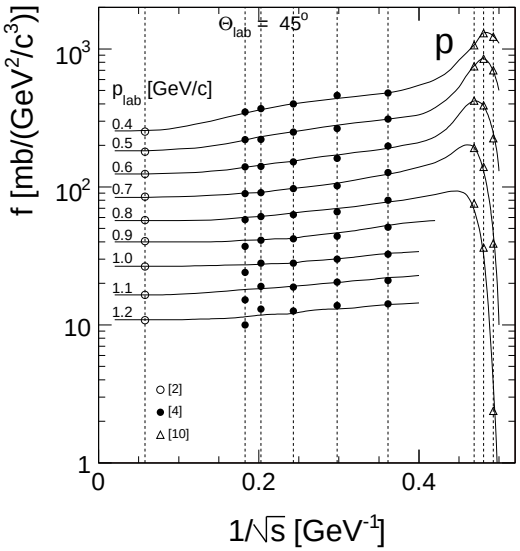
Θ_{lab} = 45°
p
p_{lab} [GeV/c]
0.4
0.5
0.6
0.7
0.8
0.9
1.0
1.1
1.2
○ [2]
● [4]
△ [10]
f [mb/(GeV²/c³)]
1/√s [GeV⁻¹]

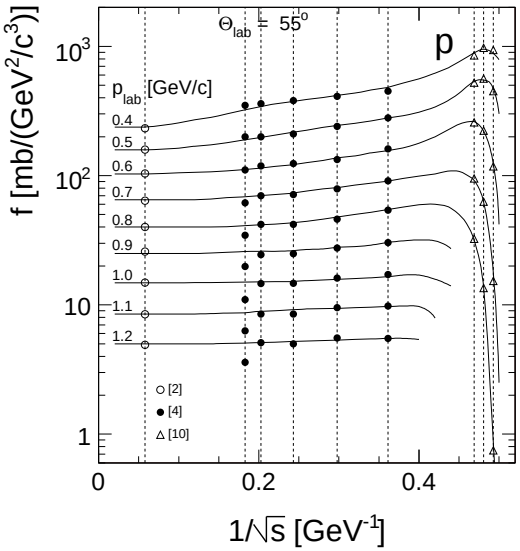
Θ_{lab} = 55°
p
p_{lab} [GeV/c]
0.4
0.5
0.6
0.7
0.8
0.9
1.0
1.1
1.2
○ [2]
● [4]
△ [10]
f [mb/(GeV²/c³)]
1/√s [GeV⁻¹]

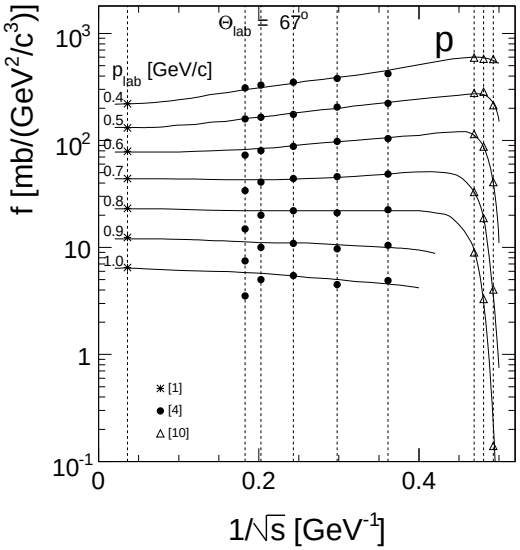
Θ_{lab} = 67°
p
p_{lab} [GeV/c]
0.4
0.5
0.6
0.7
0.8
0.9
1.0
✳ [1]
● [4]
△ [10]
f [mb/(GeV²/c³)]
1/√s [GeV⁻¹]

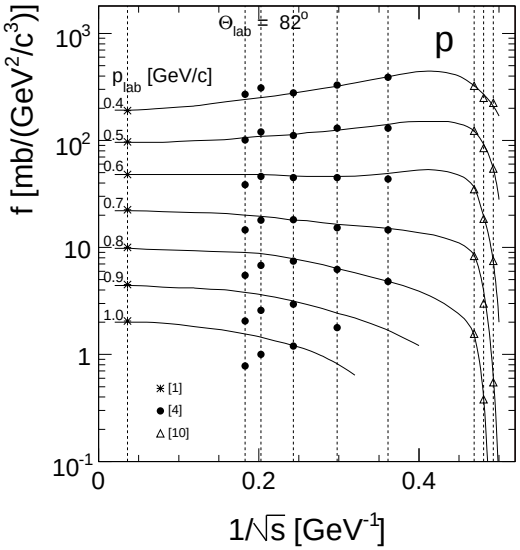
Θ_{lab} = 82°
p
p_{lab} [GeV/c]
0.4
0.5
0.6
0.7
0.8
0.9
1.0
✳ [1]
● [4]
△ [10]
f [mb/(GeV²/c³)]
1/√s [GeV⁻¹]

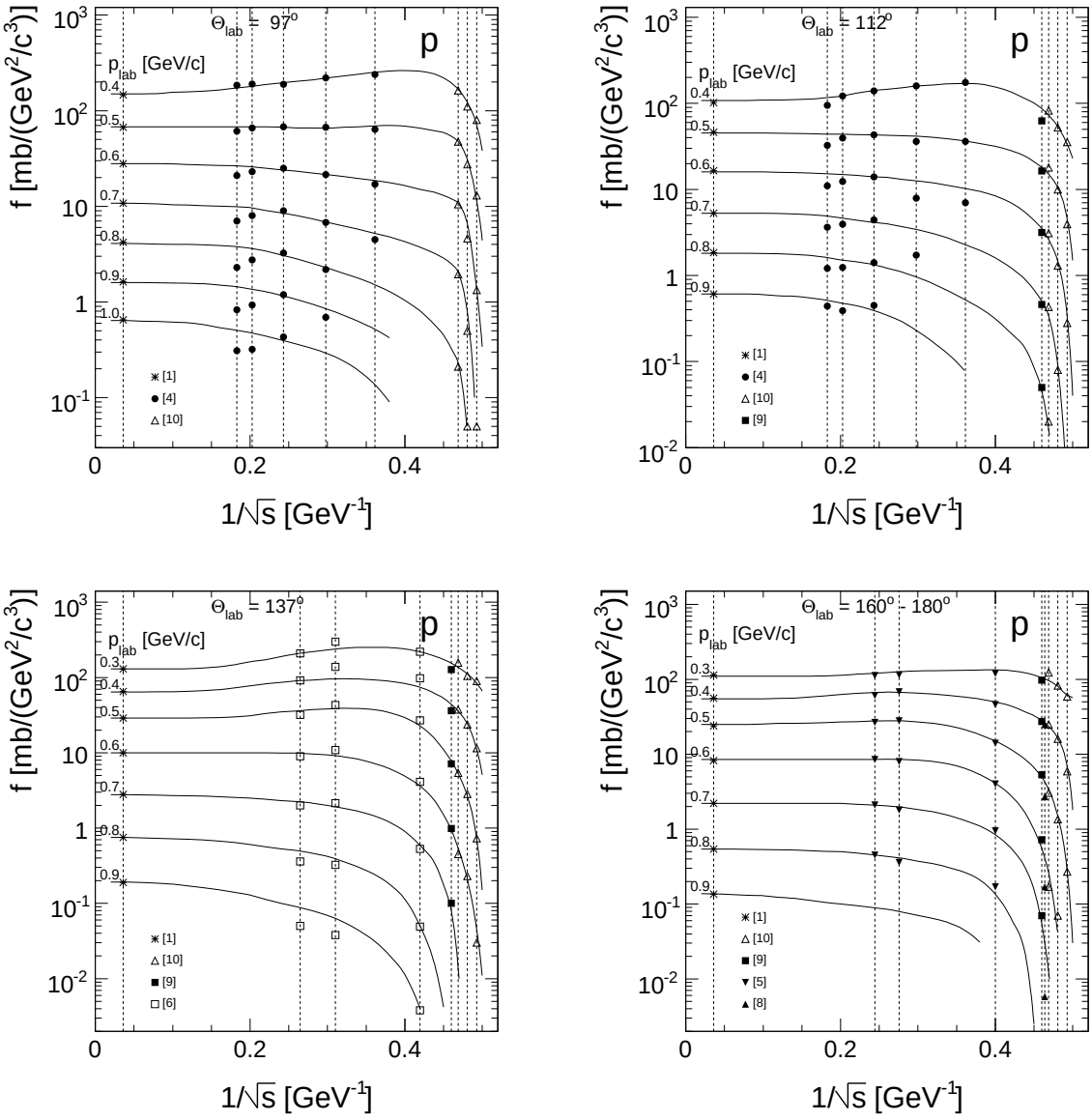

Figure 7: Invariant cross sections for protons in p+C collisions as a function of $1/\sqrt{s}$ at fixed p_{lab} and Θ_{lab}. The interpolated data points are indicated by symbols corresponding to the respective experiments in each panel. The solid lines represent the interpolation of the data

- there is a well-defined asymptotic behaviour of the cross sections for $1/\sqrt{s}$ below about 0.2 or beam momenta above about 12 GeV/c
- for the lower Θ_{lab} region and/or low p_{lab} the asymptotic region is approached from above

The latter point is reminiscent of the behaviour of the proton yields in p+p interactions, as shown in Fig. 8.

Another feature of Fig. 7 is the systematic droop of the cross sections from HARP-CDP at their highest beam momentum of 15 GeV/c or $1/\sqrt{s}$ = 0.18, demonstrating the discriminative power of the approach. This decrease is quantified in Fig. 9 where the ratio R^H between the measured invariant cross sections and the data interpolation is shown as a function of p_{lab} for the complete angular range from 25 to 97 degrees. Here deviations of up to 50% are visible.

The abruptness of this decrease would necessitate a rather violent variation of the cross sections with increasing energy including a minimum between PS and SPS energies. A final

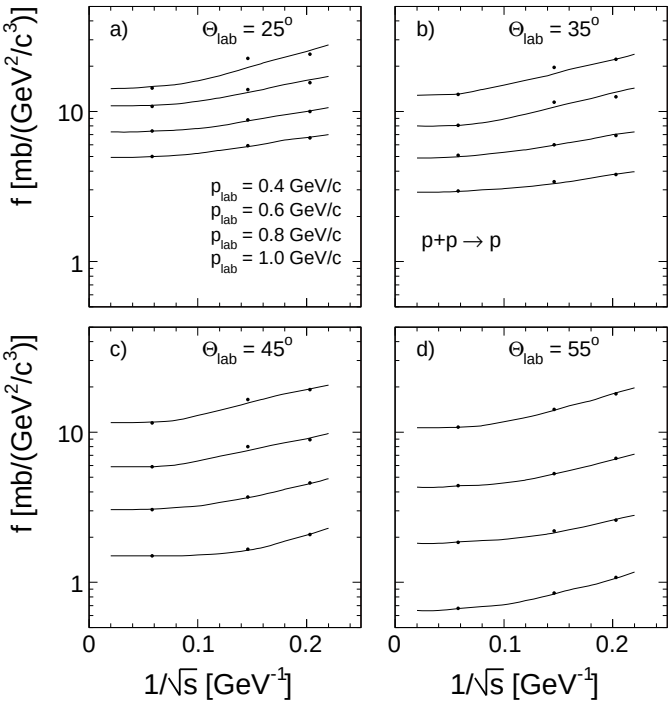

Figure 8: Invariant proton cross sections as a function of $1/\sqrt{s}$ for p+p interactions at the four lab angles a) 25, b) 35, c) 45 and d) 55 degrees for p_{lab} values from 0.4 to 1 GeV/c. The data are interpolated from Blobel [24] and NA49 [25]. The lines are drawn to guide the eye

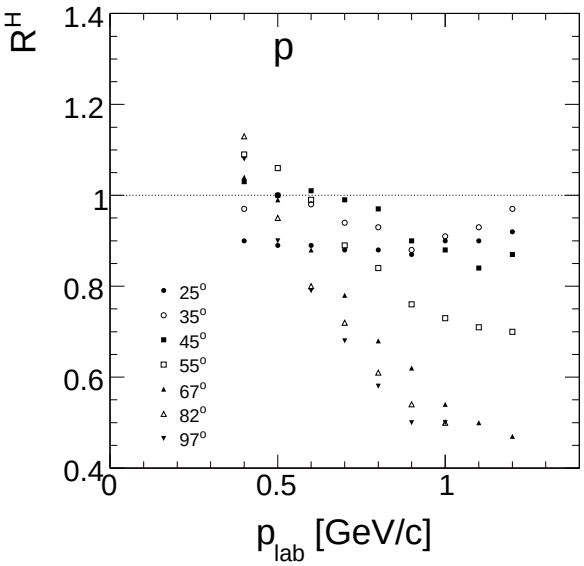

Figure 9: Ratio R^H between the interpolated invariant proton cross sections from HARP-CDP [4] and the global interpolation as a function of p_{lab} for the angular range $25 < \Theta_{\text{lab}} < 97$ degrees

clarification of this situation is given by the proton data from Serpukhov [3] which, although suffering from a different and independent problem, at least exclude such variations in the region between 17 and 67 GeV/c beam momentum, see Sect. 9.2 below.

5.2 $\cos(\theta_{\mathbf{lab}})$ dependence

In addition to the description of the energy dependence, the global interpolation has of course also to result in a smooth and continuous verification of the angular dependence presenting the third dimension of the present study. This constraint has to be fulfilled at any value of $1/\sqrt{s}$.

In a first example the situation at $1/\sqrt{s}$ = 0.05 is shown in Fig. 10. This value lies in between the Fermilab [1] and NA49 [2] data in the region of negligible s-dependence. It therefore allows for the direct comparison of the two experiments in their respective angular regions which have no overlap.

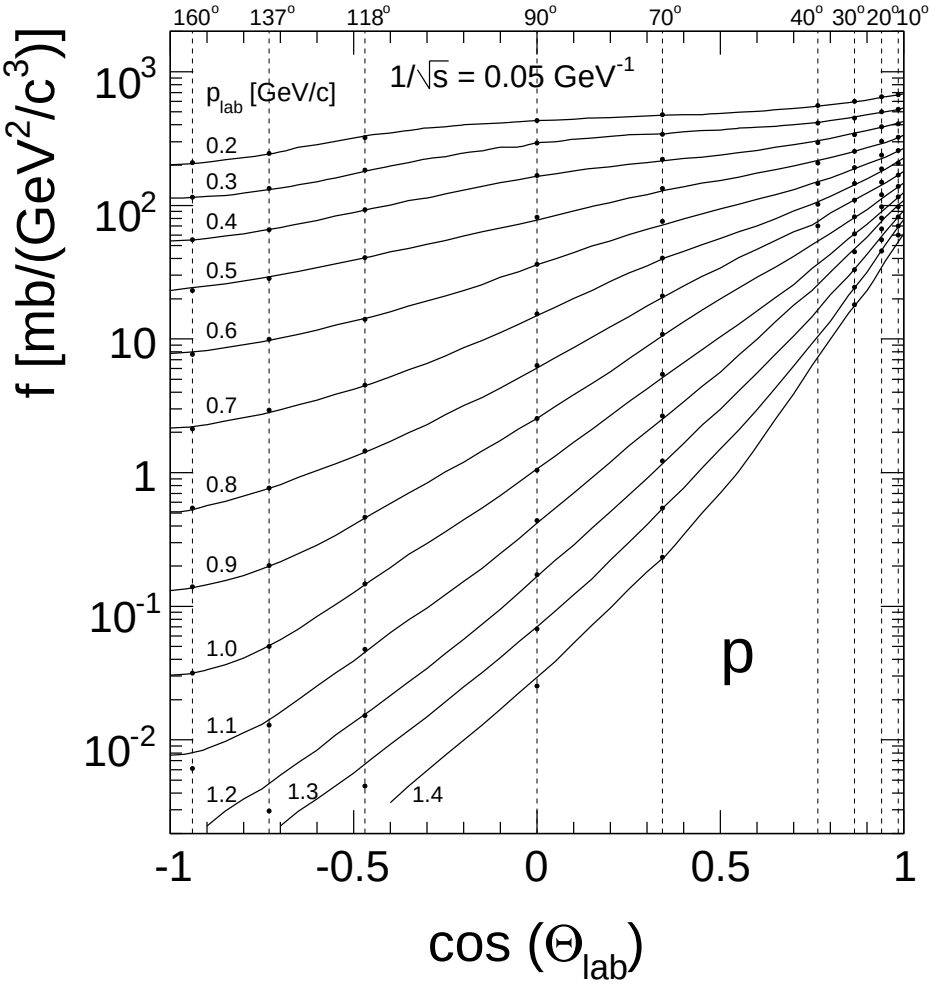

Figure 10: Invariant proton cross sections at $1/\sqrt{s}$ = 0.05 as a function of $\cos(\theta_{\rm lab})$ combining the Fermilab and NA49 data for $p_{\rm lab}$ between 0.2 and 1.4 GeV/c. The global interpolation is shown as full lines. The measured cross sections in the angular ranges from 70 to 160 degrees [1] and from 10 to 40 degrees [2] are given on the vertical broken lines

Several observations are in place here:

– the two experimental results connect perfectly through the gap between the NA49 ($\theta_{\rm lab} < 40$ degrees) and the Fermilab ($\theta_{\rm lab} > 70$ degrees) data
– there is at most a few percent variation of the cross sections between the angles of 160 and 180 degrees taking into account the constraint of continuity through 180 degrees

discussed in Sect. 4 above. This allows the combination of results in this angular region as it is applied in the determination of the $1/\sqrt{s}$ dependence, Fig. 7

– the angular distributions are smooth and close to exponential in shape. In particular, no instability in the region around 90 degrees is visible where an eventual diffractive peak from target fragmentation would appear, see also [2]

Further angular distributions at four $1/\sqrt{s}$ values between 0.1 and 0.4 GeV^{-1} are given in Fig. 11. In fact such distributions at arbitrary values of $1/\sqrt{s}$ may be obtained from the global interpolation as it is presented in numerical form at the NA49 web page [26].

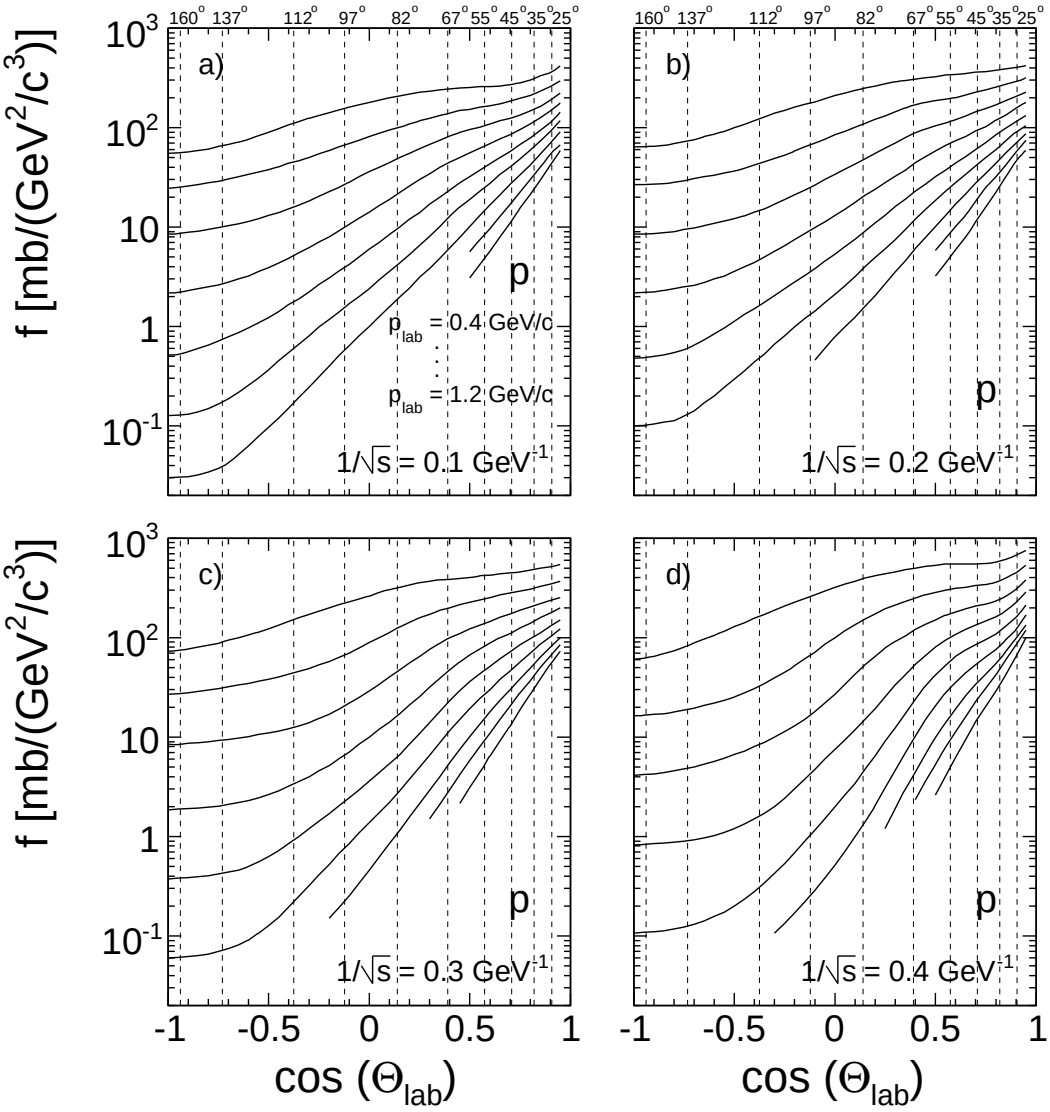

Figure 11: Invariant proton cross sections as a function of $\cos(\theta_{\text{lab}})$ for four values of $1/\sqrt{s}$: a) 0.1, b) 0.2, c) 0.3, d) 0.4 GeV^{-1} and for p_{lab} values between 0.4 and 1.2 GeV/c. The standard grid of 10 angles, Fig. 7, is indicated by the vertical broken lines

Evidently the angular distributions maintain their smooth and continuous shape, specifically through 90 degrees, at all interaction energies. With the approach to low beam momenta however, a progressive rounding of the shape towards higher lab angles manifests itself.

6 The data for positive pions

The global interpolation of the π^+ data is presented in this section in close analogy to the preceding section for protons.

6.1 $1/\sqrt{s}$ dependence

The invariant π^+ cross sections are shown in Fig. 12 as a function of $1/\sqrt{s}$ for the standard grid of ten lab angles between 25 and 180 degrees and for constant lab momenta between 0.2 and 1.2 GeV/c. The interpolated data points in each panel are identified by symbols corresponding to the different experiments.

The solid lines represent the global interpolation by eyeball fits of both the energy and the angular dependences. Again the $1/\sqrt{s}$ dependence is in general smooth and continuous, with an impressive overall consistency of all data with only few exceptions discussed below. There are some general trends to be pointed out:

- at the lowest lab momentum, the pion cross sections are practically s-independent, with variations of only 10–20% in the range from 1 to 400 GeV/c beam momentum
- this fact suggests π^+ production at low momentum transfer in the nuclear cascade
- for all lab momenta, the approach to high energies is very flat for $1/\sqrt{s} < 0.2$ or beam

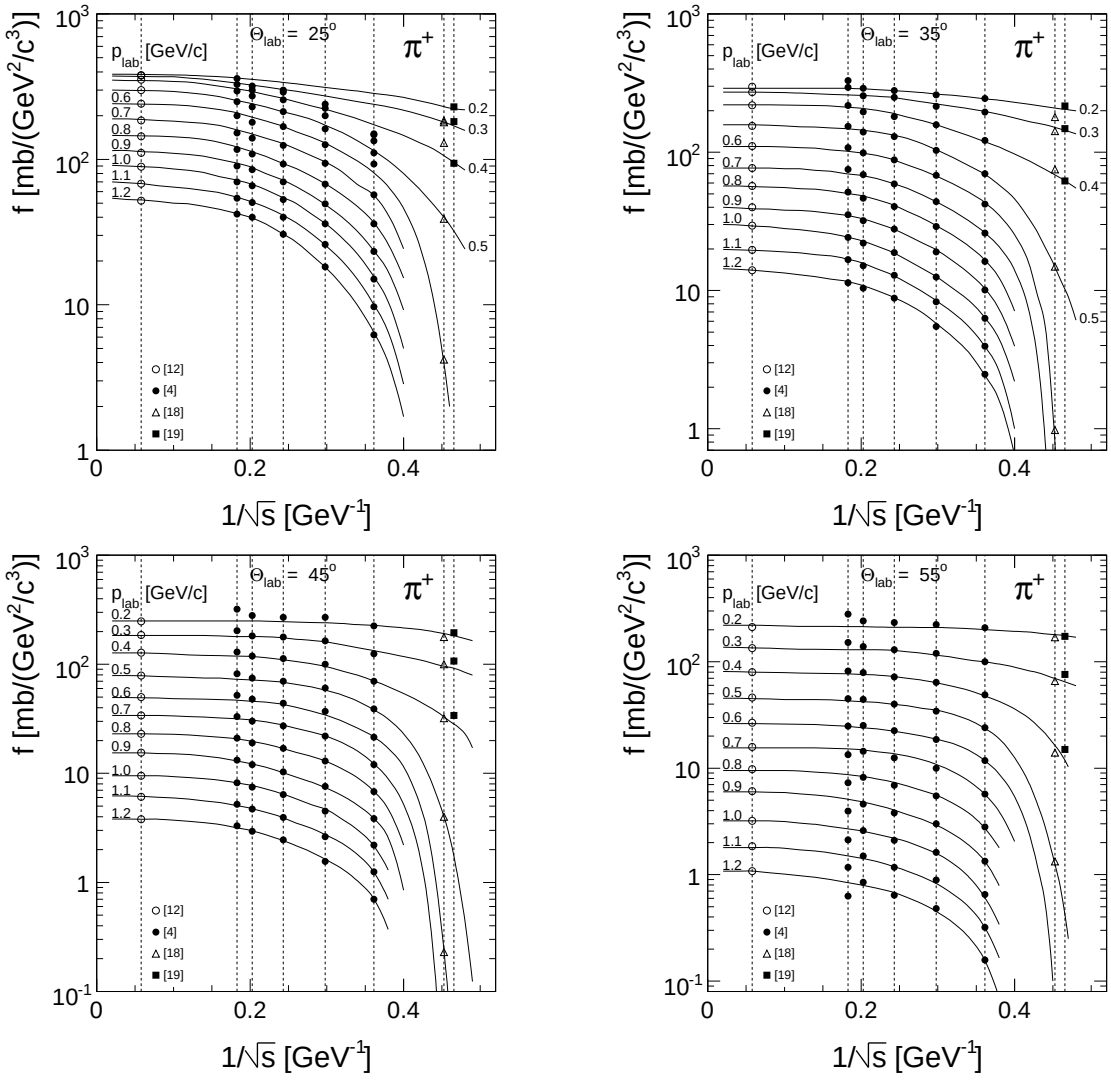

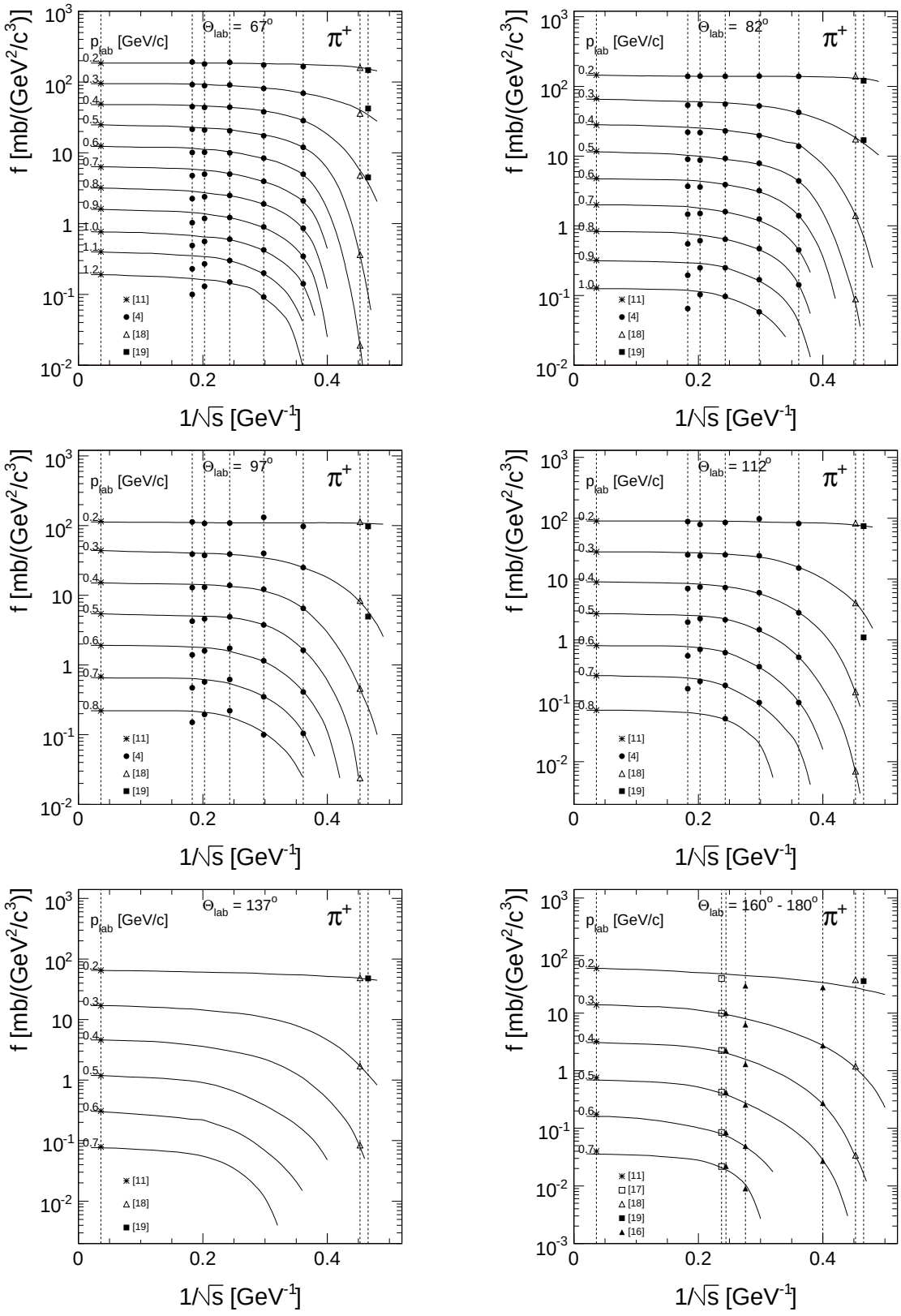

Figure 12: Invariant cross sections for π^+ in p+C collisions as a function of $1/\sqrt{s}$ at fixed $p_{\rm lab}$ and $\theta_{\rm lab}$. The interpolated data points are indicated by symbols corresponding to the respective experiments in each panel. The solid lines represent the global data interpolation

momenta above 12 GeV/c.

– the high energy cross sections are approached for all angles and beam momenta from below

There are two areas of deviation from the global interpolation which are both connected to the HARP-CDP data [4]. At their lowest angle of 25 degrees, the cross sections are systematically low by up to a factor of two below $p_{\rm lab} \sim 0.5$ GeV/c and $1/\sqrt{s}$ above 0.2. This is in contradiction to the available low energy data from other experiments also shown in Fig. 12. The second area concerns, as for the protons, the data at 15 GeV/c beam momentum where a characteristic pattern of deviations is visible: At low angles and low $p_{\rm lab}$, the data tend to overshoot the interpolation, whereas at angles above 45 degrees a progressive droop with increasing lab momentum is evident. This is quantified by the ratio R^H between the HARP-CDP data and the global interpolation shown in Fig. 13.

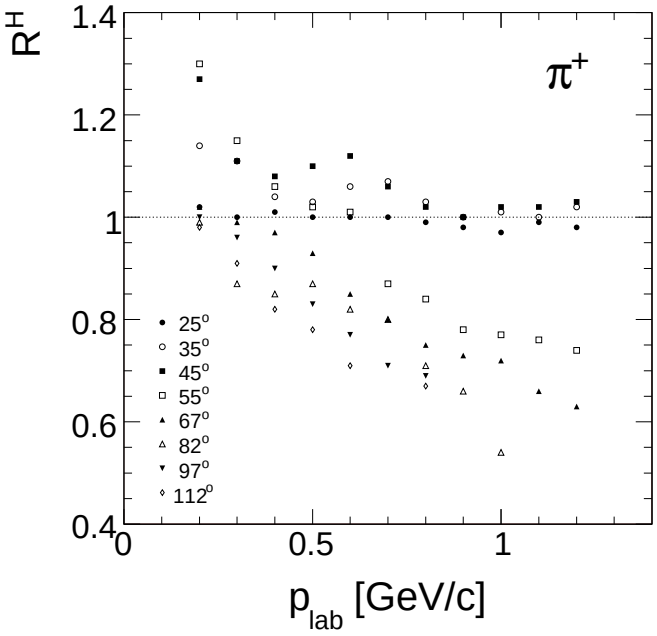

Figure 13: Ratio R^H between the interpolated invariant π^+ cross sections from HARP-CDP [4] and the global interpolation as a function of $p_{\rm lab}$ for the angular range $25 < \theta_{\rm lab} < 112$ degrees

These deviations are rather consistent with the ones found for protons. Also in this case a rapid variation of the cross sections with increasing beam momentum can be excluded by the comparison with the pion data from the Serpukhov experiment [13] between 17 and 67 GeV/c beam momentum, see Sect. 9.2 below.

6.2 $\cos(\theta_{\rm lab})$ dependence

As already shown in Sect. 5.2 for protons, the angular distributions at $1/\sqrt{s}$ = 0.05, in between the Fermilab [11] and NA49 [12] energies, are presented in Fig. 14. This allows the comparison of the two data sets and their connection across the gap in lab angles between 40 and 70 degrees which represent the upper and lower limit of the respective experiment.

Further angular distributions at four $1/\sqrt{s}$ values between 0.1 and 0.4 GeV^{-1} are given in Fig. 15.

The angular distributions are characterized by a smooth, close to exponential shape. At backward angles, the $p_{\rm lab}$ dependence is very steep with four orders of magnitude already be-

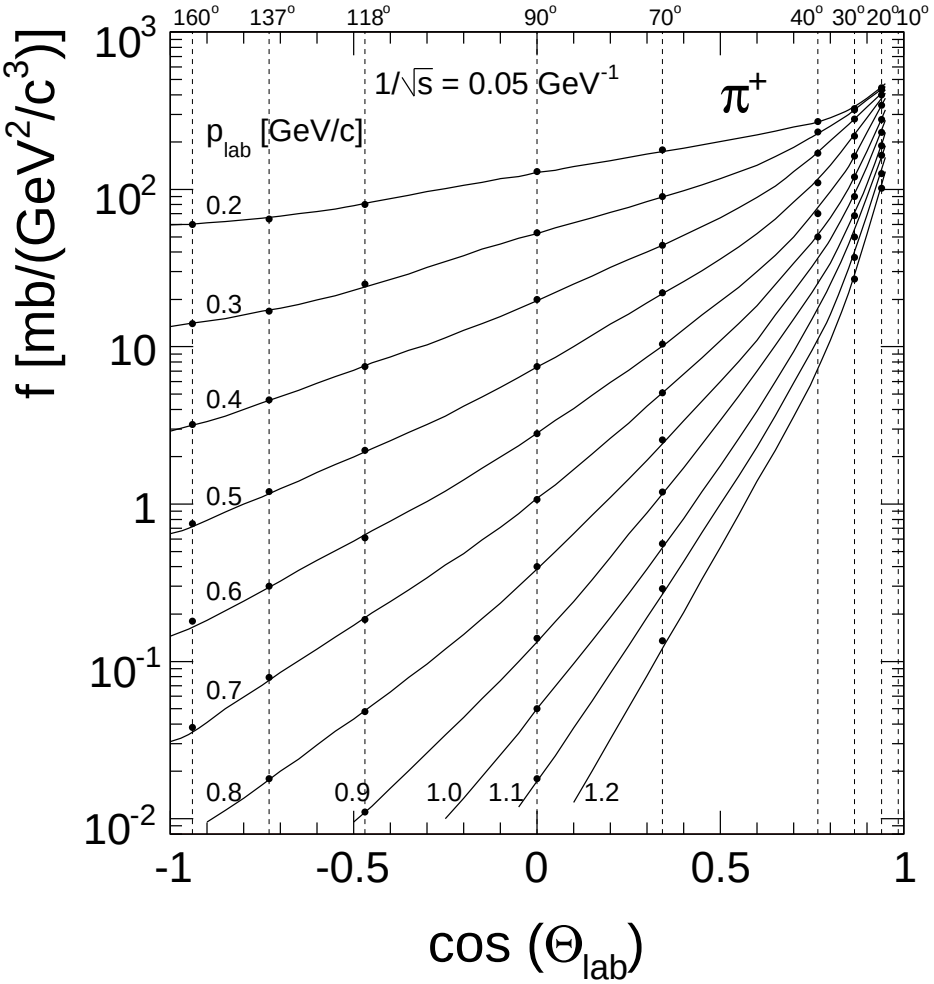

Figure 14: Invariant π^+ cross sections at $1/\sqrt{s}$ = 0.05 as a function of $\cos(\theta_{\rm lab})$ combining the Fermilab [11] and NA49 [12] data for $p_{\rm lab}$ between 0.2 and 1.2 GeV/c. The global interpolation is shown as full lines. The measured cross sections in the angular ranges from 70 to 160 degrees ([11]) and from 10 to 40 degrees ([12]) are given on the vertical broken lines

tween $p_{\rm lab}$ = 0.2 and 0.8 GeV/c. In forward direction this dependence is much reduced with less than one order of magnitude between $p_{\rm lab}$ = 0.2 and 1.2 GeV/c. This is due to the prevailance of target fragmentation in this region, see Sect. 10 for a quantitative study of this phenomenology.

7 The data for negative pions

This section follows closely the discussion of the π^+ cross sections in the preceding section.

7.1 $1/\sqrt{\rm s}$ dependence

The invariant π^- cross sections are shown in Fig. 16 as a function of $1/\sqrt{s}$ for the standard grid of ten lab angles between 25 and 180 degrees and for constant lab momenta between 0.2 and 1.2 GeV/c. The interpolated data points in each panel are identified by symbols corresponding to the different experiments.

The solid lines represent the global interpolation by eyeball fits to the data, with several features which are worth noticing:

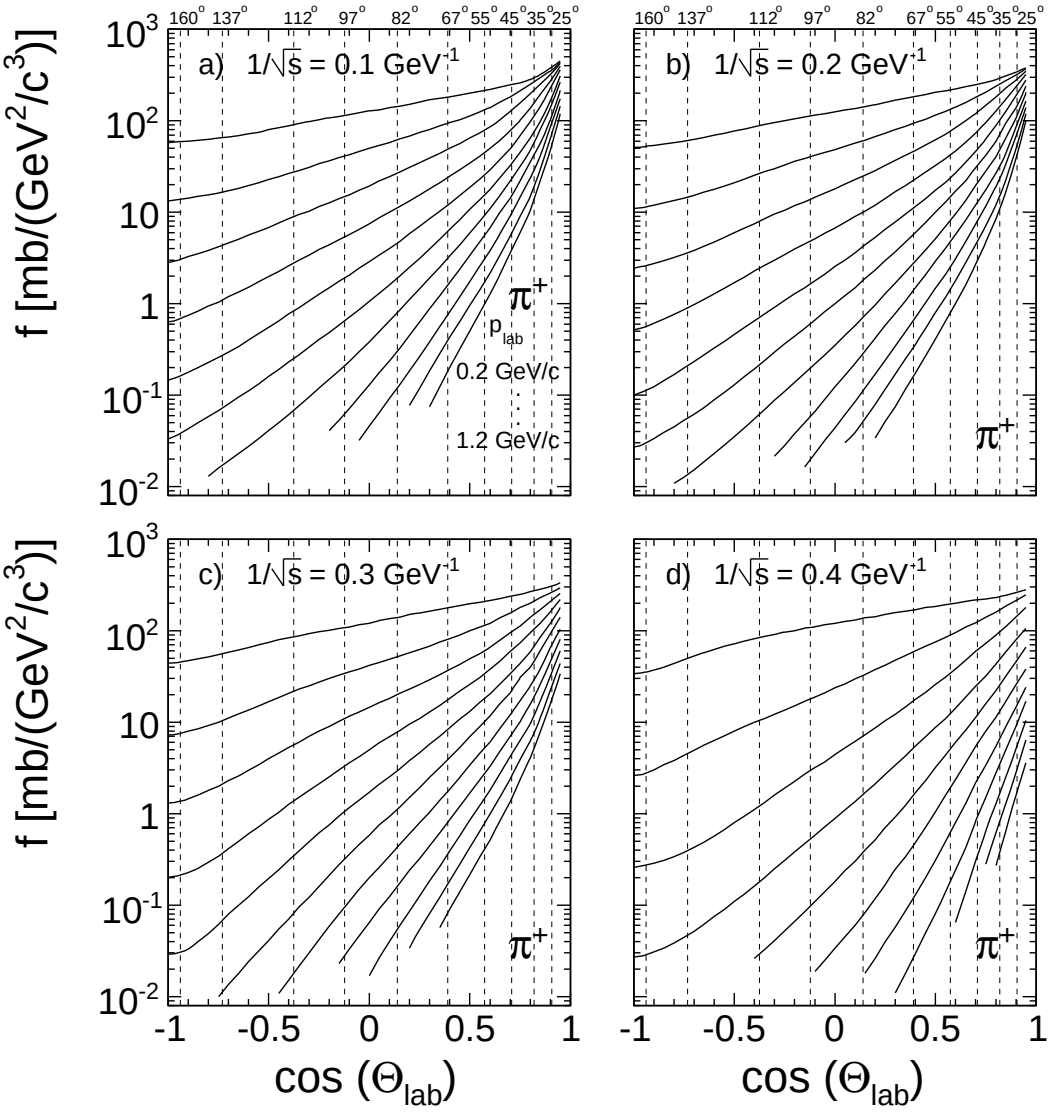

Figure 15: Invariant π^+ cross sections as a function of $\cos(\theta_{\rm lab})$ for four values of $1/\sqrt{s}$: a) 0.1, b) 0.2, c) 0.3, d) 0.4 GeV^{-1} and for $p_{\rm lab}$ values between 0.2 and 1.2 GeV/c. The standard grid of 10 angles, Fig. 7, is indicated by the vertical broken lines

- all the different data sets form a consistent ensemble without the systematic deviations visible in some regions of the proton and π^+ results
- the approach to large beam momenta happens from below for all $p_{\rm lab}$
- the s-dependence is in general stronger than for π^+, Fig. 12. If it is again flat up to $1/\sqrt{s} \sim 0.2$ at low $p_{\rm lab}$, it becomes more pronounced both towards higher $p_{\rm lab}$ and in the approach to the production threshold at large $1/\sqrt{s}$ indicating a marked increase of the π^+/π^- ratio
- this effect has as physics origin the progressive change of the production mechanism from pion exchange at low energy to gluon or Pomeron exchange at SPS energy. This will be discussed in relation to the charge ratios in Sect. 8.

It is again interesting to compare the energy dependence to the one observed in p+p interactions as presented in Fig. 17.

Although for both reactions the asymptotic high energy region is approached from below,

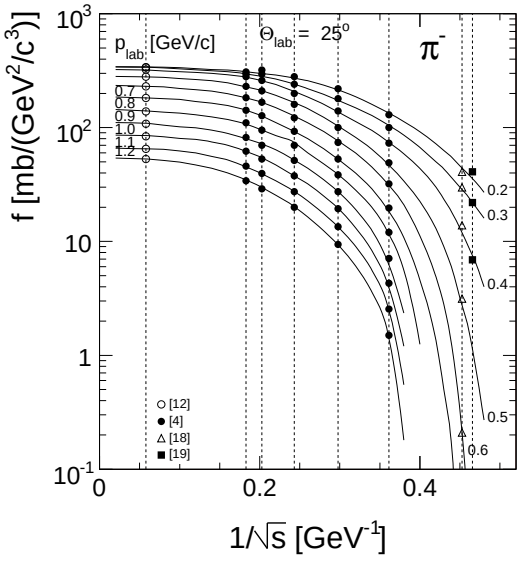
p_{lab} [GeV/c]
Θ_{lab} = 25°
π^-
f [mb/(GeV^2/c^3)]
1/√s [GeV^{-1}]
[12]
[4]
[18]
[19]

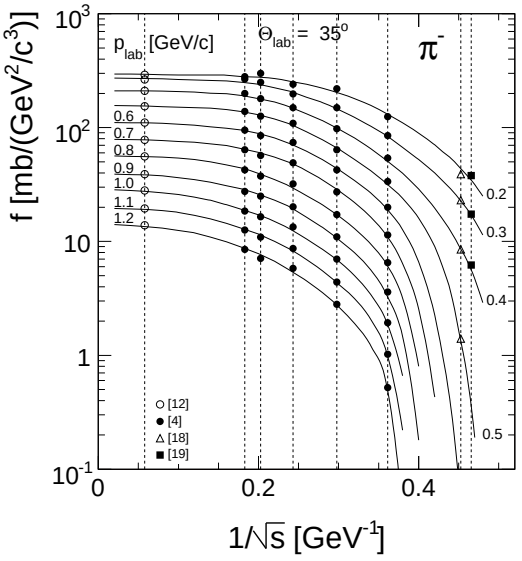
p_{lab} [GeV/c]
Θ_{lab} = 35°
π^-
f [mb/(GeV^2/c^3)]
1/√s [GeV^{-1}]
[12]
[4]
[18]
[19]

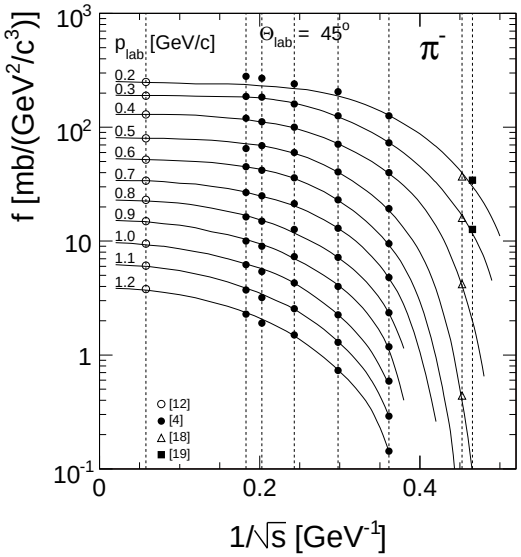
p_{lab} [GeV/c]
Θ_{lab} = 45°
π^-
f [mb/(GeV^2/c^3)]
1/√s [GeV^{-1}]
[12]
[4]
[18]
[19]

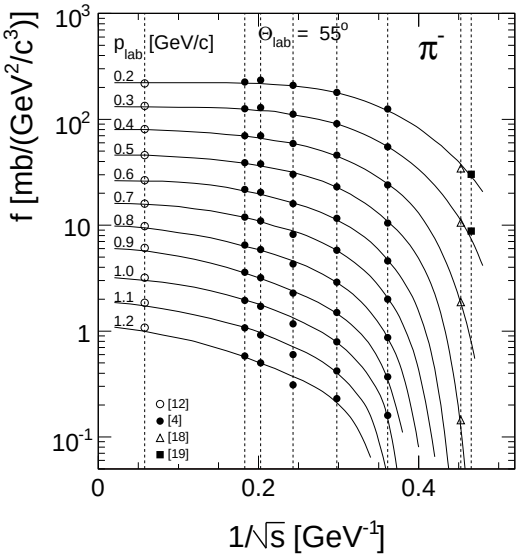
p_{lab} [GeV/c]
Θ_{lab} = 55°
π^-
f [mb/(GeV^2/c^3)]
1/√s [GeV^{-1}]
[12]
[4]
[18]
[19]

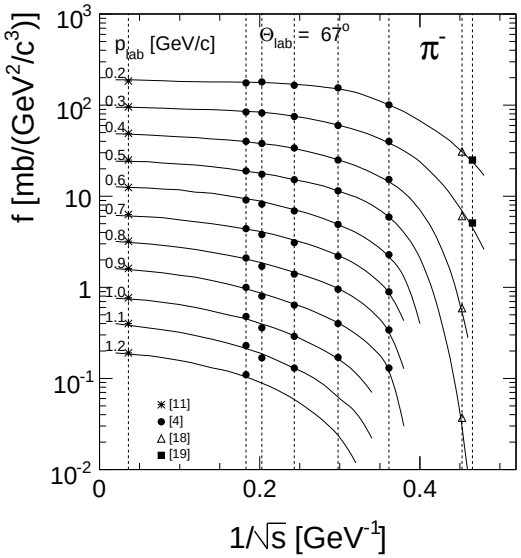
p_{lab} [GeV/c]
Θ_{lab} = 67°
π^-
f [mb/(GeV^2/c^3)]
1/√s [GeV^{-1}]
[11]
[4]
[18]
[19]

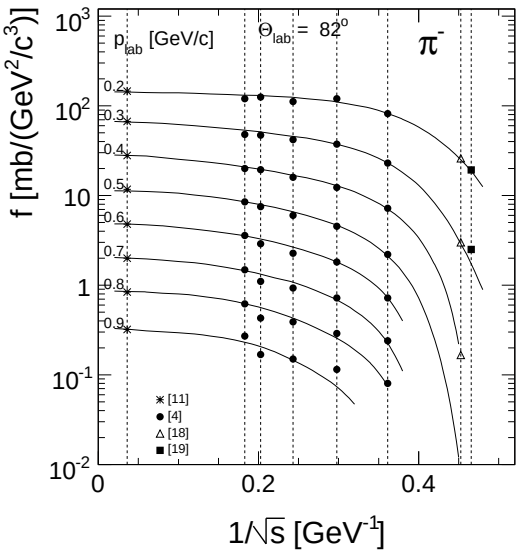
p_{lab} [GeV/c]
Θ_{lab} = 82°
π^-
f [mb/(GeV^2/c^3)]
1/√s [GeV^{-1}]
[11]
[4]
[18]
[19]

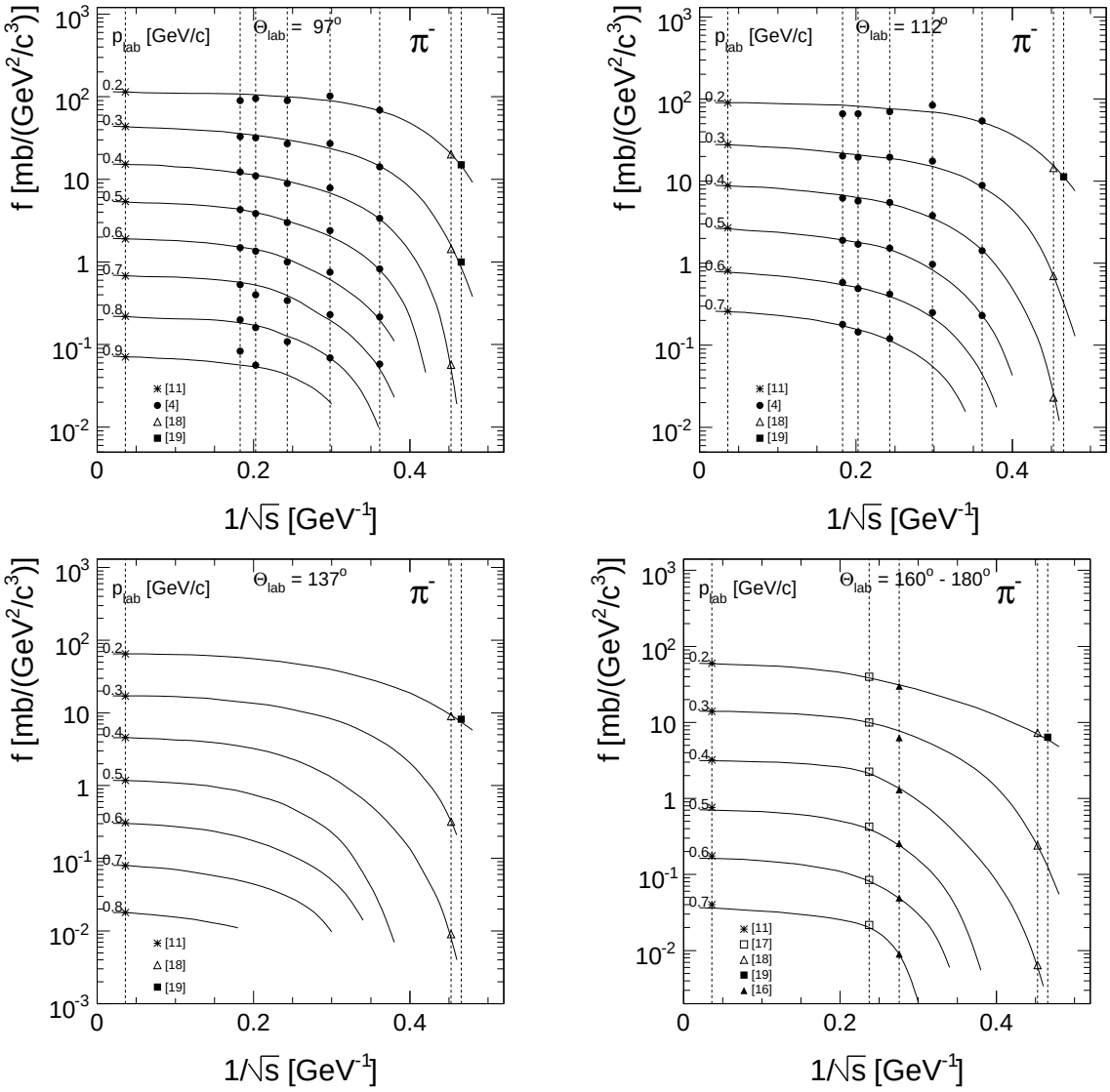

Figure 16: Invariant cross sections for π^- in p+C collisions as a function of $1/\sqrt{s}$ at fixed $p_{\rm lab}$ and $\theta_{\rm lab}$. The interpolated data points are indicated by symbols corresponding to the respective experiments in each panel. The solid lines represent the global data interpolation

this comparison shows a stronger s-dependence, at the same lab angle, in p+C than in p+p collisions. This is due to the component of nuclear cascading which contributes, in the given angular range, with equal strength than the target fragmentation to the total yield (see Sect. 10 below).

7.2 $\cos(\theta_{\rm lab})$ dependence

As for protons and π^+ in Figs. 10 and 14, the π^- cross sections from the Fermilab [11] and NA49 [12] experiments are compared and combined as a function of $\cos(\theta_{\rm lab})$ in Fig. 18.

Further angular distributions at four $1/\sqrt{s}$ values between 0.1 and 0.4 GeV^{-1} are given in Fig. 19.

Concerning smoothness and continuity these distributions are similar to the π^+ data, including the large asymmetry between the forward and backward directions. The reduction of the cross sections for π^- with respect to π^+ with increasing $1/\sqrt{s}$ is however very apparent.

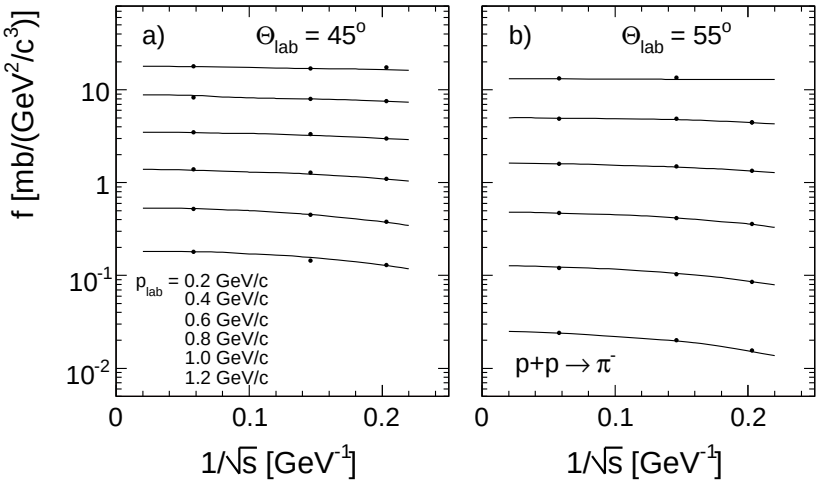

Figure 17: Invariant π^- cross sections as a function of $1/\sqrt{s}$ for p+p interactions at the two lab angles a) 45, and b) 55 degrees for p_{lab} values from 0.2 to 1.2 GeV/c. The data are interpolated from Blobel [27] and NA49 [21]. The lines are drawn to guide the eye

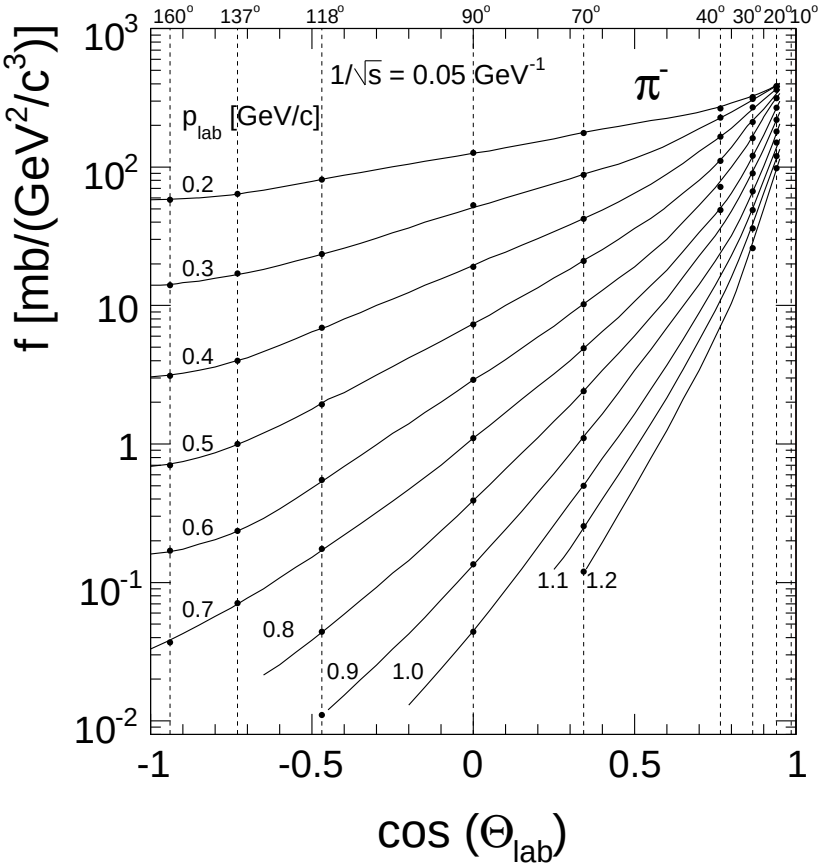

Figure 18: Invariant π^- cross sections at $1/\sqrt{s}$= 0.05 as a function of $\cos(\theta_{\text{lab}})$ combining the Fermilab [11] and NA49 [12] data for p_{lab} between 0.2 and 1.2 GeV/c. The global interpolation is shown as full lines. The measured cross sections in the angular ranges from 70 to 160 degrees ([11]) and from 10 to 40 degrees ([12]) are given on the vertical broken lines

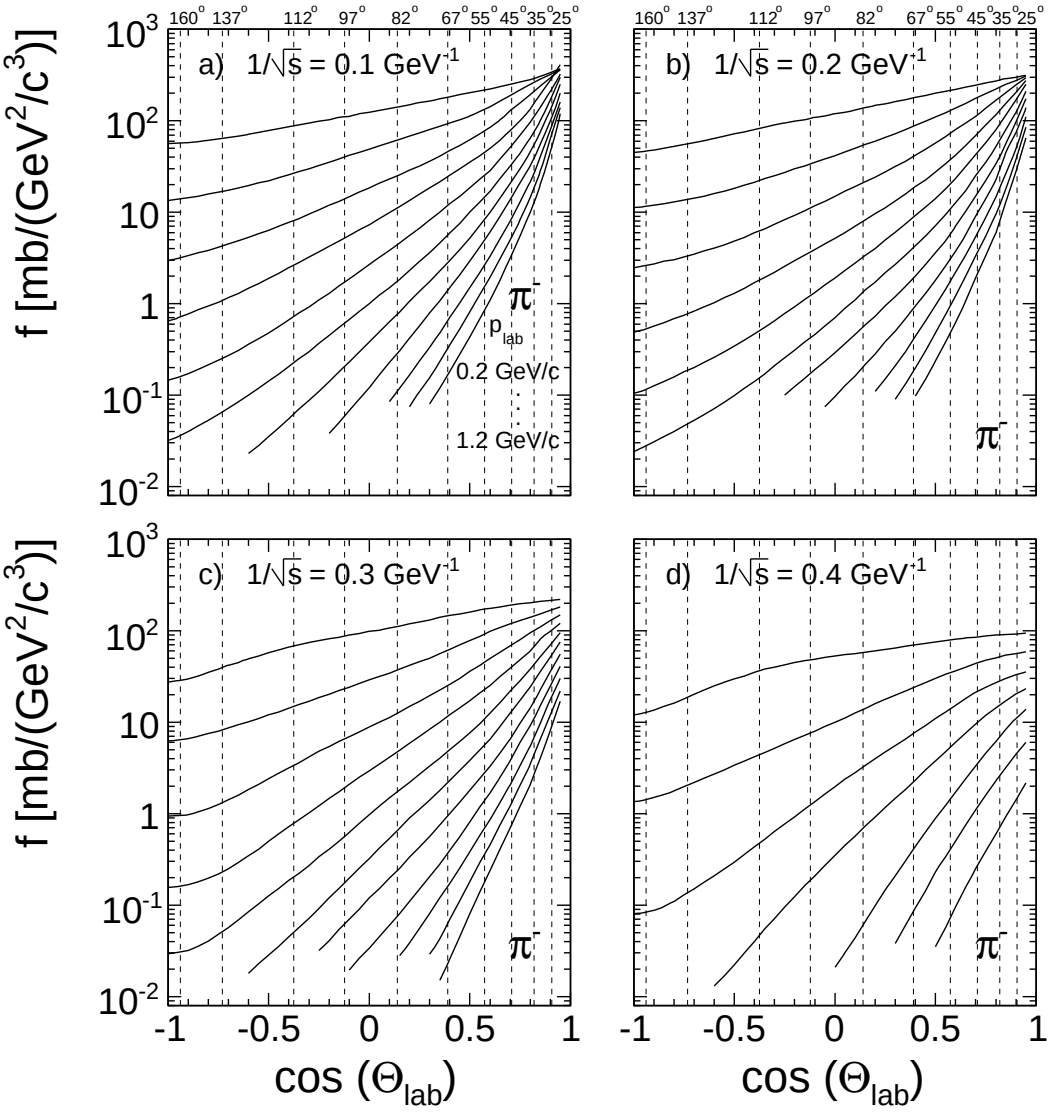

Figure 19: Invariant π^- cross sections as a function of $\cos(\theta_{\rm lab})$ for four values of $1/\sqrt{s}$: a) 0.1, b) 0.2, c) 0.3, d) 0.4 GeV^{-1} and for $p_{\rm lab}$ values between 0.2 and 1.2 GeV/c. The standard grid of 10 angles, Fig. 7, is indicated by the vertical broken lines

This will be quantified in the following Section on π^+/π^- ratios.

8 The π^+/π^- ratio

As already evoked in Sect. 4.5.3 above, the study of π^+/π^- ratios has two main advantages. Firstly, in this ratio a major fraction of the experimental systematic uncertainties cancels. Secondly, the ratio is constrained by very fundamental and model-independent physics arguments like charge conservation and isospin symmetry. In addition, its s-dependence is governed by the hadronic meson exchange process which leads to a power-law behaviour that will be shown to be common to a wide range of interactions. In the following argumentation the ratio between the global data interpolation for π^+ and π^- as described in the preceding Sects. 6 and 7 will be used:

$$R_{\pm}(1/\sqrt{s}, p_{\text{lab}}, \theta_{\text{lab}}) = \frac{f(\pi^+)}{f(\pi^-)} \tag{8}$$

As a by-product, the fluctuation of this ratio as a function of angle and interaction energy will allow for the estimation of the local precision of the interpolation procedure.

8.1 The high energy limit

It has been established by numerous experimental results that at collision energies in the SPS/Fermilab range and above the hadronic interactions are characterized by the absence of charge and flavour exchange. It has also been shown that the feed-over of pions from the projectile hemisphere into the backward region of x_F is sharply limited to the range of $x_F \gtrsim$ -0.05, see [28] for a detailed discussion. This range is outside the coverage in Θ_{lab} and p_{lab} considered in this publication.

It is therefore to be expected that the backward production of pions off an isoscalar nucleus should be charge-symmetric at high energy. This is indeed verified by the results on pion production shown in the preceding sections. It is quantified in Fig. 19 which shows the π^+/π^- ratio at $1/\sqrt{s}$ = 0.04 or 330 GeV/c beam momentum for all lab angles and lab momenta treated in this publication. This number distribution has a mean value of 1.0125 with an rms deviation of 3.2%. This rms value may be seen as a first estimate of the local precision of the three-dimensional interpolation scheme at this energy which has been established independently for both pion charges.

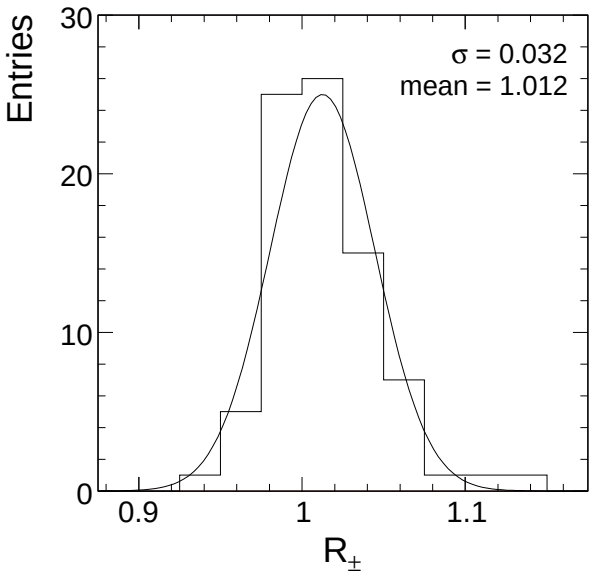

Figure 20: π^+/π^- ratio $R^{\pm}$ at $1/\sqrt{s}$ = 0.04 GeV^{-1} for 25 $<$ Θ_{lab} $<$ 162 degrees and 0.2 $<$ p_{lab} $<$ 1.2 GeV/c

8.2 Energy, momentum and angle dependence of $R_{\pm}$

With decreasing interaction energy or increasing $1/\sqrt{s}$ the π^+/π^- ratio develops a strong increase at all lab momenta and lab angles. This is shown in Fig. 21 which gives $R_{\pm}$ as a function of $1/\sqrt{s}$ for four lab momenta. The ratio of the global data interpolation is given in steps of 0.02

in $1/\sqrt{s}$. At each value of $1/\sqrt{s}$ the number of points corresponds to the standard grid of angles available at this energy.

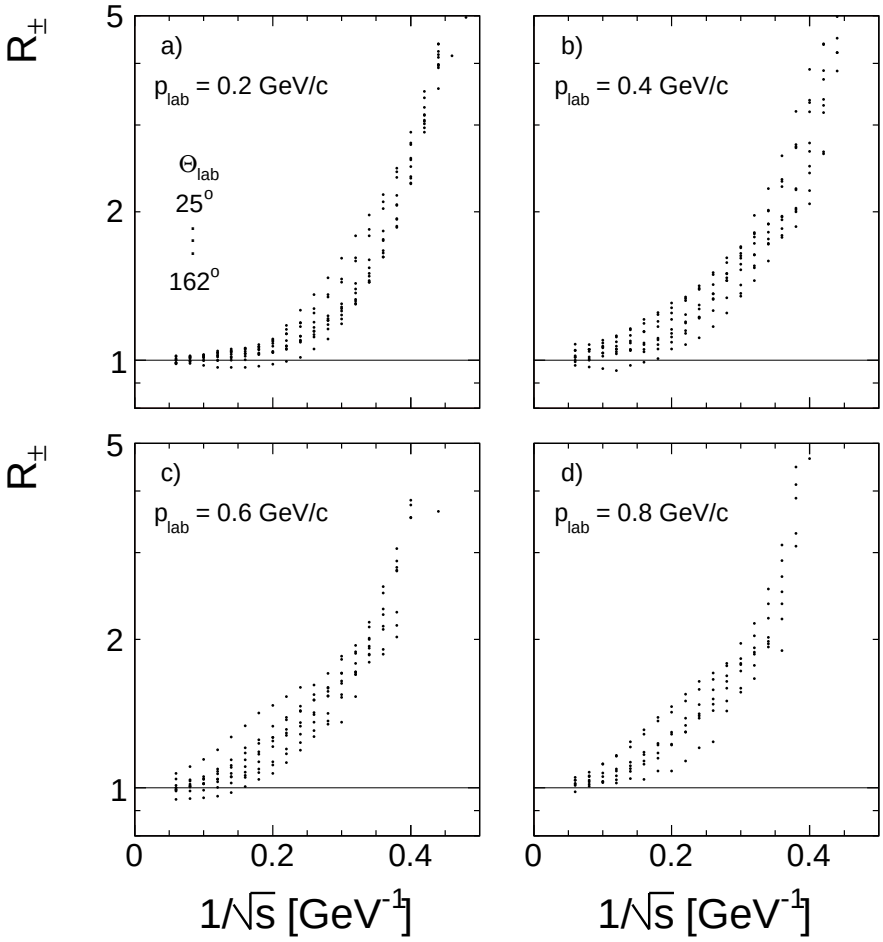

Figure 21: $R_{\pm}$ as a function of $1/\sqrt{s}$ for four values of $p_{\rm lab}$. The dots represent the ratio of the global data interpolation for π^+ and π^- in steps of 0.02 in $1/\sqrt{s}$ and for the chosen grid of 10 angles. a) $p_{\rm lab}$ = 0.2, b) $p_{\rm lab}$ = 0.4, c) $p_{\rm lab}$ = 0.6, d) $p_{\rm lab}$ = 0.8 GeV/c

Several features of Fig. 21 are noteworthy:

– considering the wide range of lab angles, $R_{\pm}$ is at each value of $1/\sqrt{s}$ confined to a narrow band indicating an approximative angle independence
– large $R_{\pm}$ values in excess of 5 are reached at the upper limit of the available scale in $1/\sqrt{s}$
– there is a systematic increase of $R_{\pm}$ with $p_{\rm lab}$

8.2.1 Mean π^+/π^- ratios and estimation of the local systematic fluctuations of the interpolation process

The features pointed out above may be quantified and at the same time the local systematic fluctuations of the interpolation may be estimated by establishing the mean values $\langle R_{\pm}\rangle$ averaged over the angular range at each $1/\sqrt{s}$. These mean values are well defined as shown in Fig. 22 which presents the normalized distribution of the point-by-point deviations from the mean in percent,

$$\Delta R_{\pm} = 100 \frac{R_{\pm} - \langle R_{\pm} \rangle}{\langle R_{\pm} \rangle} \tag{9}$$

for four values of $1/\sqrt{s}$, summing the four p_{lab} values used in Fig. 21.

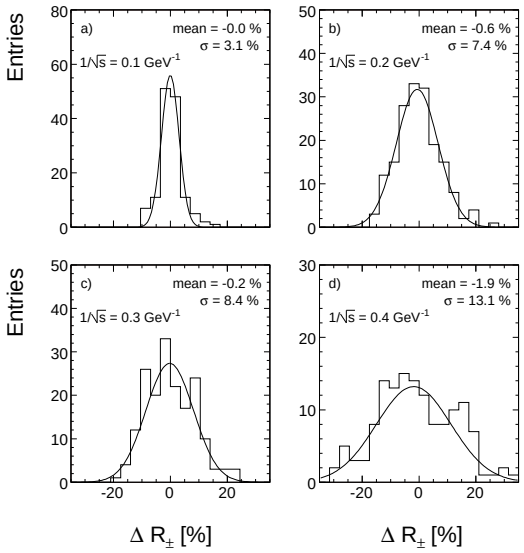

Figure 22: Number distribution of the normalized percent deviations $\Delta R_{\pm}$ from the mean over the angular range, a) $1/\sqrt{s}$ = 0.1, b) $1/\sqrt{s}$ = 0.2, c) $1/\sqrt{s}$ = 0.3, d)$1/\sqrt{s}$ = 0.4. The four p_{lab} values shown in Fig. 21 are summed up

These distributions are of Gaussian shape with an rms which increases with $1/\sqrt{s}$ as indicated in Fig. 23.

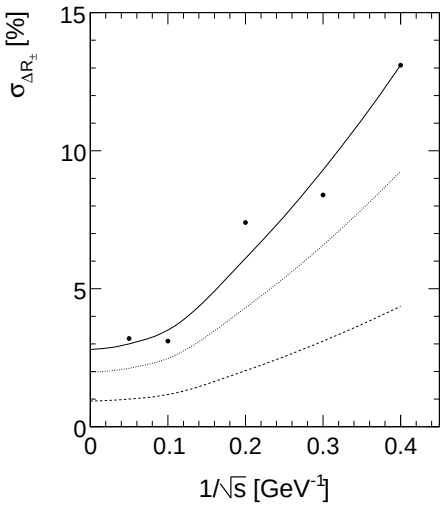

Figure 23: Rms values of the number distributions of the normalized point-by-point deviations from the mean charge ratio $\langle R_{\pm} \rangle$ as a function of $1/\sqrt{s}$. The full line represents a hand interpolation. Broken line: corresponding error margin of the mean values $\langle R_{\pm} \rangle$. Dotted lines: corresponding errors for π^+ and π^- separately

The observed energy dependence of the rms deviations is due to the fact that the invariant pion cross sections decrease, after a relatively flat behaviour up to $1/\sqrt{s} \sim 0.15$, progressively

steeper towards the production threshold, see Figs. 12 and 16. This leads inevitably to larger variations in the corresponding energy interpolation.

From the rms values given in Fig. 23 the error of $\langle R_{\pm} \rangle$ may be derived which varies between 1% and 5% for the highest and lowest interaction energy, respectively (broken line). Also the corresponding error margins for the mean pion yields may be extracted as indicated by the dotted lines in Fig. 23. From these plots it appears that the global interpolation induces fluctuations which increase from a few percent in the high s region to about 10% in the approach to the pion threshold.

8.2.2 Dependence of $R_{\pm}$ on Θ_{lab}

The dependence of $R_{\pm}$ on Θ_{lab} is shown in Fig. 24 for four values of $1/\sqrt{s}$ and four values of p_{lab}.

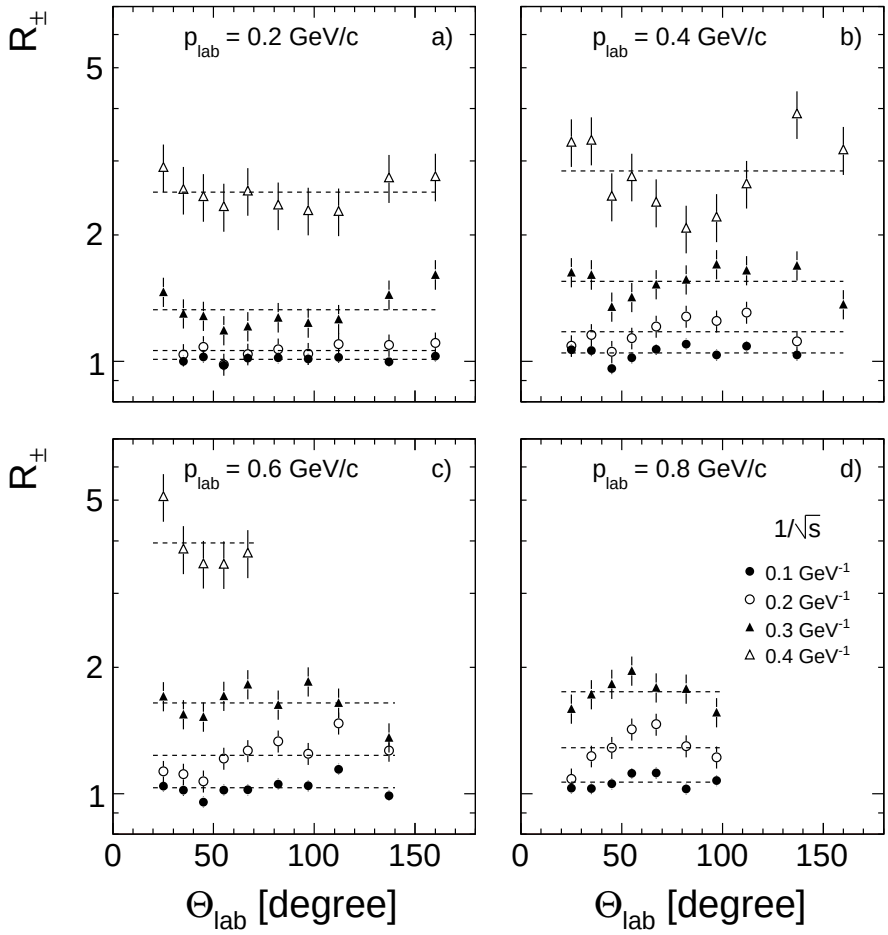

Figure 24: $R_{\pm}$ as a function of Θ_{lab} for four values of $1/\sqrt{s}$, a) p_{lab} = 0.2, b) p_{lab} = 0.4, c) p_{lab} = 0.6, and d) p_{lab} = 0.8 GeV/c. The mean values $\langle R_{\pm} \rangle$ including their errors are indicated as the horizontal bands in each panel

Evidently no systematic Θ_{lab} dependence is visible over the complete angular range within the quoted errors.

8.2.3 Dependence of $\langle R_{\pm} \rangle$ on $1/\sqrt{s}$ and p_{lab}

In the absence of angular dependence of $R_{\pm}$ as shown above, the mean values $\langle R_{\pm} \rangle$ may now be used in order to establish a precise view of the $1/\sqrt{s}$ dependence for different p_{lab} values. This dependence is presented in Fig. 25.

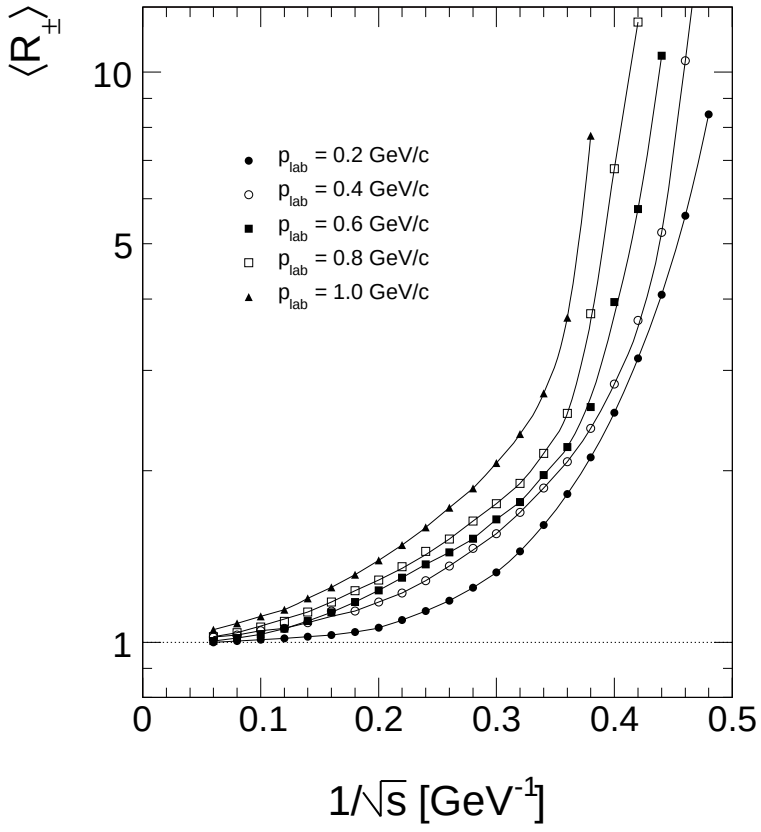

Figure 25: $\langle R_{\pm} \rangle$ as a function of $1/\sqrt{s}$ for five values of p_{lab} between 0.2 and 1.0 GeV/c. The full lines are hand interpolations through the data points

Within the errors of $\langle R_{\pm} \rangle$ extracted above, a clear p_{lab} dependence is evident superposing itself to the strong common increase of $\langle R_{\pm} \rangle$ with $1/\sqrt{s}$. This increase may be parametrized up to $1/\sqrt{s} \sim 0.3$ by the functional from $1 + c/s^{\beta(p_{\text{lab}})}$ which is, as discussed below, typical of meson exchange processes. Indeed the exponent beta varies from 2 to 1.2 for p_{lab} increasing from 0.2 to 0.8 GeV/c.

8.3 Interpretation of the observed energy and momentum dependences

The strong increase of $R_{\pm}$ with $1/\sqrt{s}$ merits a detailed study as it is directly connected to the basic hadronic production mechanisms in p+A interactions. The fact that the pion yields in the complete backward fragmentation region of an isoscalar nucleus remember the isospin of the projectile is clearly incompatible with charge and flavour independent exchange processes. Instead a meson exchange mechanism may be invoked which has indeed been used successfully in a wide range of work at low projectile momenta, see for instance [18] and references therein. Close to the pion production threshold in the nuclear hemisphere, single excitation processes via pion exchange of the type

$$\mathrm{p} + (\mathrm{p}) \quad \rightarrow \quad \Delta^{++} + (\mathrm{n}) \quad \rightarrow \quad \pi^{+} \tag{10}$$
$$\mathrm{p} + (\mathrm{p}) \quad \rightarrow \quad \Delta^{+} \ + (\mathrm{p}) \quad \rightarrow \quad \pi^{+}, \pi^{0} \tag{11}$$
$$\mathrm{p} + (\mathrm{n}) \quad \rightarrow \quad \Delta^{+} \ + (\mathrm{n}) \quad \rightarrow \quad \pi^{0}, \pi^{+} \tag{12}$$

only allow π^+ and π^0 production, whereas π^- production needs double excitation like

$$\mathrm{p} + (\mathrm{p}) \quad \rightarrow \quad \Delta^{++} + (\Delta^{0}) \quad \rightarrow \quad \pi^{+}, \pi^{0}, \pi^{-} \tag{13}$$
$$\mathrm{p} + (\mathrm{n}) \quad \rightarrow \quad \Delta^{+} \ + (\Delta^{0}) \quad \rightarrow \quad \pi^{+}, \pi^{0}, \pi^{-} \tag{14}$$
$$\mathrm{p} + (\mathrm{n}) \quad \rightarrow \quad \Delta^{++} + (\Delta^{-}) \quad \rightarrow \quad \pi^{+}, \pi^{-} \tag{15}$$

with in general an additional penalty for π^- due to the isospin Clebsch–Gordan coefficients. All meson exchange mechanisms are characterized by a strong decrease with projectile energy. This energy dependence and its interplay with processes governing the high energy sector is studied here for the first time in p+A collisions using the π^+/π^- ratio.

In this context it seems mandatory to first refer to the study of exclusive charge exchange reactions in elementary nucleon-nucleon collisions as the complete energy range discussed here has been covered there by a number of experiments [29–35].

8.3.1 The charge exchange mechanism in elementary nucleon-nucleon collisions

Charge exchange processes may be cleanly isolated experimentally in nucleon-nucleon interactions by studying the following exclusive channels:

– charge exchange scattering of the elastic type

$$\mathrm{n} + \mathrm{p} \quad \rightarrow \quad \mathrm{p} + \mathrm{n} \tag{16}$$

– single dissociation with pion production

$$\mathrm{p} + \mathrm{p} \quad \rightarrow \quad \mathrm{n} + \Delta^{++} \quad \rightarrow \quad \mathrm{n} + (\mathrm{p} + \pi^{+}) \tag{17}$$

– double dissociation with pion production

$$\mathrm{p} + \mathrm{p} \quad \rightarrow \quad (\mathrm{p} + \pi^{-}) + (\mathrm{p} + \pi^{+}) \tag{18}$$

These channels are characterized by a very steep energy dependence.

This is to be confronted with non-charge-exchange exclusive channels like

– elastic scattering

$$\mathrm{p} + \mathrm{p} \quad \rightarrow \quad \mathrm{p} + \mathrm{p} \tag{19}$$

– single dissociation

$$\mathrm{p} + \mathrm{p} \quad \rightarrow \quad \mathrm{p} + (\mathrm{p} + \pi^{+} + \pi^{-}) \tag{20}$$

– double dissociation

$$\mathrm{p} + \mathrm{p} \quad \rightarrow \quad (\mathrm{p} + \pi^{+} + \pi^{-}) + (\mathrm{p} + \pi^{+} + \pi^{-}) \tag{21}$$

which show a constant or logarithmically increasing s-dependence.

Charge exchange scattering has been measured by five experiments in the range of neutron beam momenta from 3 to 300 GeV/c. [29–33]. This is exactly covering the energy range discussed in this paper. The single and double dissociation has been studied at the CERN ISR by two experiments [34, 35] extending the energy scale to s = 3700 GeV^2. The two ISR experiments may be directly compared to the charge exchange measurements after appropriate re-normalization of the cross sections in the overlap region at the lowest ISR energy.

The resulting s-dependence at a momentum transfer t = 0.032 GeV^2 is presented in Fig. 26.

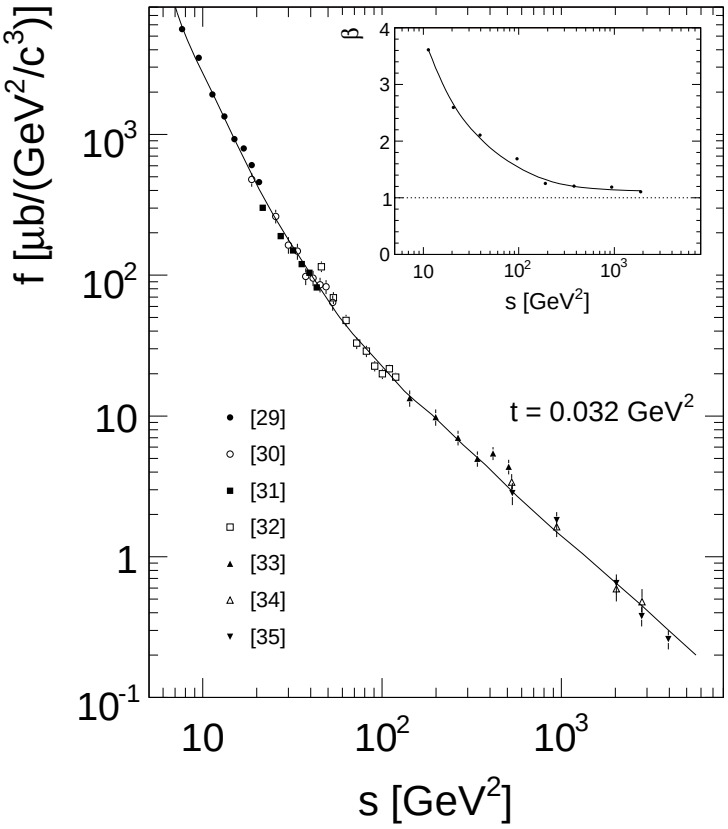

Figure 26: Invariant cross sections of charge exchange and single and double dissociation in nucleon-nucleon interactions as a function of s at a momentum transfer t = 0.032 GeV^2. The full line represents an interpolation of the data points. The insert gives the local slope β in the parametrization $f \sim s^{-\beta}$ as a function of s

Several features of Fig. 26 are of interest:

- there is a decrease of about 4 orders of magnitude in cross section between the lowest and highest s value. This decrease is to be compared to the constant or logarithmically increasing elastic and nucleon diffraction cross sections. The charge exchange contribution is therefore negligible compared to the inclusive baryon yields already at SPS energy
- there is a steady decrease of the local slope df/ds with energy, from about 3.6 at 3 GeV/c to about 1.1 above 80 GeV/c beam momentum
- a characteristic change of slope manifests itself at around 30 GeV/c beam momentum

These features have been interpreted in the 1970's when the relevant experiments were performed, in the framework of Regge theory which predicts an s-dependence of the form

$$f \sim s^{2\alpha-2} = s^{-\beta}, \tag{22}$$

where α is the intercept of the leading trajectory. This should in the case of one-meson exchange at low energy be given by the pion trajectory with zero intercept. The actual beta values above 3 at low s seem to contradict however this expectation. Here threshold effects may play a role which are not included in the parametrization (22).

With increasing energy the slopes move through the region of pion exchange with $\beta \sim 2$ down to values of about 1.1 at high energy which could be connected to ρ and a_2 exchange with correspondingly higher intercepts α in the region of 0.5. At ISR energy the ratio of ρ/π contributions has indeed been estimated to be about 2 [35]. Anyway the simple parametrization given by (22) should not be expected to hold over the full energy scale. What is interesting here is rather the strong decline of the charge exchange cross sections with energy and the experimentally rather precisely determined slope variation.

8.3.2 A remark concerning baryon resonance production in hadronic interactions

The single (17) and double (18) dissociation processes defined above are determined by the formation of Δ resonances in the final states. They therefore constitute a source of direct Δ production in nucleon-nucleon interactions. These channel cross sections decrease rapidly to the μbarn level at SPS energies. In contrast, the non-charge exchange channels like (20) and (21) have no s-dependence and stay on the mb level of cross sections. Their final states have been shown to be governed by N^* resonances [36] which may be excited by Pomeron exchange. Moreover, the p+π^+ combination of the p+π^++π^- final states has been shown to be dominated by Δ^{++} [37]. This is an indirect source of Δ resonances as a decay product of N^* states which have large decay branching fractions into Δ+π and Δ+ρ. It is therefore questionable if, at SPS energies and above, any direct Δ production is persisting. This is an interesting question for the majority of microscopic models which produce final states by string fragmentation. In the baryonic sector, diquark fragmentation is generally invoked with a prevailing direct production of Δ resonances which by isospin counting will dominate over N^*. Indeed in practically all such models there is no or only negligible N^* production. As shown below, the decrease of charge exchange processes can be traced well into the non-diffractive, inelastic region of particle production. The multi-step, cascading decay of primordial N^* resonances into Δ resonances and final state baryons should therefore be seriously considered, in particular also concerning the consequences for the evolution of final state energy densities with time.

8.3.3 The charge exchange mechanism in p+C interactions as a function of interaction energy

The very characteristic decrease of $\langle R_\pm \rangle$ with increasing s derived from the global data interpolation, Fig. 25, offers a tempting possibility of comparison to the phenomenology discussed above for the elementary nucleon-nucleon sector. Indeed, two components should contribute to the observed π^+/π^- ratios: at high energy this ratio should approach unity due to the absence of charge and flavour exchange in this region. At low energy on the contrary it should be governed by meson exchange with its strong s-dependence. These two components may be tentatively separated by using instead of $\langle R_\pm \rangle$ the quantity

$$\langle R_\pm^{me} \rangle = \langle R_\pm \rangle - 1 \tag{23}$$

in order to extract the meson exchange contribution. This quantity is plotted in Fig. 27 as a function of s for four $p_{\rm lab}$ values from 0.2 to 0.8 GeV/c.

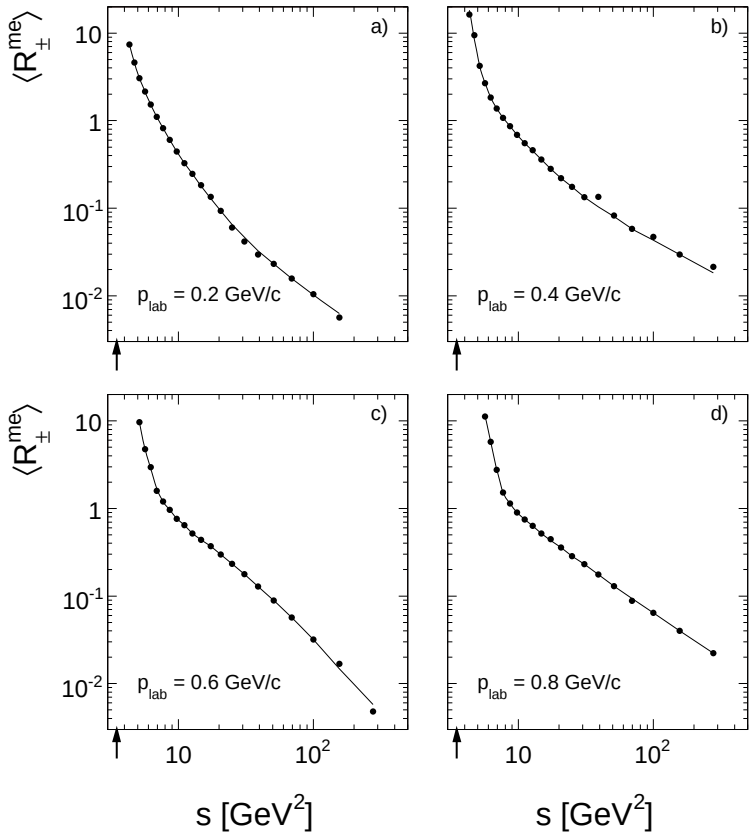

Figure 27: $\langle R^{me}_{\pm}\rangle$ as a function of s for different values of $p_{\rm lab}$, a) $p_{\rm lab}$ = 0.2, b) $p_{\rm lab}$ = 0.4, c) $p_{\rm lab}$ = 0.6, and d) $p_{\rm lab}$ = 0.8 GeV/c. The elastic limit is indicated by the arrows

A very characteristic pattern emerges which resembles the s-dependence for the charge exchange in elementary interactions described above, see Fig. 26. In general $\langle R^{me}_{\pm}\rangle$ follows a power law dependence on s

$$\langle R^{me}_{\pm}\rangle \sim cs^{-\beta^{me}} \tag{24}$$

with local slopes β^{me} which are in turn a function of s. Three different regions with distinct local slopes can be identified in Fig. 27:

- a first region with large slopes is located at s below about 6 GeV^2. This region is strongly influenced by threshold effects as the threshold for inelastic production is placed at the elastic limit $s = 4m_p^2 = 3.5GeV^2$ indicated in Fig. 27. In the approach to pion threshold the π^+/π^- ratio has to diverge as π^- is progressively suppressed, see above. With increasing $p_{\rm lab}$ this suppression will of course be more pronounced
- an intermediate region between about 8 and 40 GeV^2 with an s dependence decreasing with increasing $p_{\rm lab}$
- a third region with flattening s-dependence above about 40 GeV^2

At the lowest $p_{\rm lab}$ value of 0.2 GeV/c corresponding to the lowest momentum transfer, the similarity to the charge exchange process in nucleon-nucleon interactions, Fig. 26, is absolutely striking. This concerns both the detailed shape and the overall suppression factors. With increasing $p_{\rm lab}$, the s dependence is modified in a systematic way by a general reduction of slopes, with the exception of the threshold enhancement. This is quantified in Fig. 28 which shows the local slopes as a function of s for $p_{\rm lab}$ values between 0.2 and 1 GeV/c.

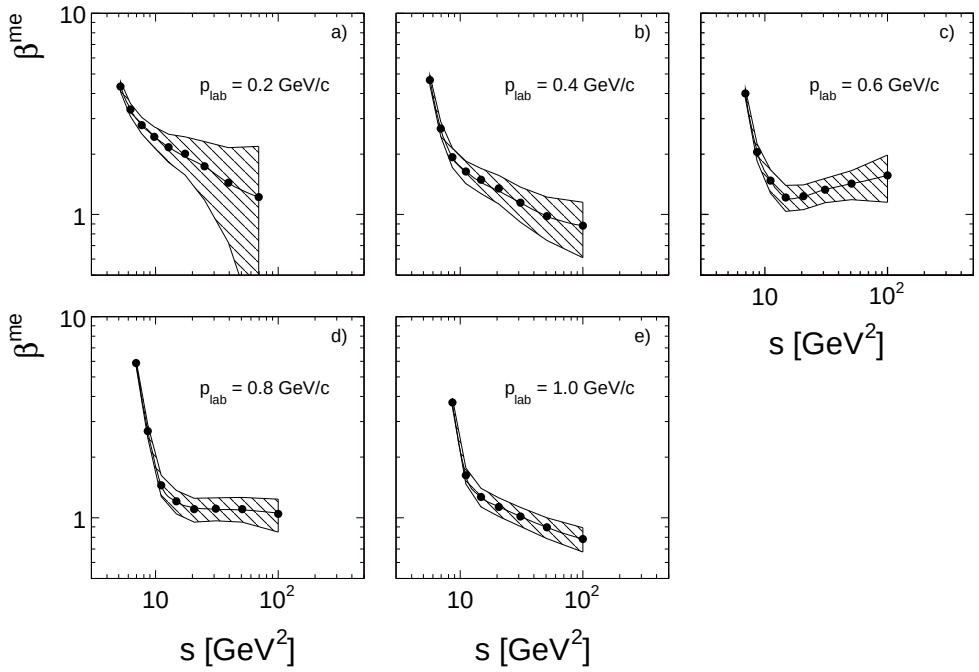

Figure 28: Slopes β^{me} of the s-dependence of $\langle R_{\pm}^{me} \rangle$ as a function of s: a) p_{lab} = 0.2, b) p_{lab} = 0.4, c) p_{lab} = 0.6, d) p_{lab} = 0.8, and e) p_{lab} = 1.0 GeV/c. The shaded regions mark the error margins

With the exception of the threshold region, the slopes are confined to the region between 2 and 1 typical of meson exchange processes. The dependence on p_{lab} is given in Fig. 29 where the slopes in the three regions of s specified above are presented.

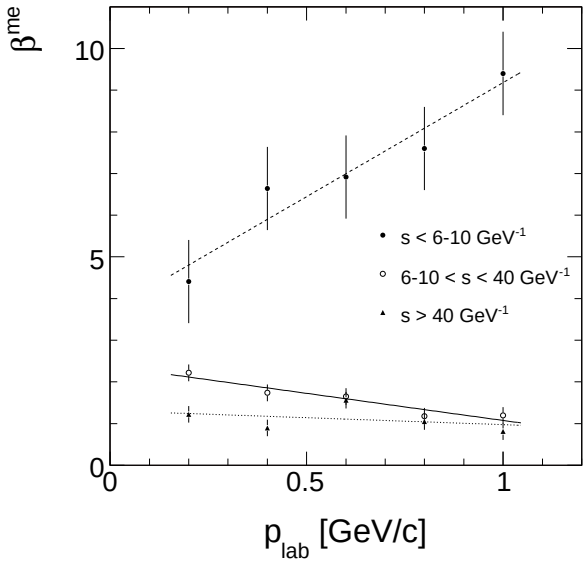

Figure 29: Local slopes in the regions $s < 6$ GeV^2 (broken line), $6 < s < 40$ GeV^2 (full line) and $s > 40$ GeV^2 (dotted line) as a function of p_{lab} between 0.2 and 1 GeV/c

This Figure shows clearly the different nature of the low s enhancement where the slopes increase strongly with p_{lab}. The two other regions, full and dotted lines, are compatible with a Regge parametrization with trajectory intercepts which increase with p_{lab}. This is insofar in-

teresting as the region of measurements regarded here covers the complete backward angular range and the corresponding interactions are by no means confined to diffractive or low momentum transfer collisions. It is shown in Sect. 10 of this paper that in the backward hemisphere the pion yields from nuclear cascading and target fragmentation are comparable. If the nuclear component is characterized by low momentum transfer reactions [2] the target fragmentation is manifestly inelastic and non-diffractive. It governs the total yield at all angles below about 70 degrees.

In conclusion of this study of π^+/π^- ratios in p+C interactions the following points should be stressed:

- the global data interpolation leads to a precise and consistent description of the behaviour of the π^+/π^- ratios in the full backward hemisphere, thus offering an additional tool for the discrimination of experimental deviations
- the inspection of the detailed s-dependence of the ratios opens a new window on the underlying exchange processes.
- In particular the comparison to the elementary nucleon-nucleon collisions establishes a close relation between apparently disjoint sectors of the different hadronic interactions

9 Deviating experiments

The global data interpolation scheme discussed in the preceding sections has considerable discriminative power against the deviation of particular data sets. Although deviations of data points in certain restricted regions of phase space are well visible in Figs. 7, 12 and 16, it is the systematic aberration of whole data sets by several standard deviations from the interpolation which asks for comment. In this sense 4 of the 19 experiments contained in Tables 1 and 2 have been identified as deviating. These will be discussed in some detail below.

9.1 The proton data by Geaga et al. [7]

J. V. Geaga et al. [7] have obtained proton data in p+C interactions at the Bevalac with beam momenta of 1.75, 2.89 and 5.89 GeV/c ($1/\sqrt{s}$ = 0.427, 0.366 and 0.281 GeV^{-1}). The measurements span a lab momentum range from 0.3 to 0.9 GeV/c at a lab angle of 180 degrees.

The resulting cross sections are consistently about a factor of two below the global data interpolation. This is visible in Fig. 30 which gives their data in comparison to the global interpolation in the range from $0.26 < 1/\sqrt{s} < 0.44$ GeV^{-1}.

Here the full lines correspond to the interpolation and the broken lines give the interpolation divided by a factor of 2.

As the angular bin from 160–180 degrees is mostly covered by data around 160–162 degrees, with only a few data points at 180 degrees, a steep angular dependence in this region cannot be a priori excluded. The study of the detailed $\cos(\Theta_{\text{lab}})$ distributions at the $1/\sqrt{s}$ values of [7] helps however to obtain a clear picture of the situation as shown in Fig. 31.

The smooth and gentle angular dependence of the interpolated data together with the physics constraint of the approach to 180 degrees with tangent zero (Sect. 4.5) clearly excludes the possibility of a drop of the invariant cross sections by a factor of two between 160 and 180 degrees. If the shape of the $1/\sqrt{s}$ dependence traces the interpolation rather precisely, the presence of a large normalization error of order 2 in the data of [7] is clearly indicated.

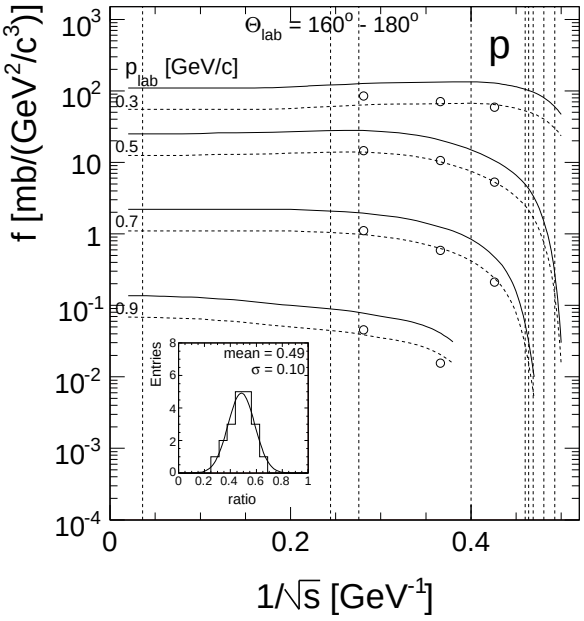

Figure 30: The proton cross sections from Geaga et al. [7] in comparison to the global data interpolation (full lines) in the lab angle bin from 160 to 180 degrees. The broken lines correspond to a reduction of the interpolation by a factor of two. The inserted histogram gives the number distribution of the ratio between data and interpolation

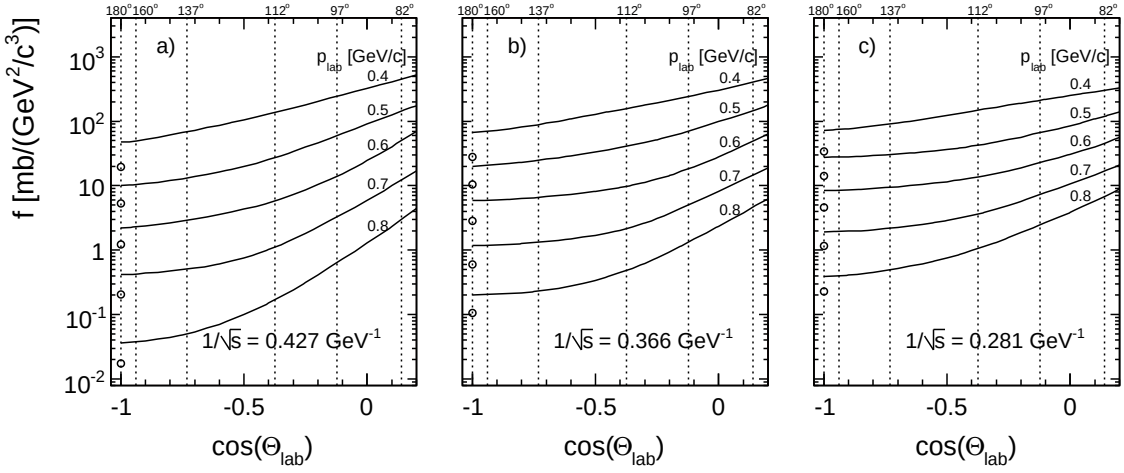

Figure 31: Invariant proton cross sections as a function of $\cos(\Theta_{\rm lab})$ for three values of $1/\sqrt{s}$; a) 0.427, b) 0.366 and c) 0.281 GeV^{-1}. The full lines give the global data interpolation, the open circles the data from [7]

9.2 The proton and pion data of Belyaev et al. [3, 13]

This experiment has obtained a sizeable set of data on proton [3] and pion [13] production at the Serpukhov accelerator. This data set is important as it spans the range of beam momenta between 17 and 57 GeV/c and hence fills the gap between PS and SPS energy where no other measurements are available. The data cover a lab momentum range from 0.25 to 1.2 GeV/c at $\Theta_{\rm lab}$ = 159 degrees.

A first view of these data is presented in Fig. 32 in comparison to the global data interpo-

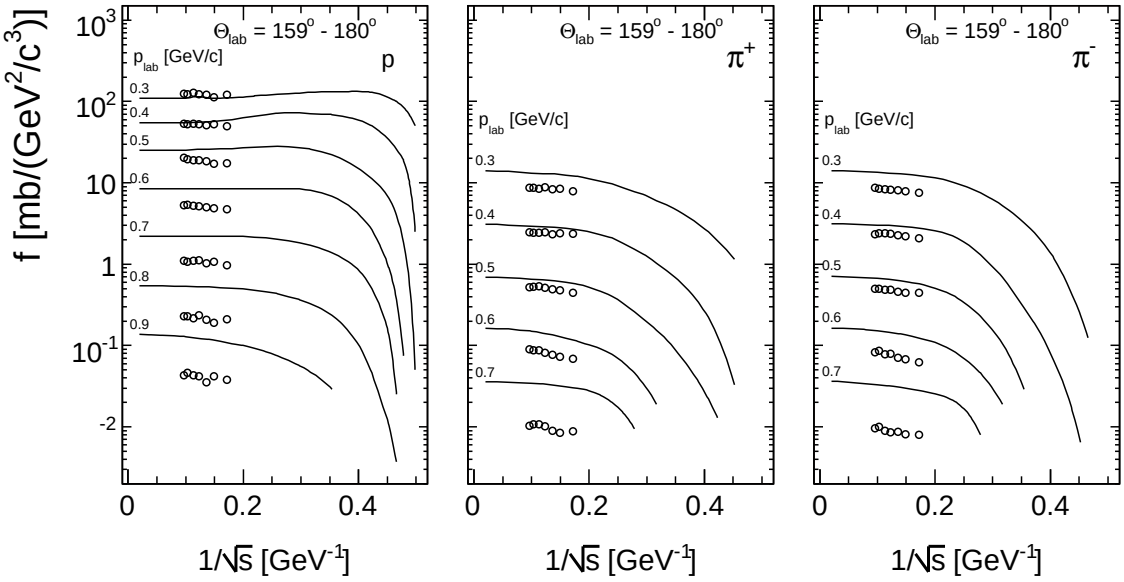

Figure 32: The data of Belyaev et al. [3, 13] as a function of $1/\sqrt{s}$ at $\Theta_{\rm lab}$ = 159 degrees (full circles) in comparison to the global data interpolation at 160 degrees (full lines)

lation.

Four main features of this comparison are apparent:

- the shape of the $1/\sqrt{s}$ dependences traces the global interpolation rather precisely
- there is a pronounced suppression of the Serpukhov data with respect to the interpolation with increasing $p_{\rm lab}$. This suppression reaches factors of three for protons and pions at their upper $p_{\rm lab}$ ranges
- the π^+ and π^- data show an identical phenomenon
- there are systematic differences in the suppression between protons and pions. If the proton data exactly match the interpolation at $p_{\rm lab}$ = 0.3 and 0.4 GeV/c, the pion data deviate already at $p_{\rm lab}$ of 0.3 GeV/c. At the higher end of the pion range of $p_{\rm lab}$ at 0.7 GeV/c there is a suppression by a factor of 3 for the pions and by a factor of 2 for the protons

These facts lead to the hypothesis that the momentum scale of this experiment has a systematic deviation. Indeed it is the non-invariant density distribution $d^2\sigma/dp_{\rm lab}d\Omega$ which is affected by a possible momentum shift, and this distribution is characteristically different for protons and pions. One example of this fact is given in Fig. 33 for $1/\sqrt{s}$ = 0.113 GeV^{-1} separately for protons and pions.

The proton distribution shows a broad maximum around $p_{\rm lab} \sim$ 0.2–0.3 GeV/c followed by an increasingly steep slope with increasing $p_{\rm lab}$. A shift of the momentum scale by a fixed percentage will therefore have a small to negligible effect around this maximum whereas at higher $p_{\rm lab}$ a strongly increasing suppression will appear. This is pointed out by the full and broken lines in Fig. 33. For pions on the contrary the density distribution decreases for all momenta measured by [13] because the maximum density which must be present due to the constraint $d^2\sigma/dp_{\rm lab}d\Omega$ = 0 at $p_{\rm lab}$ = 0 GeV/c, is not reached even at $p_{\rm lab}$ = 0.2 GeV/c. A momentum shift will therefore suppress the pion density already at low momentum. As the slope of the pion distributions is steeper than the one for protons, the same momentum shift will create bigger deviations for pions than for protons at fixed $p_{\rm lab}$.

In order to verify this hypothesis, a constant upward momentum shift of 9% has therefore

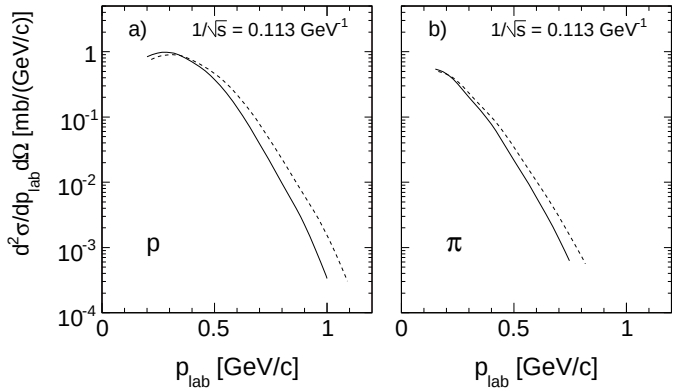

Figure 33: Non-invariant particle density $d^2\sigma/dp_{\rm lab}d\Omega$ as a function of $p_{\rm lab}$ at $1/\sqrt{s}$ = 0.113 GeV^{-1}, a) for protons [3] and b) for pions [13]. Full lines: interpolated results from the Serpukhov experiment. Broken lines: result of an upward momentum shift by 9%

been applied to the Serpukhov data. The result is shown in Fig. 34 where a perfect fit of the corrected data to the global interpolation is evident for the protons. For the pions the result is not as satisfactory since deviations of order 20–30% are still visible. However also here the very large deviations of up to 300% are completely eliminated.

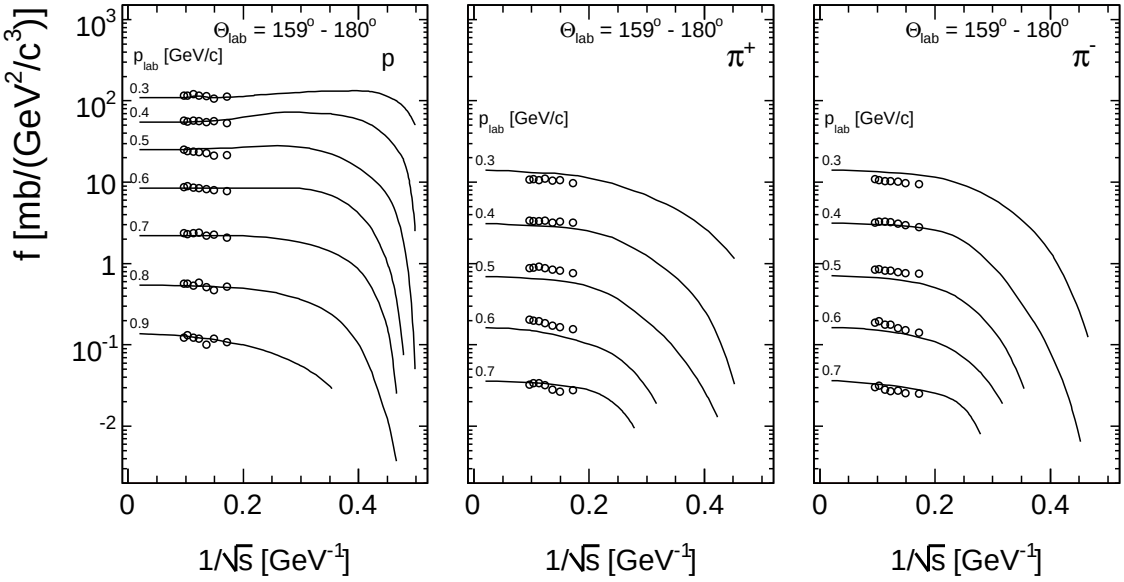

Figure 34: The data of Belyaev et al. [3, 13] as a function of $1/\sqrt{s}$ (full circles) after re-adjustment of the momentum scale by an upward shift of 9%

Further evidence for the basic validity of the Serpukhov data comes from a study of the π^+/π^- ratios $R_\pm$ as a function of $p_{\rm lab}$. This is shown in Fig. 35 where their data are averaged over the beam momentum scale from 17 to 57 GeV/c.

The data verify the predicted ratios $R_\pm$ in this energy range with a precision of about 1% up to $p_{\rm lab} \sim 0.7$ GeV/c, see in this context the discussion of $R_\pm$ errors in Sect. 8.2.1. Above this $p_{\rm lab}$ value a sharp and unexplained decrease of $R_\pm$ by up to 20% is visible which corresponds,

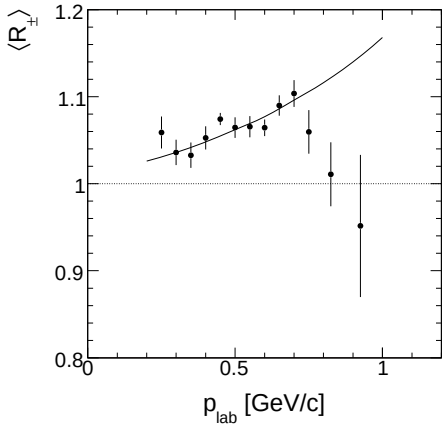

Figure 35: Pion charge ratio $R_{\pm}$ from [13] as a function of p_{lab} averaged over beam momentum between 17 and 57 GeV/c. The full line gives the result of the global interpolation averaged over the same beam momentum scale, Sect. 8

in view of the large statistical errors in this region, to about 2 standard deviations. In conclusion it may be stated that the Serpukhov data constitute an important verification of some basic facts:

- the shape of the $1/\sqrt{s}$ dependence is compatible with the one extracted from the comparison of the PS and SPS energy ranges
- the measured π^+/π^- ratios verify the ones predicted by the global data interpolation on a percent level in this energy region
- from a detailed study of the momentum dependences for protons and pions it seems indicated to assume a momentum scale error in this experiment

9.3 The HARP data for π^+ and π^- [15]

These results occupy an unusual and special place since they arise from the analysis of an identical set of input data as they have been published by the HARP-CDP collaboration [4]. The publication of independent analyses of identical input data is extremely rare in particle physics although it constitutes in principle a most welcome verification of the way from raw to final data and of the systematic problems encountered along this way. It must however be expected that this procedure results in identical output data with small to negligible relative deviations. As no direct comparison between these two groups of results has been attempted so far, with the exception of one single Θ_{lab} value [4], this general comparison will be attempted here especially also in relation to the global data interpolation as a point of reference.

9.3.1 Phase space coverage and errors

The information contained in Table 2 shows that the two data sets have distinct differences. If the beam momenta, with the exception of 15 GeV/c not treated by HARP, and the overall angular ranges are identical, HARP limits the lab momentum range to about half that of HARP-CDP. In addition, the binning both in angle and in momentum is different which again necessitates data interpolation.

For a first overview of these different data, momentum distributions of the invariant pion cross sections in the two closest angular bins at about 25 degrees and 82 degrees are shown in Fig. 36 for two typical projectile momenta.

Several observations may be deduced from these plots:

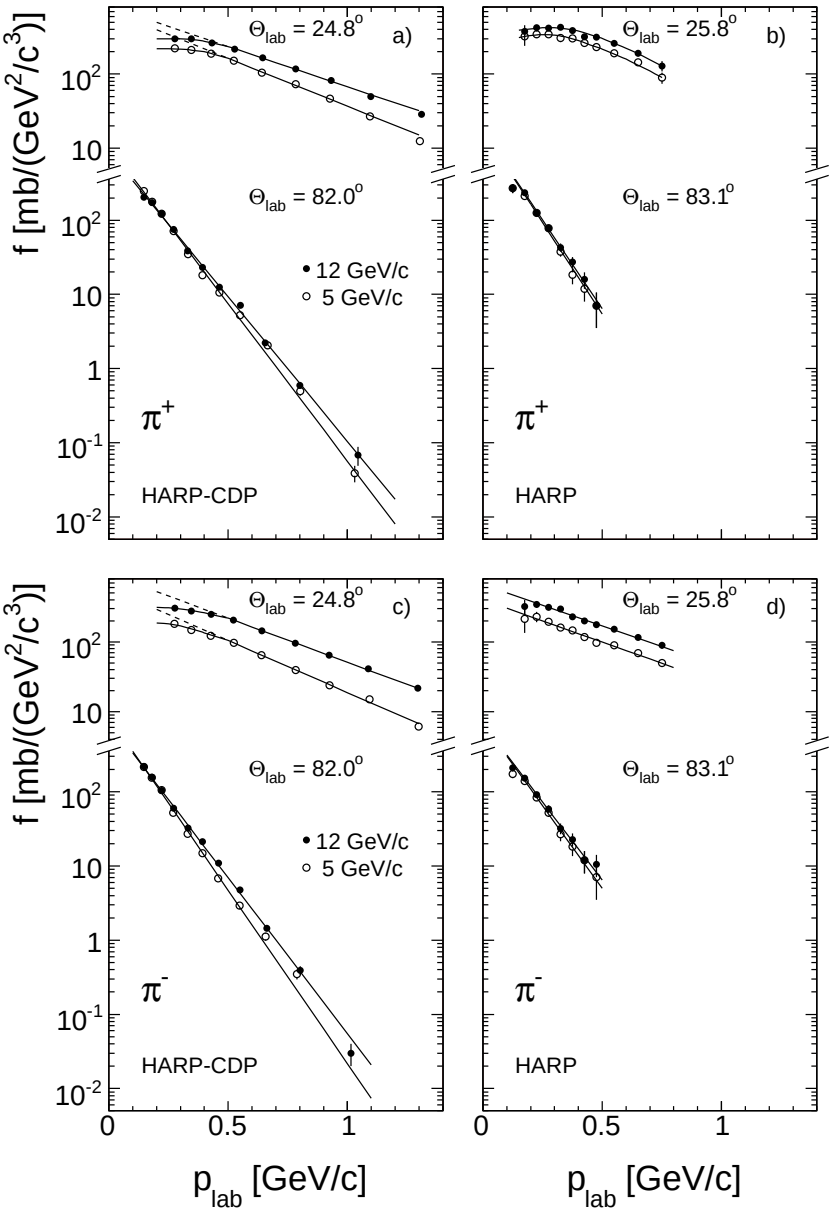

Figure 36: Invariant cross sections as a function of $p_{\rm lab}$ for π^+ and π^- as a function of $p_{\rm lab}$ at two lab angles and two beam momenta. π^+ a) HARP-CDP, b) HARP, π^- c) HARP-CDP, d) HARP. The full lines correspond to the data interpolation chosen for the HARP data; the ones for HARP-CDP represent the global data interpolation

- the reduced $p_{\rm lab}$ range of the HARP data is evident
- differences in invariant cross sections and in the shapes of the $p_{\rm lab}$ distributions are visible
- the deviations from exponential shape in the lowest $p_{\rm lab}$ bin of HARP has been argued in Sect. 4.4 to be of physics origin
- the at least partial exponential shape of the $p_{\rm lab}$ distributions is valid in both cases

The error treatment is clearly different in both analyses. HARP only gives a combined error value whereas HARP-CDP distinguishes between statistical and systematic errors. The statistical errors should of course be similar in the limit of comparable bin widths. This can be shown by regarding the residual distributions with respect to exponential fits of both data sets as

discussed below. Fig. 37 gives the number distributions of the statistical and systematic errors for HARP-CDP and for the combined errors for HARP over the complete data sets.

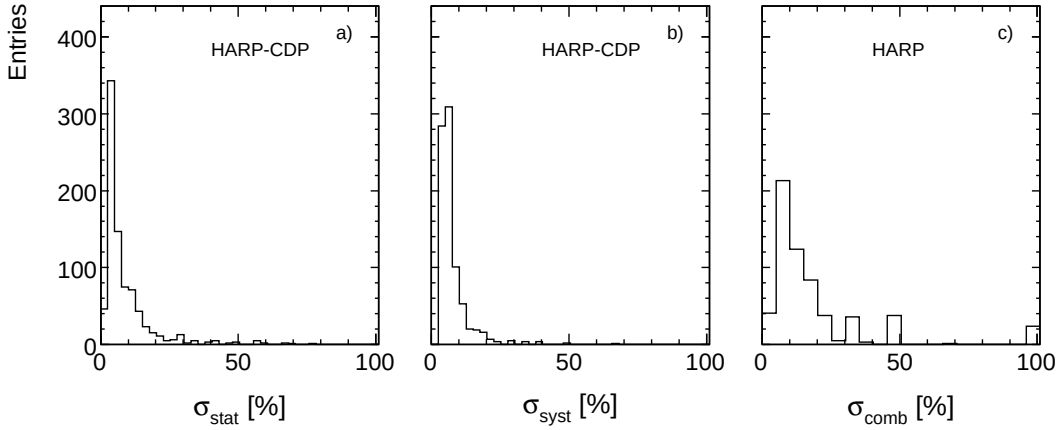

Figure 37: Number distributions of the statistical and systematic errors of HARP-CDP and for the combined errors of HARP in percent: a) σ_{stat} and b) σ_{syst} for HARP-CDP, c) σ_{comb} for HARP

The difference in size between the HARP-CDP and HARP errors should be noted. The dependence on p_{lab} and on p_{beam} in two angular ranges is presented in Fig. 38

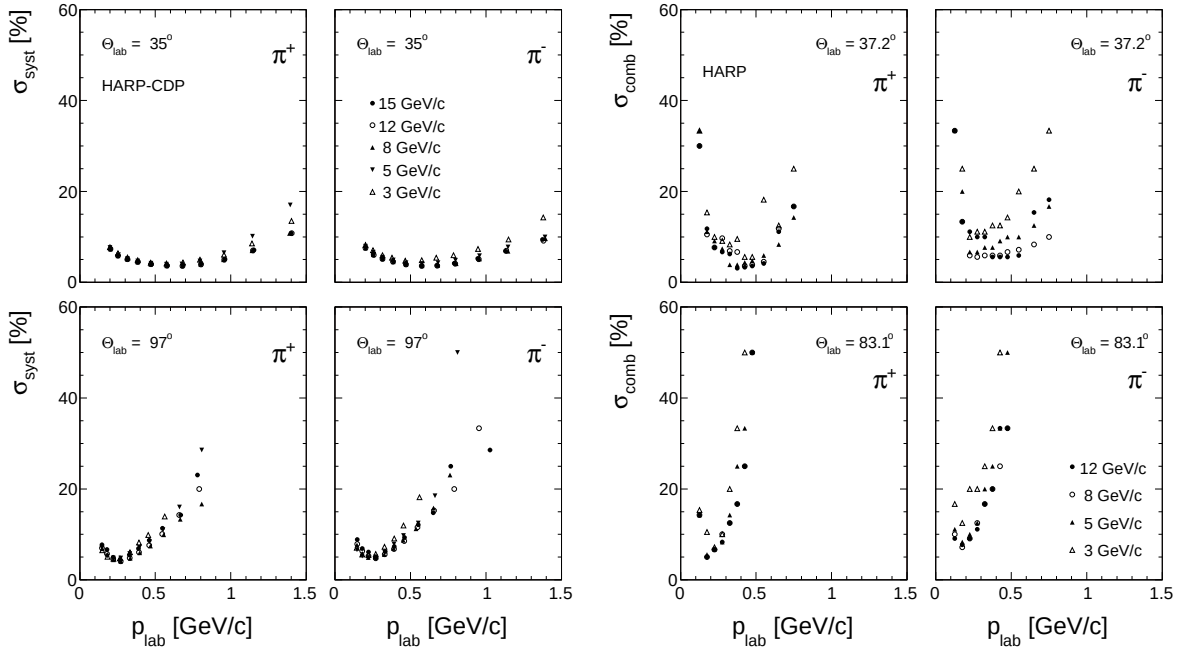

Figure 38: Systematic errors from HARP-CDP and combined errors from HARP as a function of p_{lab} for two lab angles, for all beam momenta. Left four panels: pions from HARP-CDP at 35 and 97 degrees; right four panels: HARP at 37 and 83 degrees

If the errors approach a similar level at low Θ_{lab} in a small region around 0.2–0.4 GeV/c, there is a strong increase of the HARP errors both towards low and high p_{lab}. The divergence of the error margin at larger angles to values of 50% already at $p_{\text{lab}} \sim 0.5$ GeV/c makes this the experiment with the highest error estimate amongst all other data discussed here. This has probably contributed to the decision to limit the momentum range as compared to HARP-CDP.

9.3.2 Data interpolation

The interpolation of the HARP-CDP data has been discussed above and is part of the establishment of the global interpolation scheme. For the HARP analysis one may again make use of an approximate exponential momentum dependence as shown for some typical angles and beam momenta in Fig. 39.

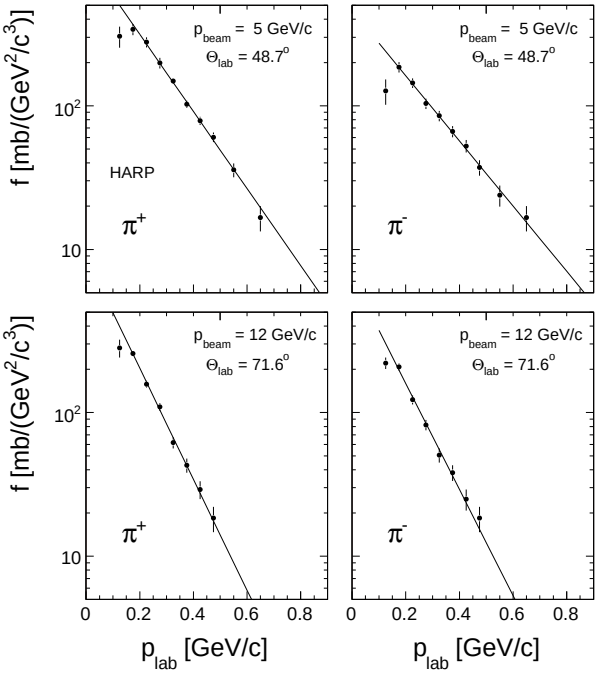

Figure 39: Invariant cross sections as a function of $p_{\rm lab}$ for π^+ and π^- at some values of beam momentum and angle

With the exception of the points at their lowest lab momentum of 0.125 GeV/c, see Sect. 4.4, these fits allow the extraction of well-defined slope parameters. The distributions of the normalized residuals of the data points

$$r_{\rm norm} = \frac{\Delta}{\sigma} \tag{25}$$

where Δ is the difference between data and fit and σ the given experimental error, are shown in Fig. 40 for π^+ and π^- for the complete set of beam momenta and angles with the exception of a few points at low momenta and angles which clearly show a non-exponential behaviour.

If the given errors describe the local stochastic fluctuations of the data points, these distributions should have an rms of unity. The actual σ of about 0.5 indicates, assuming a wider-range, non-local behaviour of the systematic errors, that the statistical errors are about half the total given errors and of order 5–15%. This is comparable, as expected for an identical data sample and comparable momentum and angular bins, to the statistical errors given by HARP-CDP. Consequently the statistical errors used for the establishment of the exponential momentum fits and thereby the data interpolation have been adjusted by the corresponding factors.

9.3.3 Fit parameters

Figs. 41 and 42 show the inverse slope parameters for the HARP data as a function of $\Theta_{\rm lab}$ for the four beam momenta for π^+ and for π^-, respectively. These values can be directly

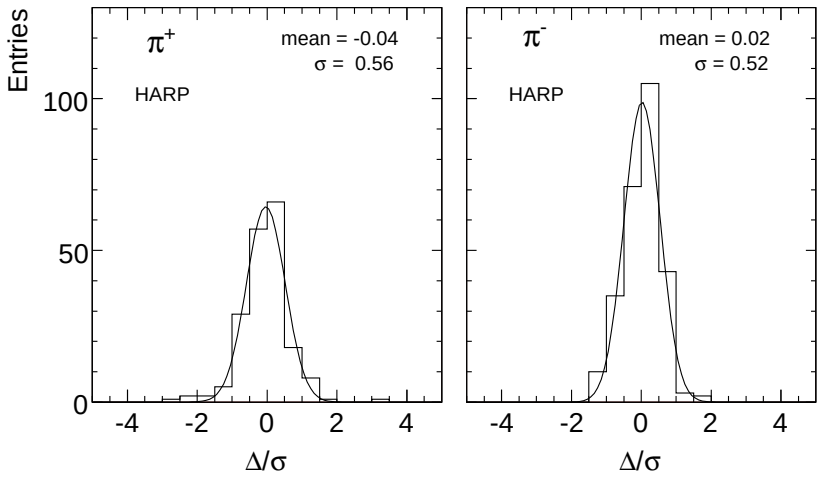

Figure 40: Normalized residual distributions for π^+ and π^- for the complete set of beam momenta and angles with the exception of a few points at low angles and momenta which clearly exhibit non-exponential behaviour

compared to the corresponding parameters for HARP-CDP also given in the Figures.

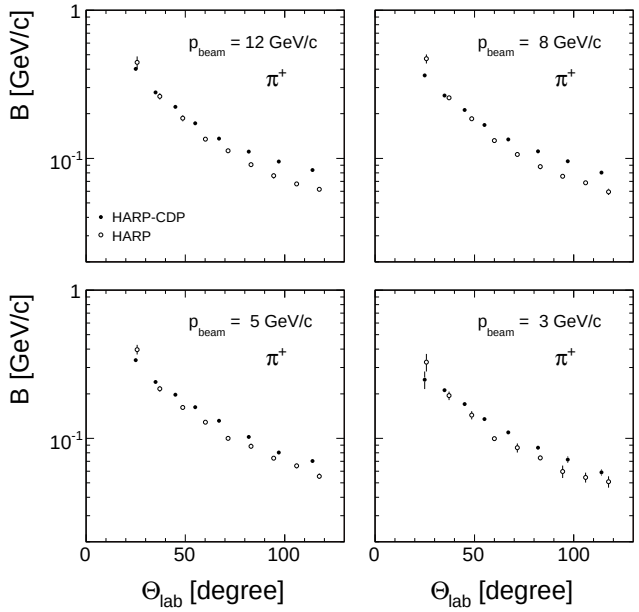

Figure 41: Inverse slopes B (5) as a function of $\cos(\theta_{\rm lab})$ for the beam momenta 3, 5, 8 and 12 GeV/c for π^+

A complex pattern of systematic differences is visible in these Figures. For π^- the inverse slopes are comparable in the region above $\Theta_{\rm lab} \sim 65$ degrees. Below this angle a systematic and progressive increase of B for HARP with respect to HARP-CDP is visible. For π^+ an opposite tendency is apparent. If the inverse slopes are equal around $\Theta_{\rm lab}$ = 35 degrees, HARP falls below HARP-CDP for larger angles and rises above for 25 degrees. This systematics will reflect in characteristic cross section differences as shown below.

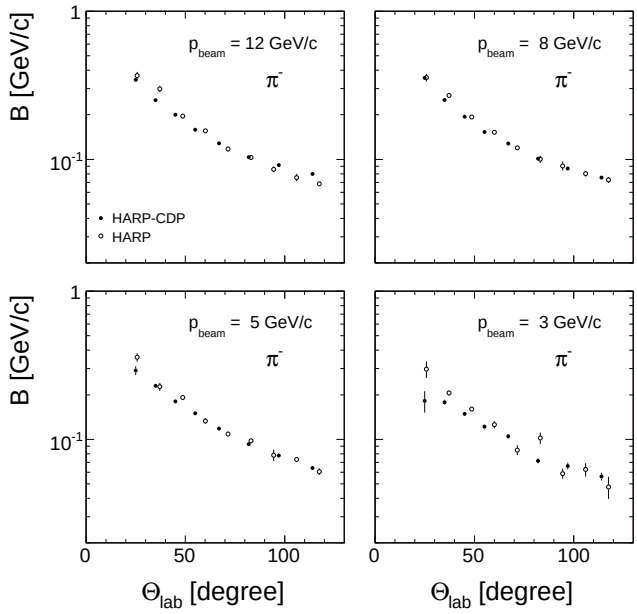

Figure 42: Inverse slopes B (5) as a function of $\cos(\theta_{\rm lab})$ for the beam momenta 3, 5, 8 and 12 GeV/c for π^-

9.3.4 Angle interpolation

In order to allow a direct comparison of the cross sections the HARP data are interpolated to the angular values of HARP-CDP which represents the standard grid of angles used for the global data interpolation. This step is well defined since the angular distributions as they are obtained from the fits to the $p_{\rm lab}$ dependences are continuous and smooth in $\cos(\Theta_{\rm lab})$ as shown for two beam momenta in Fig. 43.

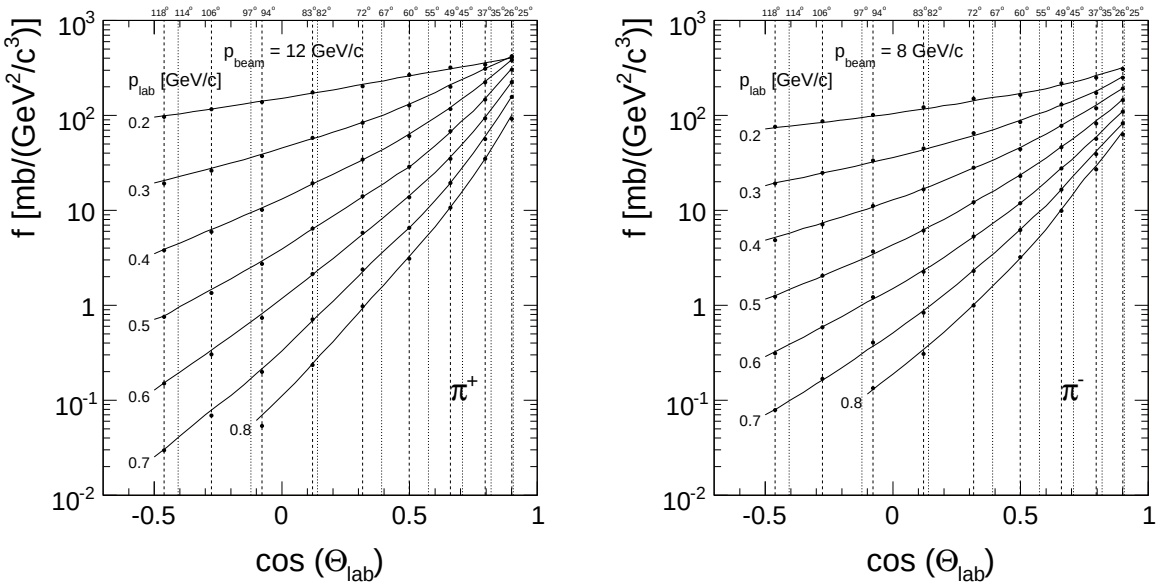

Figure 43: Invariant pion cross sections as a function of $\cos(\theta_{\rm lab})$ for the HARP data. Panel a) π^+ at 12 GeV/c beam momentum, panel b) π^- at 8 GeV/c beam momentum. Full lines: hand interpolation of the angle dependence. The angles of the HARP-CDP data are indicated by the vertical lines

The angular dependence of the invariant cross sections between the values of HARP-CDP (dotted vertical lines) and of HARP (broken vertical lines) shows that indeed also an interpolation in angle is indispensable for a quantitative comparison.

9.3.5 Cross section differences

In the following cross section differences are defined as

$$\Delta = \frac{f(\text{HARP}) - f(\text{HARP-CDP})}{f(\text{HARP})} \tag{26}$$

Fig. 44 shows the comparison of the two analyses for the example of Θ_{lab} = 67 degrees as a function of $1/\sqrt{s}$ for π^+ and π^- and the momenta 0.2, 0.4, 0.6 and 0.8 GeV/c.

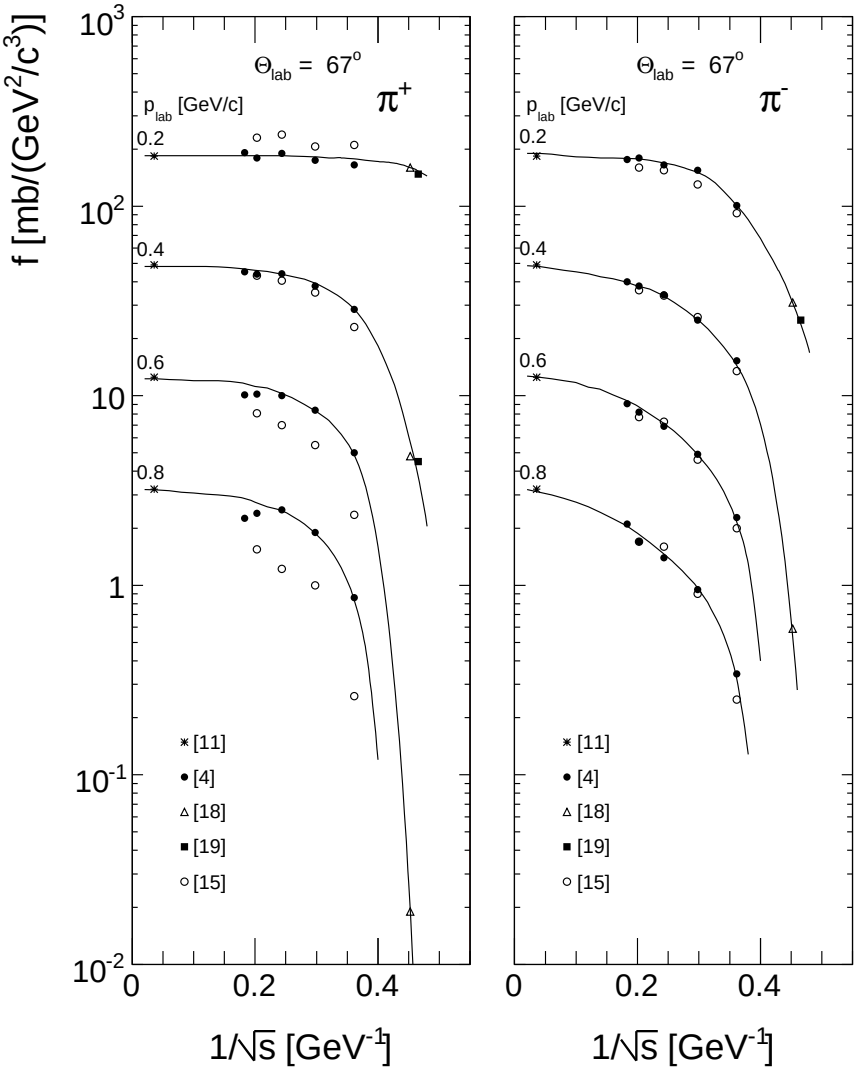

Figure 44: Invariant pion cross sections for Θ_{lab} = 67 degrees as a function of $1/\sqrt{s}$ and for the lab momenta of 0.2, 0.4, 0.6 and 0.8 GeV/c. Panel a) π^-, panel b) π^+. Open circles: HARP, full circles: HARP-CDP and additional data interpolated to this angle from Fermilab [11] at 400 GeV/c beam momentum and from Cochran et al. [18] and Crawford et al. [19] at 1.38 and 1.2 GeV/c beam momentum. Full lines: interpolation in $1/\sqrt{s}$ from Figs. 12 and 16 of this paper

In this example, the importance of the additional data at high and low beam momentum for the cross-check of the internal consistency is directly apparent as a strong constraint concerning both the absolute value of the cross sections and the shape of the $1/\sqrt{s}$ dependence. For π^- all data sets follow at this angle a reasonably continuous and smooth s-dependence. The HARP and HARP-CDP data are consistent within a margin of about $\pm$10% at all momentum values. For π^+ on the other hand sizeable differences between the HARP analysis and all other data sets are visible. At low $p_{\rm lab}$ HARP is above by about 20% for all beam momenta. This trend is inverted at $p_{\rm lab}$ above 0.4 GeV/c to -35% at 0.6 and -55% at 0.8 GeV/c, this latter momentum implying a slight extrapolation of the HARP data. This systematics is a result of the differences in the inverse slopes, see Figs. 41 and 42.

A more complete picture of the percent deviations between the HARP and HARP-CDP results is presented in Fig. 45 for π^- and Fig. 46 for π^+ as a function of $p_{\rm lab}$ for the eight $\Theta_{\rm lab}$ values of HARP-CDP and for the two beam momenta of 12 and 5 GeV/c.

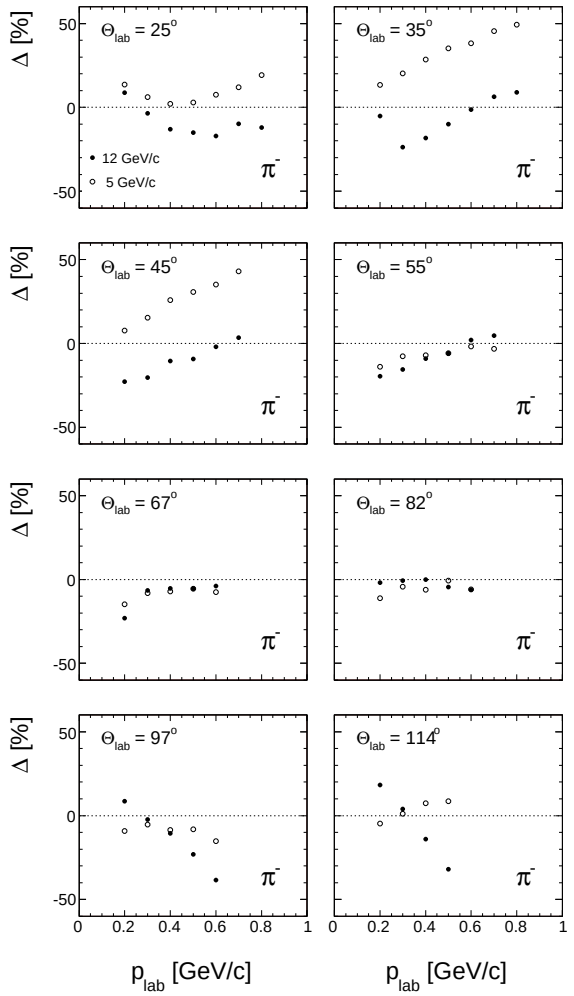

Figure 45: Percent difference between the HARP and HARP-CDP analyses for π^- as a function of lab momentum for eight angles and the beam momenta of 12 and 5 GeV/c

For π^- the differences stay generally on a level of less than $\pm$40% with rather similar momentum dependences. For π^+ (note the different vertical scales) the differences are generally positive with up to 40% in the low angle range, developing with increasing angle into very important negative deviations reaching values which exceed -100%.

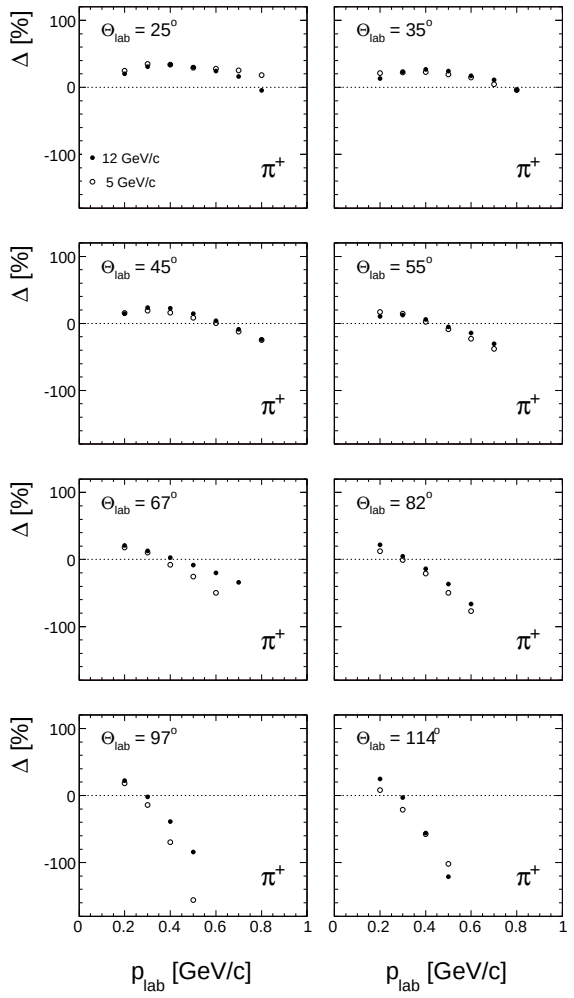

Figure 46: Percent difference between the HARP and HARP-CDP analyses for π^+ as a function of lab momentum for eight angles and the beam momenta of 12 and 5 GeV/c

Histograms of the cross section differences for all angles and beam momenta are given in Fig. 47.

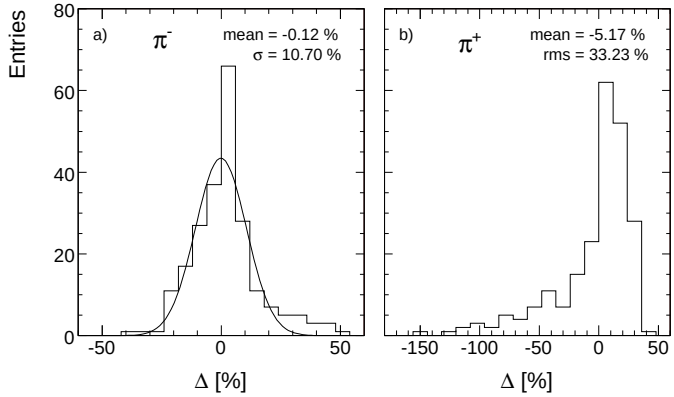

Figure 47: Histograms of the percent differences for all angles and beam momenta. Panel a) π^-, panel b) π^+

The mean values of these histograms turn out to be close to zero. The rms deviations are however very sizeable with 10.7% for π^- and 33% for π^+. Here it should be kept in mind that one is looking at the same input data so that ideally two independent analyses should produce difference distributions as δ functions at $\Delta = 0$.

9.3.6 π^+/π^- ratios $R_\pm$

The importance of π^+/π^- ratios for the study of systematic effects and the constraints imposed on $R_\pm$ by conservation laws and the basic exchange mechanisms in hadronic interactions has been discussed in detail in Sect. 8 of this paper. Here the results from HARP concerning $R_\pm$ will be discussed. Figs. 48 and 49 show $R_\pm$ as a function of $p_{\rm lab}$ for four lab angles and for the beam momenta of 5 GeV/c (Fig. 48) and 12 GeV/c (Fig. 49). The full lines give the results of the HARP data interpolation, the data points the ratios of the measured cross sections with their adjusted statistical errors (Sect. 9.3.2).

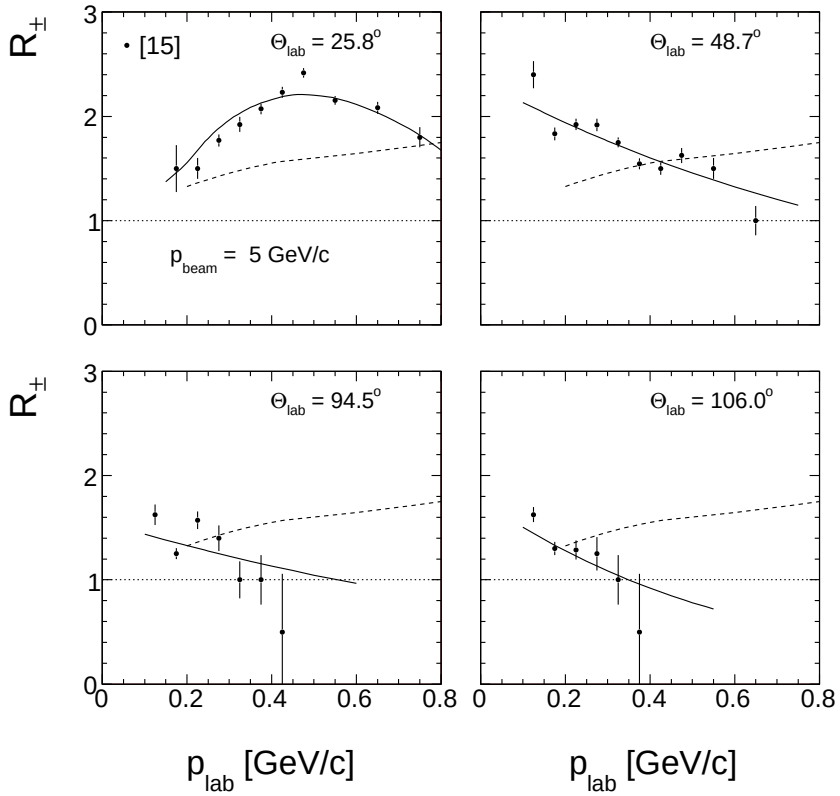

Figure 48: Charge ratio $R_\pm$ from HARP as a function of $p_{\rm lab}$ for four lab angles and a beam momentum of 5 GeV/c. The full lines give the results of the data interpolation, the full circles correspond to the ratios of the measured cross sections with the statistical errors derived in Sect. 9.3.2. The broken lines give the result of the global interpolation of all available data sets

These figures show the large deviations between the HARP results and the global data interpolation indicated by the broken lines in Figs. 48 and 49. In fact the HARP results are diametrical to the general trend of $R_\pm$ and touch for the larger angle region unphysical values at $R_\pm < 1$. At the same time they complement the argumentation of the $1/\sqrt{s}$ dependence for π^+ based on Fig. 44. If a priory it is conceivable to imagine a dependence combining the HARP measurements with the data of the independent results at low and high interaction energy, the unphysical behaviour of $R_\pm$ definitely excludes such an option.

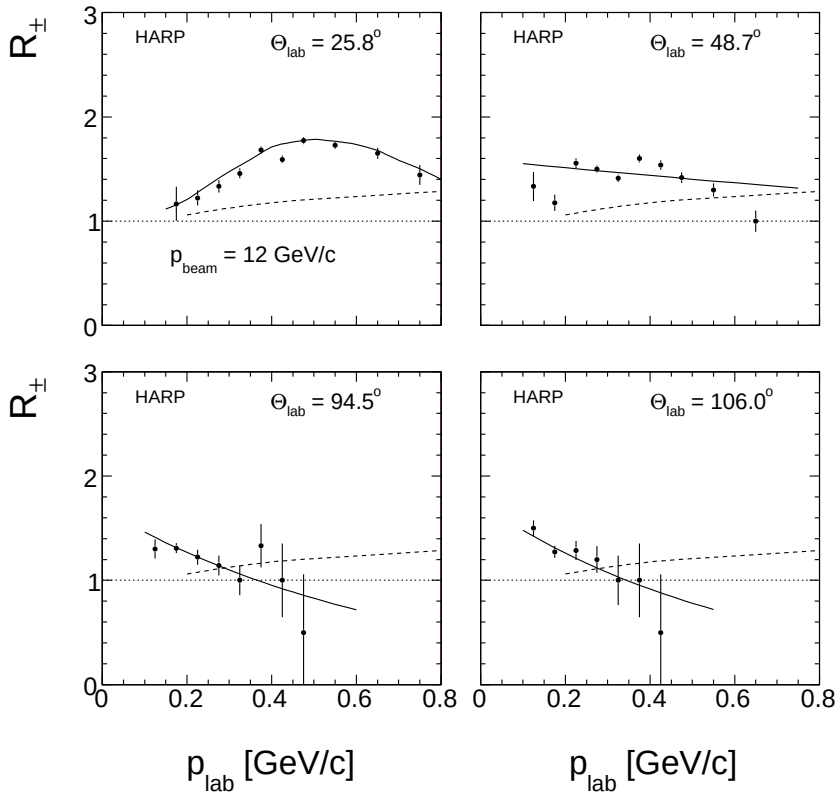

Figure 49: Charge ratio $R_{\pm}$ from HARP as a function of $p_{\rm lab}$ for four lab angles and a beam momentum of 12 GeV/c. The full lines give the results of the data interpolation, the full circles correspond to the ratios of the measured cross sections with the statistical errors derived in Sect. 9.3.2. The broken lines give the result of the global interpolation of all available data sets

9.3.7 A possible source of the observed deviations

Regarding the comparison of the π^+ cross sections from HARP with the global data interpolation, Fig. 44, a close similarity to the behaviour of the Serpukhov data for pions, Sect. 9.2 and Fig. 32 above, becomes evident. In fact the systematic pattern of the deviations, in particular their $p_{\rm lab}$ dependence, follows the same trend. It is therefore tempting to apply a corresponding upward momentum shift of a constant percentage to the HARP data. This is resulting in the "corrected" HARP data presented in Fig. 50 for angles between 55 and 112 degrees.

Fig. 50 shows the published HARP data as open circles and the momentum-corrected data as stars in comparison to the global interpolation as well as the other experimental results used in its establishment. Evidently this single-parameter correction brings the HARP cross sections into close agreement with the HARP-CDP data and with the other experiments. Several puzzles remain however unclear in connection with these data:

- in contrast to the Serpukhov data, the momentum effect only touches the π^+ data whereas the π^- data seem to first order unaffected. This charge asymmetry in the cylindrical HARP TPC detector remains to be explained
- the simple correction described above does not work out for angles below 55 degrees. It has however to be realized that only in the large angle region shown in Fig. 50 the HARP TPC volume is used over its complete radial extension. For smaller angles the exploited area contracts to a smaller radial region closer to the inner field cage
- the necessary shift of 15% in momentum would indicate and necessitate, if true, very

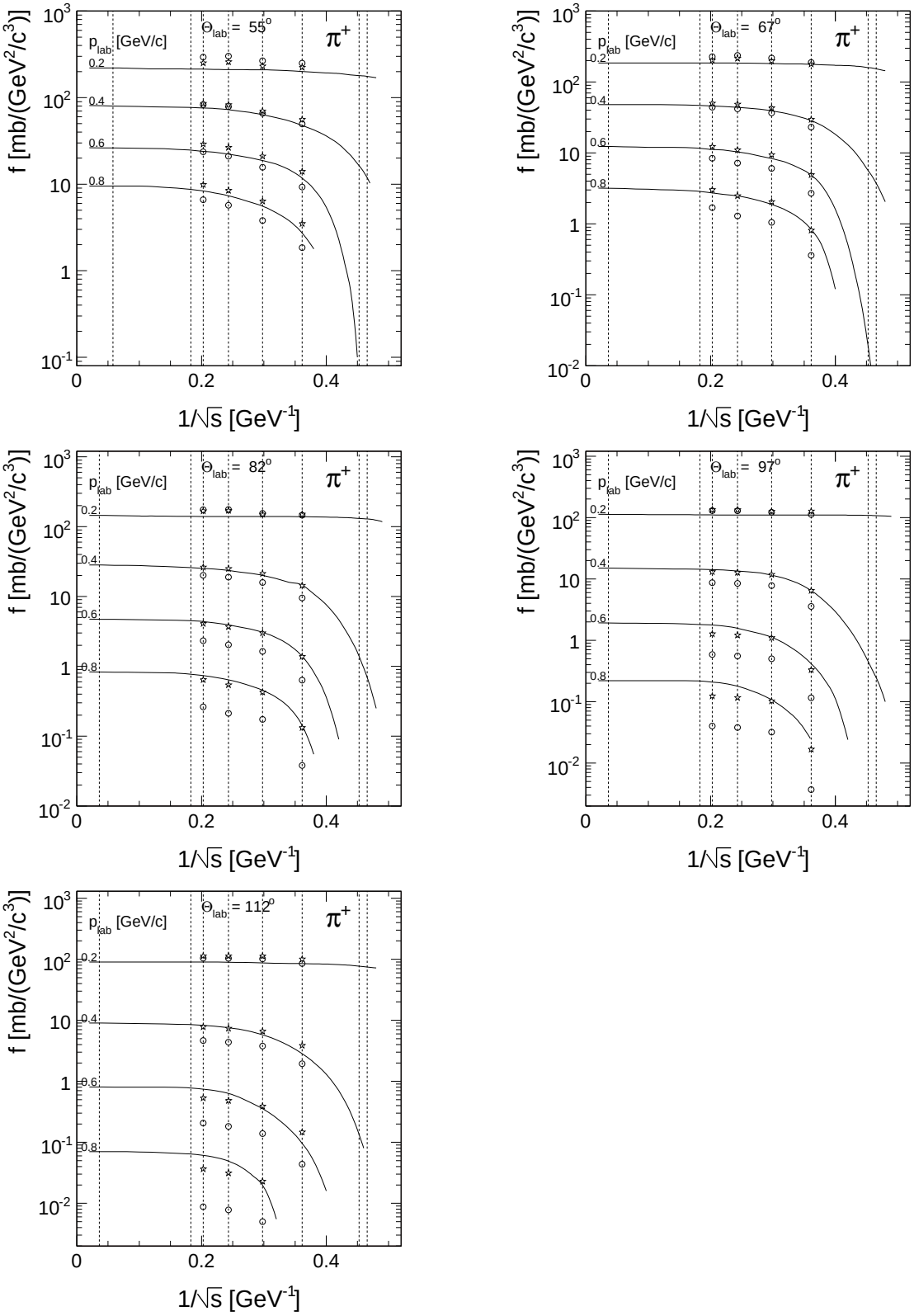

Figure 50: $1/\sqrt{s}$ dependence as a function of $1/\sqrt{s}$ for Θ_{lab} between 55 and 112 degrees. The open circles describe the HARP data, the stars the HARP data after application of an upward momentum shift by 15%. The data at p_{lab} = 0.8 GeV/c has been obtained by extrapolation with exponential fit

substantial track distortions.

The correction procedure undertaken above should of course be taken with great precaution. It may however be regarded as yet another indication of the importance of precise momentum scales in the work on backward hadron production.

9.4 The pion data from NA61, "SHINE" [14]

SHINE has published in 2011 the most recent data set discussed in this paper. These results are obtained at 31 GeV/c beam momentum and cover ranges from 0.6 to 22.3 degrees lab angle and from 0.2 to 18 GeV/c lab momentum (Table 2). If a large part of the given angular and momentum coverage falls outside the backward region regarded here, the low-momentum range up to $p_{\rm lab} \sim 0.5$ GeV/c for all angles and the range $0.6 < p_{\rm lab} < 1$ GeV/c for angles above about 9 degrees correspond to negative x_F and are therefore to be considered here.

The complete $1/\sqrt{s}$ dependence discussed in the preceding sections has a lower angular limit at 25 degrees corresponding to the lowest angular bin of the HARP-CDP data. This angle is very close to the highest SHINE angle of 22.3 degrees allowing for a safe interpolation between the two angular ranges. The cross sections from the global interpolation are therefore presented in Figs. 51 and 52 for $1/\sqrt{s}$ = 0.13 GeV^{-1} (corresponding to 31 GeV/c beam momentum) as a function of $\cos(\Theta_{\rm lab})$, for lab momenta down to 25 degrees. The SHINE data are given in this Figure for their $\Theta_{\rm lab}$ values of 12, 15.5, 18.9, and 22.3 degrees.

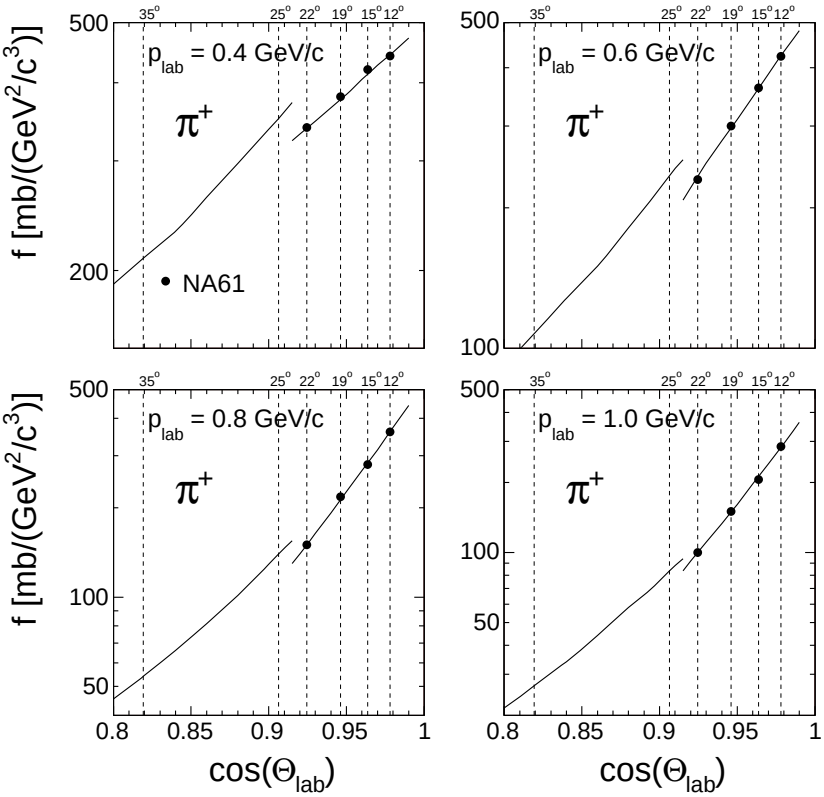

Figure 51: Invariant π^+ cross sections as a function of $\cos(\Theta_{\rm lab})$ at $1/\sqrt{s}$ = 0.13 GeV^{-1} in the $\Theta_{\rm lab}$ region from 12 to 30 degrees and for the lab momenta from 0.4 to 1 GeV/c

A systematic offset between the two angular regions is apparent. It corresponds to differences of about 15% for π^+ and about 25% for π^- in the intermediate angular region at

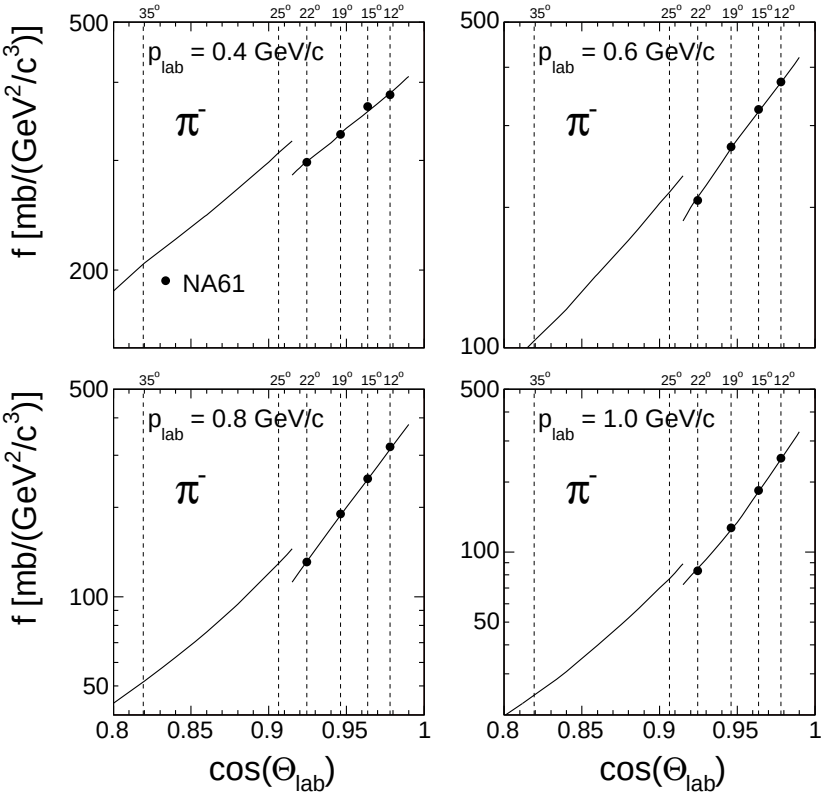

Figure 52: Invariant π^- cross sections as a function of $\cos(\Theta_{\text{lab}})$ at $1/\sqrt{s}$ = 0.13 GeV^{-1} in the Θ_{lab} region from 12 to 30 degrees and for the lab momenta from 0.4 to 1 GeV/c

$\Theta_{\text{lab}} \sim 24$ degrees. The difference between π^+ and π^- is also visible in the π^+/π^- ratios as compared to the global interpolation shown in Fig. 53.

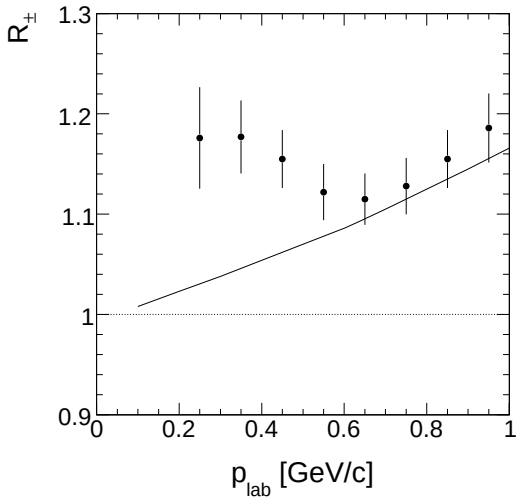

Figure 53: $R_\pm$ for the SHINE results as a function of p_{lab} averaged over the angular region from 12 to 22.3 degrees. The full line gives $R_\pm$ for the global interpolation at 31 GeV/c beam momentum

As the global interpolation is limited to $\Theta_{\text{lab}} > 25$ degrees, another way of comparison is offered by the NA49 data at 158 GeV/c beam momentum [12]. These data cover the

complete angular range of the SHINE results. For this comparison the ratio of the global interpolation at 158 GeV/c beam momentum ($1/\sqrt{s}$ = 0.058 GeV^{-1}) to the one for 31 GeV/c ($1/\sqrt{s}$ = 0.13 GeV^{-1}) may be formed for the available Θ_{lab} from 160 to 25 degrees. For the lower angular range the ratio between the invariant cross sections from NA49 and from SHINE may be used. This comparison is shown in Figs. 54 and 55.

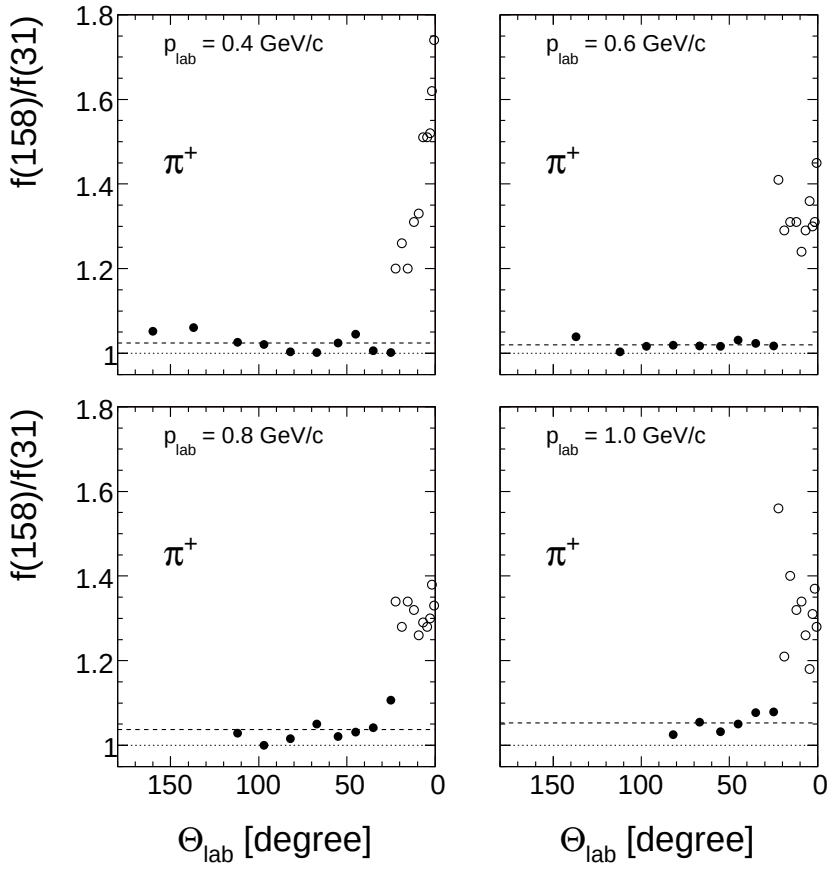

Figure 54: Ratio of invariant π^+ cross sections at 158 and 31 GeV/c as a function of Θ_{lab}. The closed circles correspond to the global data interpolation, the open circles to the direct NA49/SHINE ratio. The broken lines give the mean over the angular range of the global data interpolation

Apparently the cross section ratio is within errors angle independent over the full range of the global data survey, with a well-defined average which is increasing with p_{lab} from 1.02 to 1.05 for π^+ and from 1.07 to 1.16 for π^- for the momentum range $0.4 < p_{\text{lab}} < 1$ GeV/c. In contrast, the ratio between NA49 and SHINE results ranges from 1.2 to 1.75 for π^+ and from 1.3 to 1.75 for π^-, with a general increase with decreasing lab angle. The reason for this discrepancy is not evident, in particular as in the forward region above $x_F \sim 0.1$ the two results are relatively close. Anyway the s-dependence at low x_F is sufficiently well known from elementary interactions to exclude deviations of this order of magnitude. See also the discussion in the following section concerning the prediction of p+C cross sections from elementary collisions.

In conclusion of this section on deviating experiments it may be stated that the global data interpolation between 15 different experiments attempted in this paper shows a considerable power of discrimination against diverging results. In some cases it becomes even possible to hint at a rational explanation for the observed discrepancies.

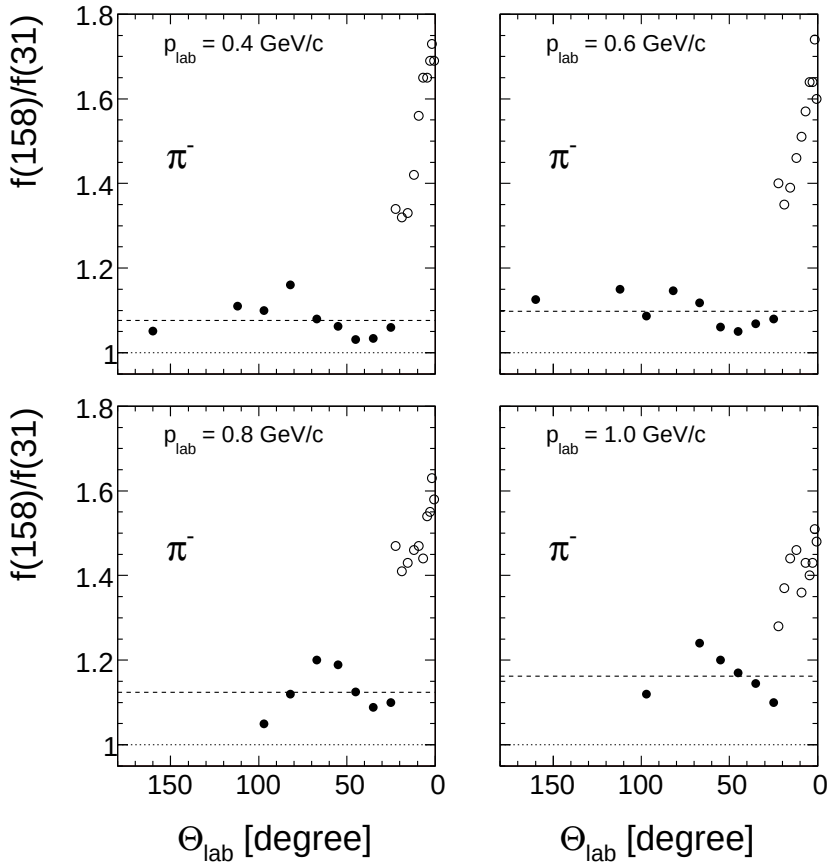

Figure 55: Ratio of invariant π^- cross sections at 158 and 31 GeV/c as a function of Θ_{lab}. The closed circles correspond to the global data interpolation, the open circles to the direct NA49/SHINE ratio. The broken lines give the mean over the angular range of the global data interpolation

10 The separation of target fragmentation and intra-nuclear component for pion production at SPS energy

Hadronic production in the backward direction of p+A collisions has two components: the fragmentation of the target nucleons which have been hit by the projectile proton, and the propagation of momentum transfer into the nucleus by secondary nucleon-nucleon interaction which follow, on a longer time scale, the initial excitation process. Both processes are governed by the mean number of collisions $\langle\nu\rangle$ suffered by the projectile on his trajectory through the nucleus.

As only the sum of these two separate mechanisms is experimentally accessible, a minimum assumption about the fragmentation of the target nucleons is needed in order to allow the separation of the components in an otherwise model-independent fashion. This minimal assumption consists in assuming that the fragmentation process of the hit nucleons is equal to the basic nucleon-nucleon interaction, taking full account of course of isospin symmetry. In addition and only valid for the relatively small value of $\langle\nu\rangle$ in the Carbon nucleus, it will be assumed that successive collisions result in hadronization at full interaction energy of the corresponding elementary interactions.

As far as the value of $\langle\nu\rangle$ is concerned, this has been determined for pion production in some detail in [28] using the forward and the backward region at x_F > -0.1 where no intra-

nuclear cascading is present, see below. This determination used three independent approaches:

- a Monte-Carlo calculation using the measured nuclear density distributions
- the relation between the inelastic cross sections of p+p and p+C interactions
- the approach to x_F = -0.1 of the ratio of pion densities in p+C and p+p collisions

The two former methods have to make the assumption that the inelastic interaction cross sections are independent of the number of subsequent collisions ν.

In [2] a similar approach is used concerning the production of protons and anti-protons, again in the regions where there is no contribution from nuclear cascading as well as in the full backward hemisphere.

All methods mentioned above result in a consistent estimate of $\langle\nu\rangle$ = 1.6 in p+C collisions, with a relative systematic uncertainty of the order of a few percent.

In the following argumentation a prediction of the mean pion density of target fragmentation in the backward hemisphere at $\sqrt{s}$ = 17.2 GeV will be used which is relying on the published pion data from NA49 [21] and the estimated mean number of collisions, $\langle\nu\rangle$. The invariant pion cross sections are divided by the inelastic cross section to yield the quantity

$$\langle f_{\rm pp}(x_F, p_T)\rangle = 0.5(f_{\rm pp}^{\pi^+}(x_F, p_T) + f_{\rm pp}^{\pi^-}(x_F, p_T)) \tag{27}$$

per inelastic event which establishes isospin symmetry, and

$$f^{\rm pred}(x_F, p_T) = 1.6\langle f_{\rm pp}(x_F, p_T)\rangle \tag{28}$$

This prediction is transformed into the appropriate coordinates $p_{\rm lab}$ and $\Theta_{\rm lab}$ and divided by the measured invariant p+C cross sections $f_{\rm pC}(p_{\rm lab}, \Theta_{\rm lab})$ per inelastic event yielding the ratio

$$R^{\rm pred}(p_{\rm lab}, \Theta_{\rm lab}) = \frac{f^{\rm pred}(x_F, p_T)}{f_{\rm pC}(p_{\rm lab}, \Theta_{\rm lab})} \tag{29}$$

This ratio is shown in Fig. 56 as a function of $p_{\rm lab}$ for the lab angles 10, 20, 30, 40 and 45 degrees.

It is evident that the ratio is close to one for the three lowest angles at all $p_{\rm lab}$ and for the region below 0.8 GeV/c for 40 and 45 degrees. This is quantified in Fig. 57 which gives the distribution of the ratio for the mentioned $p_{\rm lab}$ ranges.

The results show that indeed the measured pion cross sections correspond for lab angles up to 45 degrees precisely to the prediction from elementary collisions. This indicates that there is no contribution from intra-nuclear cascading in this region, in accordance with the results of [28]. A drop of the ratio becomes however visible in the higher $p_{\rm lab}$ range at 40 and 45 degrees. This marks the onset of a nuclear component which becomes clearly visible in the ratios at larger angles shown in Fig. 58.

It is interesting to note that the target fragmentation governs the pion density up to the highest lab angles at low $p_{\rm lab}$, with $R^{\rm pred}$ values of more than 50%. The ratio decreases however steadily with increasing $p_{\rm lab}$ and reaches zero at distinct momentum values indicating the approach to x_F = -1 in the plots of Fig. 1. This kinematic effect is more clearly brought out in Fig. 59 showing that the fraction of target fragmentation is essentially a function of x_F and rather independent on lab angle.

The correlation between $p_{\rm lab}$ and $\Theta_{\rm lab}$ for fixed values of $R^{\rm pred}$ shown in panel a traces rather exactly the kinematic correlation between the same variables for fixed values of x_F, panel b. This allows to establish a direct dependence of $R^{\rm pred}$ on x_F which is to first order angle-independent, panel c.

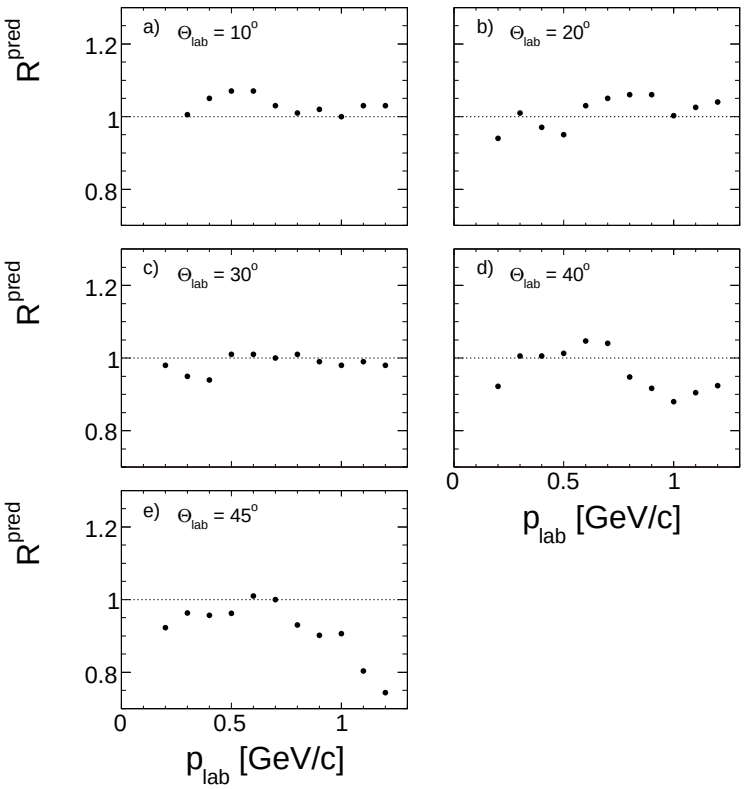

Figure 56: $R^{\text{pred}}(p_{\text{lab}}, \Theta_{\text{lab}})$ as a function of p_{lab} for the five angles 10, 20, 30, 40 and 45 degrees

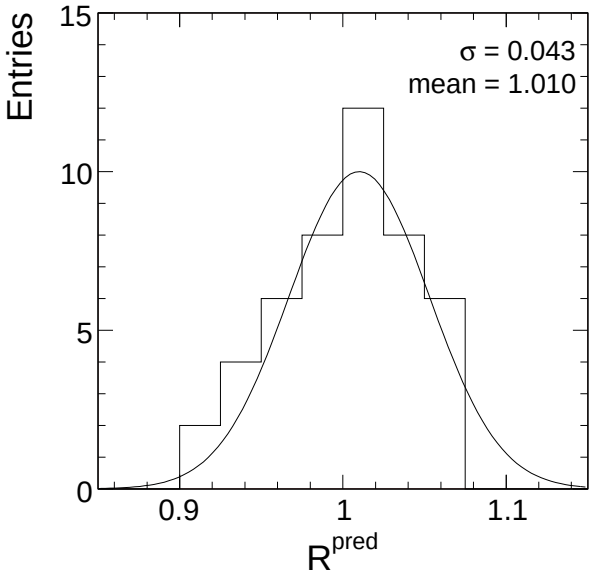

Figure 57: Distribution of $R^{\text{pred}}(p_{\text{lab}}, \Theta_{\text{lab}})$ for the lab angles 10, 20, 30 degrees and 40 and 45 degrees at $p_{\text{lab}} < 0.8$ GeV/c. Full line: Gauss fit to the distribution with a mean value at 1.01 and a relative rms of 4.3%

The invariant densities $f^{\text{pred}}(p_{\text{lab}}, \Theta_{\text{lab}})$ per inelastic event as predicted from the fragmentation of the participant target nucleons is presented in Fig. 60.

This density may be subtracted from the pion density $f(p_{\text{lab}}, \Theta_{\text{lab}})/\sigma^{\text{inel}}$ measured in p+C interactions which is within errors equal for π^+ and π^-, see Figs. 14 and 18. The resulting

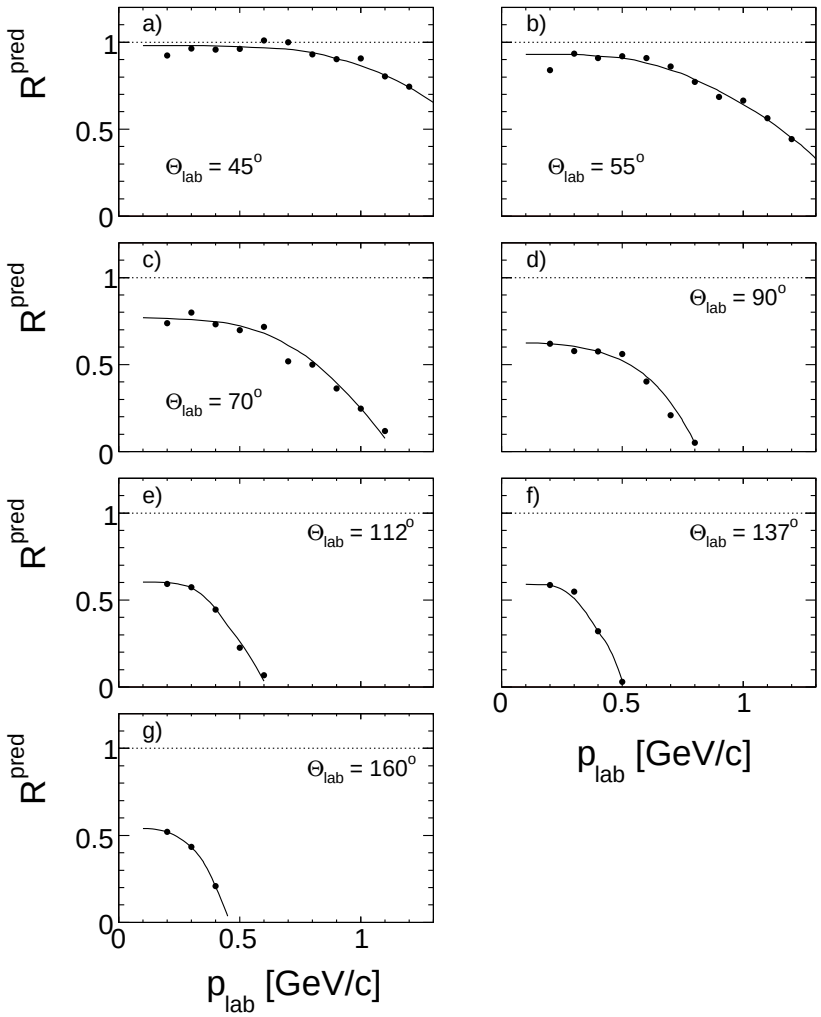

Figure 58: $R^{\text{pred}}(p_{\text{lab}}, \Theta_{\text{lab}})$ as a function of p_{lab} for the angles of 45, 55, 70, 90, 112, 137 and 160 degrees. The full lines are local interpolations

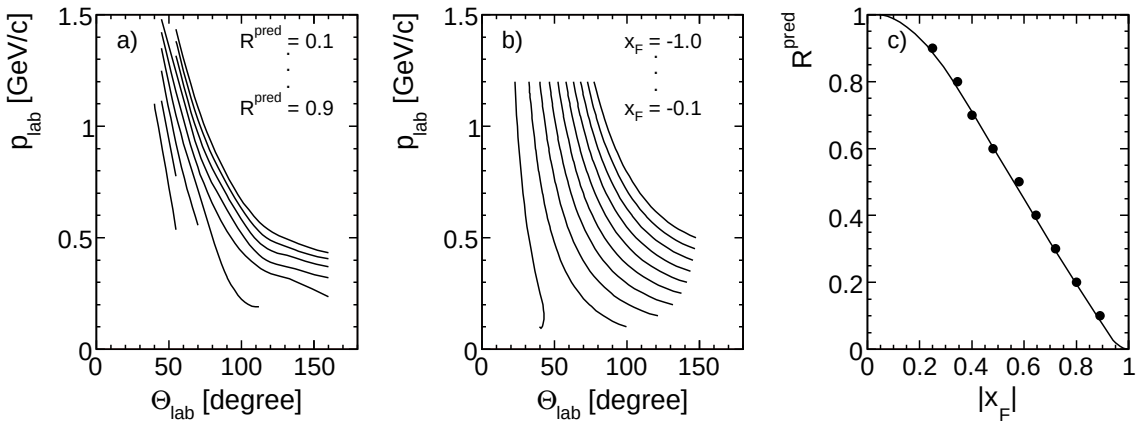

Figure 59: a) measured correlation between p_{lab} and Θ_{lab} for constant values of $R^{\text{pred}}(p_{\text{lab}}, \Theta_{\text{lab}})$ between 0.1 and 0.9, b) correlation between p_{lab} and Θ_{lab} for fixed values of x_F between -0.1 and -1.0 and c) $R^{\text{pred}}(p_{\text{lab}}, \Theta_{\text{lab}})$ as a function of x_F

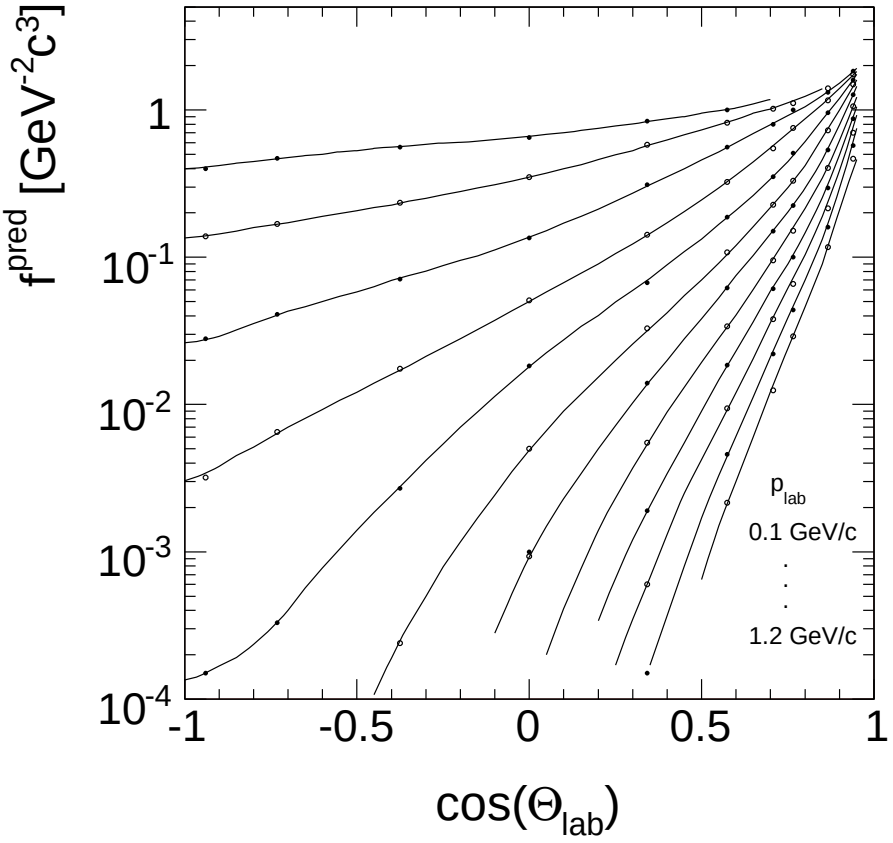

Figure 60: Predicted invariant density $f^{\text{pred}}(p_{\text{lab}}, \Theta_{\text{lab}})$ per inelastic event as a function of $cos(\Theta_{\text{lab}})$ for fixed values of p_{lab} between 0.1 and 1.2 GeV/c. The full lines represent data interpolations

invariant density

$$f^{\text{nucl}}(p_{\text{lab}}, \Theta_{\text{lab}}) = \frac{f(p_{\text{lab}}, \Theta_{\text{lab}})}{\sigma^{\text{inel}}} - f^{\text{pred}}(p_{\text{lab}}, \Theta_{\text{lab}}) \tag{30}$$

is shown in Fig. 61.

This subtraction procedure becomes of course uncertain in the small angle region where the nuclear component is on the few percent level and below with respect to the target fragmentation, see Figs. 56 and 58.

The invariant angular distributions shown in Figs. 60 and 61 may be converted into number distributions following:

$$\frac{d^2n^{\text{pred}}(p_{\text{lab}}, \Theta_{\text{lab}})}{dp_{\text{lab}}d\Theta_{\text{lab}}} = 2\pi \frac{p_{\text{lab}}^2}{E_{\text{lab}}} f^{\text{pred}}(p_{\text{lab}}, \Theta_{\text{lab}}) \tag{31}$$

and

$$\frac{d^2n^{\text{nucl}}(p_{\text{lab}}, \Theta_{\text{lab}})}{dp_{\text{lab}}d\Theta_{\text{lab}}} = 2\pi \frac{p_{\text{lab}}^2}{E_{\text{lab}}} f^{\text{nucl}}(p_{\text{lab}}, \Theta_{\text{lab}}) \tag{32}$$

Integrating these distributions over p_{lab}, the number distributions

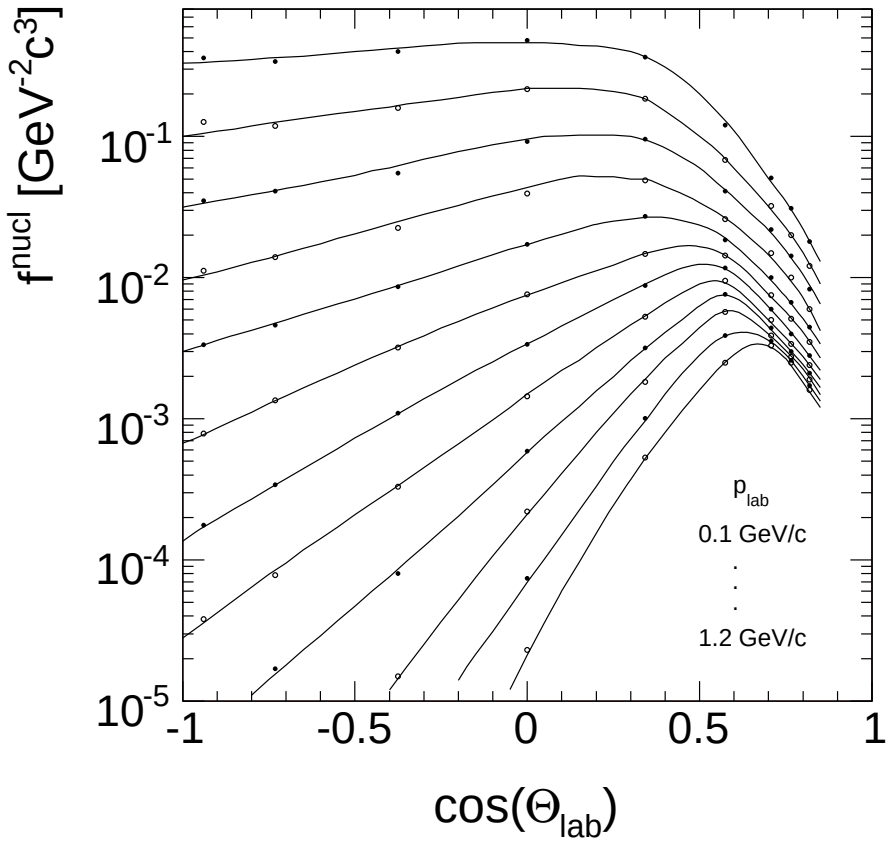

Figure 61: Invariant pion density $f^{\text{nucl}}(p_{\text{lab}}, \Theta_{\text{lab}})$ from intra-nuclear cascading as a function of $cos(\Theta_{\text{lab}})$ for fixed values of p_{lab} between 0.1 and 1.2 GeV/c. The full lines represent data interpolations

$$\frac{dn^{\text{pred}}}{d\cos(\Theta_{\text{lab}})} \tag{33}$$

and

$$\frac{dn^{\text{nucl}}}{d\cos(\Theta_{\text{lab}})} \tag{34}$$

are obtained which are shown in Fig. 62 together with the ratio

$$R^{\text{nucl}}(\cos(\Theta_{\text{lab}})) = \frac{dn^{\text{nucl}}}{d\cos(\Theta_{\text{lab}})} \Big/ \frac{dn^{\text{pred}}}{d\cos(\Theta_{\text{lab}})} \tag{35}$$

Evidently the nuclear component of pion production stays comparable to the target fragmentation in the full backward hemisphere of Θ_{lab}. It decreases rapidly for Θ_{lab} below about 60 degrees and vanishes below Θ_{lab} 25 degrees.

Integration of $dn^{\text{nucl}}/d\cos(\Theta_{\text{lab}})$ over $\cos(\Theta_{\text{lab}})$ results in the total single pion yield from nuclear cascading

$$n_{\pi}^{\text{nucl}} = 0.105 \tag{36}$$

per inelastic event. The predicted integrated yield from target fragmentation is

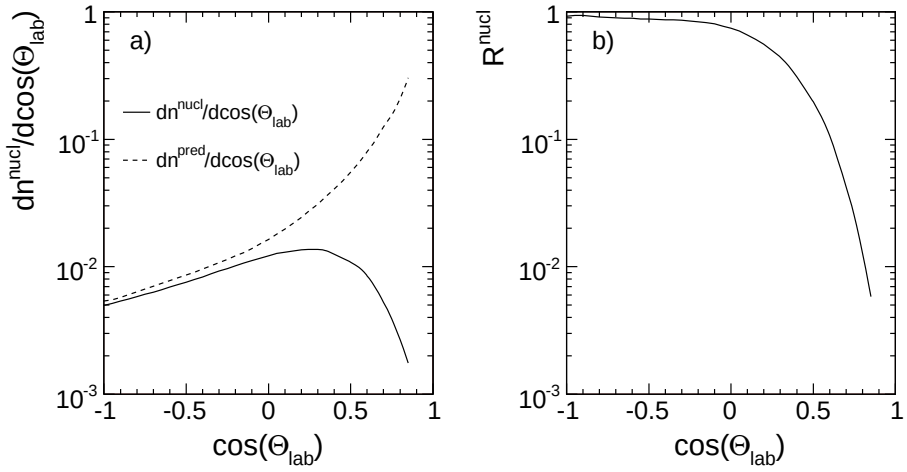

Figure 62: a) $dn^{\text{nucl}}/d\cos(\Theta_{\text{lab}})$ as a function of $\cos(\Theta_{\text{lab}})$ (full line), $dn^{\text{pred}}/d\cos(\Theta_{\text{lab}})$ as a function of $\cos(\Theta_{\text{lab}})$ (broken line), b) the ratio R^{nucl} as a function of $\cos(\Theta_{\text{lab}})$

$$n_{\pi}^{\text{pred}} = \frac{1.6(n_{\pi^+}^{\text{pp}} + n_{\pi^-}^{\text{pp}})}{4} = 2.151 \tag{37}$$

with

$$n_{\pi^+}^{\text{pp}} = 3.018 \tag{38}$$

and

$$n_{\pi^-}^{\text{pp}} = 2.360 \tag{39}$$

from p+p interactions as measured by NA49, [21]. This means that for p+C interactions the nuclear component of pion production amounts to 4.9% of the pions originating from the fragmentation of the hit target nucleons. Applying isospin symmetry on the isoscalar C nucleus with

$$n_{\pi^+} = n_{\pi^-} = n_{\pi^0} \tag{40}$$

the total pion yields are 6.45 from target fragmentation and 0.315 from nuclear cascading.

Making use of the kinematic relation between the coordinate pairs p_{lab}, Θ_{lab} and x_F, p_T, see Fig. 1c, the double differential yields for the nuclear component as functions of x_F and p_T

$$\frac{d^2n^{\text{nucl}}}{dx_F dp_T} = 2\pi p_{\text{max}} \frac{p_T}{E} f^{\text{nucl}}(x_F, p_T) \tag{41}$$

may be obtained where p_{max}, (2), and E are cms quantities. The resulting pion density distributions are shown in Fig. 63 as a function of x_F for p_T values from 0.05 to 0.7 GeV/c.

A peak at low p_T and x_F = -0.15 is apparent which corresponds to the location of pions with small lab momentum, see Fig. 1. With increasing p_T the maximum density decreases and shifts in x_F to lower values which is again in accordance with the kinematic correlation visible in Fig. 1. Integration over p_T results in the single differential density $dn^{\text{nucl}}/dx_F(x_F)$ shown in Fig. 64 together with the predicted density distribution $dn^{\text{pred}}/dx_F(x_F)$ from target fragmentation and with the ratio of the two densities.

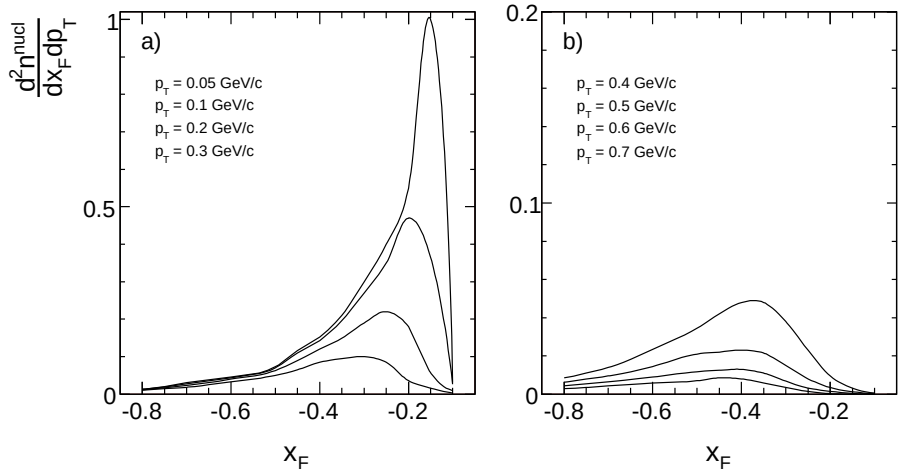

Figure 63: Double differential pion density $d^2n^{\text{nucl}}/dx_F dp_T$ as a function of x_F for a) $0.05 < p_T < 0.3$ GeV/c and b) $0.4 < p_T < 0.7$ GeV/c

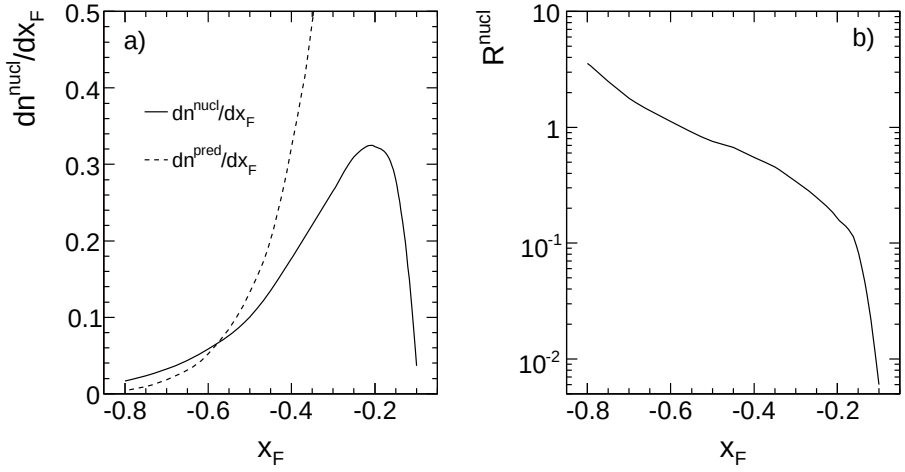

Figure 64: a) Pion density dn^{nucl}/dx_F as a function of x_F (full line). The predicted density distribution from target fragmentation dn^{pred}/dx_F is shown as the broken line; b) Ratio $R^{\text{nucl}}(x_F) = (dn^{\text{nucl}}/dx_F)/(dn^{\text{pred}}/dx_F)$ as a function of x_F

The p_T integrated pion density $dn^{\text{nucl}}/dx_F(x_F)$ shows a peak at $x_F \sim$ -0.2 and vanishes at $x_F \sim$ -0.08. As shown by the density ratio with the predicted target fragmentation $dn^{\text{pred}}/dx_F(x_F)$ in Fig. 64b, the nuclear component reaches 10% of the target fragmentation at x_F = -0.15 and exceeds this contribution for $x_F <$ -0.55.

The nuclear pion component extracted above is used in [2] in conjunction with the complementary nuclear proton component to obtain the percentage of cascading protons which are accompanied by pion emission.

11 Conclusion

This paper presents a survey of available data concerning backward proton and pion production in minimum bias p+C interactions, including new and extensive data sets obtained at the CERN PS and SPS. The backward direction being defined as the complete phase space at negative Feynman x_F, the data cover, for projectile momenta from 1 to 400 GeV/c, the ranges

from 0.2 to 1.2 GeV/c in lab momentum $p_{\rm lab}$ and from 10 to 180 degrees in lab angle $\Theta_{\rm lab}$. The paper attempts an interconnection of the different data sets by a detailed three-dimensional interpolation scheme in the variables $1/\sqrt{s}$, $p_{\rm lab}$, and $\cos(\Theta_{\rm lab})$. This attempt allows a precise control of the internal data consistency as well as the study of the evolution of the invariant inclusive cross sections in all three variables.

A literature search has provided a set of 19 different experiments with a total of more than 3500 data points. These measurements were obtained over 40 years of experimentation by collaborations employing widely different experimental techniques. In this respect it may be stated as a first positive result that the majority of the data may be combined into a surprisingly self-consistent ensemble. This global interpolation scheme results in a considerable discriminative power against the systematic deviation of particular data sets. Only 4 of the 19 quoted experiments show in fact deviations which clearly mark them as systematically diverging. These experiments are inspected in detail one by one in an attempt to clearly bring out the discrepancies. In some of the cases, possible experimental error sources are pointed out.

The underlying physics provides for additional constraints concerning basic quantities like charge conservation and isospin symmetry as well as the necessity of smoothness and continuity of the observed cross sections. Whenever possible, contact to the complementary elementary nucleon-nucleon interactions is established. This concerns in particular the evocation of mesonic exchange processes for the description of π^+/π^- ratios and the prediction of the target fragmentation from elementary interactions and its separation from the component of nuclear cascading.

As far as the dependences of the invariant cross sections on the three basic variables $p_{\rm lab}$, $\Theta_{\rm lab}$ and $1/\sqrt{s}$ is concerned, a well constrained phenomenology emerges. The $p_{\rm lab}$ dependences are exponential or close to exponential over a major part of the phase space with some exceptions mostly towards low interaction energies. This fact results in an important constraint for the data interpolation. The $\cos(\Theta_{\rm lab})$ dependences are not far from exponential and smooth and continuous through all lab angles. In particular there is no indication of an instability around 90 degrees for the proton yields. The $1/\sqrt{s}$ dependences converge, after strong variations close to production threshold, smoothly to asymptotic behaviour in the SPS energy range. This region is approached from above by the protons and from below for the pions. This convergence is confirmed by the π^+/π^- ratios which show, being governed by meson exchange at low $\sqrt{s}$ with large values marked by the projectile isospin, a smooth decline with energy towards unity as expected from the underlying elementary exchange processes.

Acknowledgements

This work was supported by the Polish State Committee for Scientific Research (P03B00630), the Polish National Science Centre (on the basis of decision no. DEC-2011/03/B/ST2/02634) the Bulgarian National Science Fund (Ph-09/05), the EU FP6 HRM Marie Curie Intra-European Fellowship Program, the Hungarian Scientific Research Fund OTKA (T68506) and the Hungarian OTKA/NKTH A08-77719 and A08-77815 grants.

References

[1] Y. D. Bayukov et al., Phys. Rev. **C20**, (1979) 764
[2] B. Baatar et al., arXiv:1207.6520v1 [hep-ex]
[3] I. M. Belyaev et al., **JINR-P1-90-551** (1990) (in Russian)
[4] A. Bolshakova et al., Eur. Phys. J. **C70** (2010) 573
[5] N. A. Burgov et al., Sov. J. Nucl. Phys. **30** (1979) 371, Yad. Fiz. **30** (1979) 720
[6] Y. D. Bayukov et al., Sov. J. Nucl. Phys. **18** (1974) 639
Y. D. Bayukov et al., Sov. J. Nucl. Phys. **19** (1974) 648
[7] J. V. Geaga et al., Phys. Rev. Lett. **45** (1980) 1993
[8] S. Frankel et al., Phys. Rev. Lett. **36** (1976) 642
[9] V. I. Komarov et al., Phys. Lett. **69B** (1977) 37
[10] J. Franz et al., Nucl. Phys. **A472** (1987) 733
[11] N. A. Nikiforov et al., Phys. Rev. **C22** (1980) 700
[12] C. Alt et al., Eur. Phys. J. **C49** (2007) 897
[13] I. M. Belyaev et al., Sov. J. Nucl. Phys. **49** (1989) 295
[14] N. Abgrall et al., Phys. Rev. **C84** (2011) 034604
[15] M. G. Catanesi er al., Phys. Rev. **C77** (2008) 055207
[16] N. A. Burgov et al., Sov. J. Nucl. Phys. **32** (1980) 219, Yad. Fiz. **32** (1980) 423
[17] A. M. Baldin et al., Sov. J. Nucl. Phys. **20** (1975) 629
[18] D. R. F. Cochran, Phys. Rev. **D6** (1972) 3085
[19] J. F. Crawford, Phys. Rev. **C22** (1980) 1184
[20] J. Whitmore et al., Phys. Lett **60B** (1976) 211
T. Ferbel, Phys. Rev. Lett. **29** (1972) 448
A. H. Mueller, Phys. Rev. **D2** (1970) 2963
[21] C. Alt et al., Eur. Phys. J. **C45** (2006) 343
[22] B. D. Anderson et al., Phys. Rev. Lett. **46** (1981) 226
[23] D. H. Boal, Phys. Rev. **C25** (1982) 3068
[24] V. Blobel et al., Nucl .Phys. **B135** (1978) 379
[25] T. Anticic et al., Eur. Phys. J. **C65** (2010) 9
[26] http://cern.ch/spshadrons
[27] V. Blobel et al., Nucl. Phys. **B69** (1974) 454
[28] G. Barr et al., Eur. Phys. J. **C49** (2007) 919
[29] E. L. Miller et al., Phys. Rev. Lett. **26** (1971) 984
[30] M. N. Kreisler et al., Nucl. Phys. **B84** (1975) 3
[31] V. Böhmer et al., Nucl. Phys. **B110** (1976) 205
[32] A. Babaev et al., Nucl. Phys. **B110** (1976) 189
[33] H. R. Barton et al., Phys. Rev. Lett. **37** (1976) 1656
[34] H. De Kerret et al., Phys. Lett. **69B** (1977) 372
[35] G. Goggi et al., Phys. Lett. **72B** (1977) 265
[36] G. Goggi et al., Phys. Lett. **79B** (1978) 165
[37] C. Conta et al., Nucl. Phys. **B175** (1980) 97